NAVAL POSTGRADUATE SCHOOL
Monterey, California

THESIS

PERFORMANCE OF A HIGH RESOLUTION DIAGNOSTIC MODEL FOR SHORT RANGE MESOSCALE WIND FORECASTS IN COMPLEX TERRAIN

by

Shawn G. Gallaher

September 2002

Thesis Advisor: Douglas K. Miller
Second Reader: Wendell A. Nuss

THIS PAGE INTENTIONALLY LEFT BLANK

REPORT DOCUMENTATION PAGE

Form Approved OMB No. 0704-0188

1. AGENCY USE ONLY *(Leave blank)*	2. REPORT DATE	3. REPORT TYPE AND DATES COVERED
	September 2002	Master's Thesis

4. TITLE AND SUBTITLE
Performance of a High Resolution Diagnostic Model for Short Range Mesoscale Wind Forecasts in Complex Terrain

5. FUNDING NUMBERS

6. AUTHOR (S) Shawn G. Gallaher

7. PERFORMING ORGANIZATION NAME(S) AND ADDRESS(ES)
Naval Postgraduate School
Monterey, CA 93943-5000

8. PERFORMING ORGANIZATION REPORT NUMBER

9. SPONSORING / MONITORING AGENCY NAME(S) AND ADDRESS(ES)

10. SPONSORING/MONITORING AGENCY REPORT NUMBER

11. SUPPLEMENTARY NOTES The views expressed in this thesis are those of the author and do not reflect the official policy or position of the U.S. Department of Defense or the U.S. Government.

12a. DISTRIBUTION / AVAILABILITY STATEMENT
Approved for public release: distribution is unlimited

12b. DISTRIBUTION CODE

13. ABSTRACT *(maximum 200 words)*

This study investigates the feasibility of using a high resolution simple diagnostic model (WOCSS) initialized from a coarser grid full physics prognostic model (COAMPS) to obtain mesoscale winds. This approach using COAMPS 81, 27, and 9 km forecast model soundings to initialize WOCSS at 3 km is compared to COAMPS forecast at 3km horizontal resolution alone. Four case studies were collected during various weather regimes in Central California. Observations were collected from 5 different agencies and were used for verification of the models. The sensitivity of various WOCSS parameters were also explored.

The results showed that overall the COAMPS(9km)/WOCSS approach provides winds as good as COAMPS at 3 km at a greatly reduced computation time. The COAMPS/WOCSS methodology performed particularly well during non-frontal situations where low-level inversions were present. Separation of the surface observation data by agency revealed large errors from data networks with low maintenance, monitoring and site specifications standards. The highest flow surface in WOCSS was the only parameter that displayed any significant sensitivity. Further work is needed to test the advantages of this sensitivity. COAMPS/WOCSS mesoscale forecast winds may prove to be very useful as input to emergency response applications such as dispersion and trajectory modeling.

14. SUBJECT TERMS	15. NUMBER OF PAGES
Mesoscale Wind Forecasting, Diagnostic Wind Models, Winds on Critical Streamline Surfaces (WOCSS), Mesoscale Modeling, Complex Terrain	146
	16. PRICE CODE

17. SECURITY CLASSIFICATION OF REPORT	18. SECURITY CLASSIFICATION OF THIS PAGE	19. SECURITY CLASSIFICATION OF ABSTRACT	20. LIMITATION OF ABSTRACT
Unclassified	Unclassified	Unclassified	UL

NSN 7540-01-280-5500 **Standard Form 298 (Rev. 2-89)**
Prescribed by ANSI Std. 239-18

THIS PAGE INTENTIONALLY LEFT BLANK

Approved for public release; distribution is unlimited

PERFORMANCE OF A HIGH RESOLUTION DIAGNOSTIC MODEL FOR SHORT RANGE MESOSCALE WIND FORECAST IN COMPLEX TERRAIN

Shawn G. Gallaher
Lieutenant, United States Navy
B.S., University of North Carolina at Asheville, 1995

Submitted in partial fulfillment of the
requirements for the degree of

MASTER OF SCIENCE IN METEOROLOGY AND PHYSICAL OCEANOGRAPHY

from the

NAVAL POSTGRADUATE SCHOOL
September 2002

Author: Shawn G. Gallaher

Approved by: Douglas K. Miller, Thesis Advisor

Wendell A. Nuss, Second Reader

Carlyle H. Wash, Chairman
Department of Meteorology

THIS PAGE INTENTIONALLY LEFT BLANK

ABSTRACT

This study investigates the feasibility of using a high resolution simple diagnostic model (WOCSS) initialized from a coarser grid full physics prognostic model (COAMPS) to obtain mesoscale winds. This approach using COAMPS 81, 27, and 9 km forecast model soundings to initialize WOCSS at 3 km is compared to COAMPS forecast at 3km horizontal resolution alone. Four case studies were collected during various weather regimes in Central California. Observations were collected from 5 different agencies and were used for verification of the models. The sensitivity of various WOCSS parameters were also explored.

The results showed that overall the COAMPS(9km)/WOCSS approach provides winds as good as COAMPS at 3 km at a greatly reduced computation time. The COAMPS/WOCSS methodology performed particularly well during non-frontal situations where low-level inversions were present. Separation of the surface observation data by agency revealed large errors from data networks with low maintenance, monitoring and site specifications standards. The highest flow surface in WOCSS was the only parameter that displayed any significant sensitivity. Further work is needed to test the advantages of this sensitivity. COAMPS/WOCSS mesoscale forecast winds may prove to be very useful as input to emergency response applications such as dispersion and trajectory modeling.

THIS PAGE INTENTIONALLY LEFT BLANK

TABLE OF CONTENTS

LIST OF FIGURES

LIST OF TABLES

THIS PAGE INTENTIONALLY LEFT BLANK

ACKNOWLEDGEMENTS

I started this endeavor in October of 2001 and had no idea how challenging and rewarding the experience would be. Doug Miller's enthusiasm for knowledge and his patience with delivering that knowledge during this process will always be greatly appreciated. Not only is he a tremendous asset to the Meteorology Department at NPS, he is a great person as well. I would also like to thank Professor Wendell Nuss for access to his expertise in mesoscale meteorology and his time.

Every organization has that support person who is invaluable to the overall success of the system, in this Department that person is Bob Creasy. Bob is an incredible source of information, and is always willing to lend a helping hand. Special thanks to Mike Cook, Arlene Guest, Dick Lind and Mary Jordan for their assistance as well.

Not sure there is a more caring or understanding women in the world than my wife Rebecca. She unselfishly sacrificed her time to ensure all of life's little concerns were taken care of so I could focus on my work. Thank you so much for all you have done over the past twenty-seven months. Finally, to my mother who has always supported me in everything I've ever done, thank you.

THIS PAGE INTENTIONALLY LEFT BLANK

I. INTRODUCTION

A. HORIZONTAL RESOLUTION DILEMMA

Advances in computer technology during the 1990's sparked a revolution in the atmospheric numerical weather prediction (NWP) community. Ten years ago 80 kilometers (km) horizontal spacing was considered high resolution modeling. Today atmospheric mesoscale models routinely operate below 10 km resolution. The National Center for Environmental Prediction (NCEP) runs the ETA model at 12 km horizontal resolution for the entire United States and even 8 km resolution over selected domains. Fleet Numerical Meteorology and Oceanography Center runs the Coupled Ocean-Atmosphere Mesoscale Prediction System (COAMPS) at 9 km resolution over selected domains world-wide and the regional METOC Centers run COAMPS as low as 7 km. The Air Force runs the Penn State/NCAR Mesoscale Model version 5 (MM5) routinely below 10 km horizontal resolution worldwide.

Most of the energy and technology has been focused toward future reductions in horizontal resolution; secondary to this objective is the verification process. Does reduced horizontal grid spacing in mesoscale models add skill to the forecast? This question is a difficult one and cannot be answered with certainty. Recently, members of the University of Washington published the results of a verification study of the UW/MM5 model over western Washington State. The results showed promising wind, temperature and precipitation statistics when horizontal resolution was reduced from 36 km to 12 km, but minimal improvements from 12 km to 4km (Mass et al. 2002).

Today’s mesoscale models are non-hydrostatic full physics models; assumptions are made in the governing equations and model physics to simplify the calculations. At what horizontal resolution do these assumptions fail? At what spatial scale do mesoscale features become so random and short-lived that predictability is not possible?

B. SIMPLE DIAGNOSTIC MODELING APPROACH

How can future fine-scale three dimensional wind parameters be forecast by a diagnostic model? The approach is to take model forecast fields from a prognostic full dynamics NWP and initialize a simple terrain-following diagnostic model at high resolution. The advantages of this approach include faster product output times, high vertical resolution at the lower levels and avoiding violation of the simplifying assumptions of the full physics mesoscale models. A simple diagnostic model can run as much as 25 times faster than a full physics mesoscale model at similar horizontal resolution. Simple diagnostic models can tune vertical level distribution to capture only the lower levels of the atmosphere where dispersion model input winds are most vital.

The reduction in horizontal resolution by full physics models challenges the validity of parameterizations made for the Planetary Boundary Layer (PBL), clouds, radiation and surface energy. The diagnostic wind model used in this study, Winds Over Critical Streamline Surfaces (WOCSS), is only limited in horizontal resolution by the resolution of the topography data. WOCSS uses a Froude Number approach; under stable conditions the flow will tend to go around the

topography and for unstable conditions the flow is more likely to go over the topography.

C. MODEL VERIFICATION

Model verification is simply the comparison of model forecasts to the actual state of the atmosphere. Model verification is a difficult process due to multiple sources of errors. Most verification processes have a controlled environment whose parameters can be measured precisely and model outputs can be compared to these measurements. This situation allows the analyzer to concentrate on errors of the simulator. The atmosphere is an infinitely more difficult problem. The true state of the atmosphere cannot be truly known. Current measurement methods only give an estimation of the current state; therefore, the analyzer must concentrate on both observational and modeling errors.

Modeling errors are a function of the modeling process. Model dynamics and scale assumptions can lead to random and systematic errors even if the initial state were known exactly. The selection of horizontal and vertical resolutions create aliasing problems of micro and mesoscale processes whose feedbacks into the larger scales are misrepresented. The misrepresentation of real topography by the simulating model smooth through the model topography causing valleys to be higher and mountain ridges to be lower due to elevation averaging and/or silhouette matching. This leads to errors in thermal gradients both vertically and horizontally (Monterrosa 1999). Barriers or the lack of barriers often times exist in the model that are not present in the real topography preventing flow

channeling and blocking from being represented properly. Kuypers (2000) found that errors in the mesoscale model boundary conditions were a major factor in the propagation of errors through the forecast as well.

Errors associated with the model itself could be more easily solved if the initial and final conditions of the atmosphere were known, but they are not. Observational errors exist in four forms. The first source of error comes from equipment systematic errors. These errors can be reduced by quality maintenance schedules and daily monitoring. The second source involves sensor location and set-up. Anemometers located in sheltered areas tend to have wind speed and direction biases. Some observation sites are controlled by different agencies creating non-uniform sensor heights above ground level (AGL) and non-uniform quality standards. The next source of error results from station positioning. Most agencies deliver site position information to an accuracy of 0.01 or 0.001 of a degree (Latitude or Longitude). Rounding errors can create position errors in the 100 meter to 1 kilometer range. These errors can make a tremendous difference in high horizontal resolution models when interpolating the model fields to the observation site position, particularly in regions having large variations in terrain elevation. The observation network itself is a source of errors for the model initialization process, as well as, the model verification process. The site density of an observation network may not be able to resolve mesoscale features the modeler is trying to simulate, making it difficult to verify model output to these observations (Perkey 1986).

D. DIRECT DEPARTMENT OF DEFENSE APPLICATIONS

Why does the Navy need mesoscale model output products? The Navy has billions of dollars in assets dispersed around the globe delivering a forward presence in protection of United States and United Nations interests. This exposes Naval Units to many different types of local weather regimes. These local weather phenomena affect the physical material condition of vessels and aircraft through damage due to high winds and seas. Combat success can rely heavily on skillful local forecasts for such operations as amphibious landings, flight operations, target area conditions and tactical decision aid inputs.

The primary customers of the results of this study are members of the Emergency Response community. Since the events of September 11, 2001 a strong emphasis has been placed on dispersion model technology for chemical, biological and radiation (CBR) agents. The success of dispersion and trajectory model output, such as HPAC, VLSTRAC and HYSPLIT, depend heavily on NWP wind fields. The dispersion modeling of CBR agents requires high resolution three dimensional wind vectors, near real-time availability and increased vertical level sampling of the lower atmosphere (levels beneath 2500m). The diagnostic wind modeling approach, using COAMPS/WOCSS, can provide all the above for a short range forecast in complex topography. This study should reveal to what level of skill this approach can provide the required output.

E. HYPOTHESIS

The common misconception is that higher horizontal resolution full physics models always provide better mesoscale forecasts. Mesoscale models are attempting to sample sub-mesoscale and microscale processes whose behaviors and time scales are not fully understood or observed. Time and spatial predictability limits decrease as model horizontal resolution increases. Time predictability limits of atmospheric models depend heavily on the accuracy of the measurement of initial state (Lorenz 1982). Department of Defense Forces normally operate in regions that have unreliable or even absent observation networks. The military cannot depend on mesoscale forecasts that are dependent on the initial in situ measurements.

We hypothesize using the mesoscale model/WOCSS approach may be as useful or more useful at high resolutions for two reasons:

1) Significantly reduced computation time
2) This approach is less prone to problems arising from violating the simplifying assumptions of full physics mesoscale models.

F. OBJECTIVES

The goal of this research is to examine the possible benefits of using a simple diagnostic model at high resolutions initialized from a coarser resolution full physics mesoscale model (COAMPS). This study will verify WOCSS 3 km resolution wind fields initialized from cold

starts of COAMPS at 81km, 27km and 9km horizontal resolution for four case studies. COAMPS will also be run at 3km resolution for comparison to each of the WOCSS 3km resolution wind fields. A statistical analysis will be run on each of the case study control runs for evaluation of forecast skill. A series of non-control experiments will be run on the WOCSS model in an attempt to improve model output. The verification process will be to compare interpolated model output fields to a fairly dense observation network located in the Central California Coastal region.

This research will attempt to answer the following question. Can WOCSS, run at 3km horizontal resolution and initialized from coarser resolution COAMPS fields, provide as good or better short range wind forecast as COAMPS run at 3km horizontal resolution?

Section II will provide background on the state of the art, as well as, information about the domain characteristics and observation network. Section III will describe the characteristics of the models used in this study. The methods used for collection of data and statistical analysis will be provided in Section IV. A discussion of the synoptic and mesoscale weather regimes present during each of the four case studies will be described in Section V. Section VI will discuss the results of both the control and experimental model outputs. Finally, Section VII will provide the findings and a possible future work on the subject.

THIS PAGE INTENTIONALLY LEFT BLANK

II. BACKGROUND

A. STATE OF THE ART

The primary users of diagnostic models have traditionally been members of the air quality management community. The general methodology is to input observations from the domain of interest directly into the diagnostic model. These observations are input into the diagnostic model through objective analysis techniques that weight the observations according to their distance from each other. There are obvious advantages to using diagnostic models, particularly in areas of complex terrain. Diagnostic models are typically equipped with simple governing equations for mass conservation in variable local topography (Sherman 1978). The simple approach allows modelers to run multiply-nested models with high horizontal resolutions over a fairly large domain. The model output is then placed into dispersion models where statistical algorithms and dispersion theory dynamics are calculated and displayed (Lange 1978). Industrial facilities, air quality managers, as well as local, state and government emergency response facilities used this approach to evaluate plumes generated by the intentional or unintentional release of toxic or radioactive material. This method provides reasonable nowcast results after an unexpected spill (Fast et al. 1995).

The use of a diagnostic model generated from local observations, although simple and fast, has several shortfalls. Observation network density may represent surface features sufficiently, but the lack of vertical

information greatly degrades the value of model simulated structures. This approach also assumes local observations are available in the domain of interest, not a good assumption for military emergency response in data-denied areas. The most current observations drive the diagnostic model, therefore model results only remain valuable while the atmospheric structure is similar to the initial state; this can be hours or minutes depending on variability (Cox et al. 1998). The greatest limitation to observationally driven diagnostic modeling is the inability to capture complex dynamic features that cannot be measured by the observations (slope flows, sea breezes, low-level jets, etc.) and the changes in these features with time (Fast et al. 1995).

Advancements in NWP have turned the focus more toward future estimates of continuous or anticipated spills using prognostic mesoscale models. Williams and Yamada (1990) used the HOTMAC-RAPTAD system at Tooele Army Depot experimenting with using high resolution mesoscale models as direct inputs into dispersion models for emergency response applications. Fast et al. (1995) and Poulos and Bossert (1995) also experimented with this approach using the RAMS/LPDM system to simulate the transport and deposition of chemical and radiological byproducts from industrial sites. The overwhelming drawback of this method is the enormous computational power required to run high horizontal and vertical resolution full physics models. Emergency response requires fast output products in order to be effective. Several techniques are incorporated to reduce computation time such as reducing model domain size

significantly and/or computing fewer vertical levels, which lowers capability and effectiveness.

Another disadvantage is the difficulty of capturing the correct phase timing associated with thermally induced mesoscale features in the full physics models. Although increased variability of the atmosphere is simulated, the exact location and magnitude of the phenomena are misrepresented, leading to large local errors (Poulos and Bossert 1995).

The final disadvantage is that the parameterizations used to estimate PBL, cloud, soil moisture and radiative processes become oversimplified at high horizontal resolutions. Arakawa and Chen (1987) stated that closure assumptions of cloud parameterizations must not sacrifice the predictability of resolvable-scale fields and that they be observationally verifiable. Model resolutions below 5 km begin to violate these assumptions since individual cloud elements are being resolved by the horizontal grid with no way to verify the processes. Traditional cloud parameterizations begin to break down at 20-25 km resolution. Explicit and hybrid parameterizations provide reasonable results below these resolutions but have had inconclusive results for resolutions higher than 5-10 km (Molinari and Dudek 1992).

The method pursued in this study takes advantage of the positive aspects of each approach mentioned above. This method employs a high horizontal resolution diagnostic model (WOCSS) initialized by the forecast fields of a coarser resolution prognostic mesoscale model (COAMPS). The diagnostic model outputs can then be relayed to an

emergency response dispersion model for plume display. This study only investigates the performance of mesoscale wind fields produced by the COAMPS/WOCSS approach, not the dispersion model results. Running the mesoscale model at coarser resolutions (9, 27, 81 km) leaves the model results less subject to the constraints mentioned above, such as model parameterizations and phase timing errors. The diagnostic model then receives vertical stability information from the mesoscale model and adjusts flow to higher resolution topography. The obvious advantage of this method is speed. Due to the simple calculations in the diagnostic model, domain size and vertical level distribution can be expanded. The flow can be adjusted to the finest horizontal resolution terrain data set available. The most significant disadvantage is the inability of diagnostic models to form small-scale mesoscale structures not related to local topographic effects. Mesoscale models operating below 5 km horizontal resolution have formed small-scale mesoscale structures, but the output is often not operationally useful due to the errors in magnitude, location and translation of these structures.

Mohammed (2000) conducted an experiment similar to this study using the MM5 mesoscale model and WOCSS diagnostic model. He compared high-density observations from the 1997 Southern California Ozone Study to MM5 wind fields at 81, 27, 9, 3 km grid spacing and WOCSS (run at 3 km grid spacing) initialized by MM5 9 km. The results showed that WOCSS wind speeds performed better and that wind directions performed just as well as MM5 at 3km resolution. These results are encouraging since the

MM5(9km)/WOCSS(3km) method provided as good or better wind forecast than MM5 (3km) while conserving considerable computational resources. Although this study and the work of Mohammed seek the same goal, this research is different in many ways. The study will be using the Navy's COAMPS mesoscale model instead of MM5. The domain will be located over Central California as opposed to Southern California. This study explores results from four different case studies containing different weather regimes and seasonal variations. The final difference is the experimentation of the sensitivity of WOCSS parameters and its effects on model output in this thesis.

B. DESCRIPTION OF MODEL DOMAIN

The model domain is located in Coastal Central California centered around San Jose. The domain extends as far south as Big Sur, as far north as Santa Rosa (70 km north of San Francisco Bay), as far east as Los Banos and approximately 120 km offshore to the west. The bottom left-hand coordinate starts at 36.23N and 123.73W and the top right hand coordinate ends at 38.48N and 120.88W (Figure 1). The verification domain dimensions are 273 km by 273 km and the highest level in WOCSS is 2500 meters (COAMPS model top was 20 km).

The terrain elevation varies from sea level near the coast to 1300 meters along the Coastal and Santa Cruz Mountains ranges. There are two major valleys in the region, the Santa Clara and Salinas Valleys (Figure 1). The Santa Clara Valley runs northwest to southeast from the San Francisco Bay to Gilroy. The Salinas Valley also runs

northwest to southeast linking Monterey Bay at Marina to the 101 corridor down to King city and Southern California.

The topography is extremely complex in this region giving way to multiple microclimates. Winds are channeled through mountain passes and valleys forced by the prevailing weather regimes. Weather regimes in this region are best described as a Mediterranean climate (Null 1995). This type of climate has a wet season and a dry season separated by short transition periods. The dry season normally begins in late Spring and continues until October. The East Pacific (EASTPAC) High is the primary synoptic feature during this time. Strong coastal northwest winds drive Ekman transport along the coast forcing surface waters offshore allowing cold deep water to flow to the surface. Strong subsidence from the EASTPAC High, coupled with the cool ocean surface temperatures, creates a very stable marine layer resulting in fog and stratus in the coastal areas. The interior valleys warm quickly during the day creating a significant thermal gradient between the coast and central valleys. A strong sea breeze develops advecting marine air into valleys linked to the coast.

The wet season begins in November and lasts until March. The EASTPAC High weakens and recedes further south allowing the Polar Jet to slide further southward and bring the storm track into Central California. Occluded low pressure systems from the North Pacific and cold fronts from the Gulf of Alaska make up the majority of precipitation events. Unstable post-frontal air can also develop thunderstorms over the ocean that translate over the coastal and central valley areas. The wet season makes

up over 80% of the annual precipitation in this region. The transition seasons, spring and fall, are marked by clear skies and warm temperatures. The EASTPAC High pressure is still not established during these seasons allowing the Southern California Thermal Low to provide offshore flow (Null 1995; Miller 1996).

C. DESCRIPTION OF OBSERVATION NETWORK

The observation network used in this study consists of 58 surface data sites, 4 vertical profilers and 1 vertical sounding (Figure 2). The network is a collection of data from five different agencies: National Oceanic and Atmospheric Administration (NOAA), Bay Area Air Quality Management District (BAAQMD), Monterey Bay Aquarium Research Institute (MBARI), Naval Postgraduate School (NPS) and California Department of Forestry (CDF). NOAA is considered the most reliable of the five agencies due to rigid maintenance, monitoring, reporting and site specification standards. The National Weather Service (NWS) San Francisco Bay/Monterey located in Monterey provides all NOAA surface stations data as well as data from the Richmond Profiler. The NOAA surface observations in this study were obtained by the Automated Surface Observation System (ASOS), which are located at various positions listed in Table 1. The Tomasini Point surface site is also maintained by NOAA but monitored and reported by the California-Nevada River Forecast Center (CNRFC) in Sacramento. NOAA observations are located near the population areas they support, therefore most sites reside in lower elevation valleys. Four of the offshore buoys

used in this study are also maintained by NOAA but data collection, monitoring and reporting are conducted by the National Data Buoy Center (NDBC) located in Mississippi.

The remaining observation sites are collected and distributed via the Bay Area Mesoscale Initiative (BAMI) effort. BAMI data are collected from government, state and local agencies as well as Bay area universities (Baskett et al. 1998). The purpose of this initiative was to provide real-time mesoscale monitoring system for research and air quality applications. This network provides observational data in both urban and rural locations. The CDF sites provide most of the high elevation observation data through Remote Automated Weather Systems (RAWS). Table 2 provides a list of BAMI site details.

The only available observations above 10 meters above ground level (AGL) is provided by the four wind profilers and the sounding at Oakland, hereafter referred to as OAKU. The sounding data is taken twice a day providing wind and temperature data for the entire column of atmosphere above Oakland. All four profilers are Ultra High Frequency (UHF) lower tropospheric profilers operating at 915 Megahertz (MHz) that are normally referred to as boundary layer radar wind profilers. These devices use Doppler technology similar to sodar, but instead of using acoustic signals they use electromagnetic (EM) signals to remotely sense winds aloft. The profilers have five beam angles, one directly vertical and the other four are tilted slightly off vertical exactly 90° from one another. The basic principle of operation is an EM pulse is emitted from the transmitter. Fractional amounts of this energy are

backscattered from the clear air small-scale turbulent fluctuations in the boundary layer, creating gradients in the radio refractive index, back to the receiver. The signal processing unit determines the Doppler frequency shift that occurs between the original and final signal states. This information allows the processor to compute wind velocities to and from the profiler. To eliminate turbulent or spurious data, the processor uses a technique referred to as consensus averaging over time (~25 minutes). Range gates are set up in the data processor to allow scattered EM energy to arrive only from select altitudes. (WebMET 2002). The four profilers and their locations are given in Table 3. Profiler observations are collected over four layers (Table 4). These particular layers were collected to obtain vertical data near 975, 950, 900 and 850 millibars.

All observation site locations, except for the Spring Valley CDF site (Temperature only) and the profilers (Wind direction and speed), provide temperature, wind speed and wind direction data for the four case studies in this research. Surface observation sites collect wind data at 10 meters above ground level (AGL), except for the CDF sites (7 meters AGL). Some case studies may be missing certain locations due to mechanical failure or data retrieval problems. Precision and maintenance data is provided for each agency on Table 5.

THIS PAGE INTENSIONALLY LEFT BLANK

III. MODEL DESCRIPTION

A. COUPLED OCEAN-ATMOSPHERE MESOSCALE PREDICTION SYSTEM

The Coupled Ocean-Atmosphere Mesoscale Prediction System (COAMPS), developed by Naval Research Laboratory, is a nonhydrostatic mesoscale model with a sophisticated atmospheric data assimilation system and an optional hydrostatic ocean model. COAMPS uses the nonhydrostatic, compressible form of the primitive equations and parameterizations for subgrid-scale mixing, surface fluxes, explicit moist physics, cumulus convective and radiation processes (Hodur 1997). The vertical levels are user-determined and in σ-coordinates. This study used COAMPS with 47 vertical levels. COAMPS also has user-specified horizontal resolution (limited to 3:1 reduction in grid spacing when nesting). The initial and lateral boundary conditions are derived from a global model or the first guess fields of a coarser grid COAMPS. COAMPS can operate in one or two-way nesting mode. Model topography is bilinearly interpolated to the model grid from Level 1 Defense Mapping Agency (DMA) Digital Terrain Elevation Database (DTED) (100-meter resolution). The model grid projection is specified and each model gridpoint is attached to a latitude and longitude, which allows the domain to be globally relocatable with several projection options (Hodur 1997). The ocean model is a barotropic model using incompressible, hydrostatic dynamics, but is not currently operational in COAMPS. COAMPS can be operated in stand alone (atmospheric model only) or coupled

mode (atmospheric and ocean model). This study uses COAMPS in stand alone mode.

COAMPS also contains an advanced atmospheric data assimilation system consisting of data quality control, analysis and initialization. The quality control (QC) algorithms in COAMPS check observational data for redundancy, exceedance of climatological limits, hydrostatic consistency and vertical wind shear, wind speed, and direction in soundings, and check radiosondes against first guess and neighboring observations and ship positions relative to their last report (Baker 1992; Hodur 1997).

The multivariate optimum interpolation (MVOI) analysis technique, developed by Lorenc (1986), uses a volume method based on observation density that produces a separate analysis for each nested grid. Observed winds, heights and thicknesses are obtained from radiosondes, pibals, air reports (AIREPS), Aircraft Communication Addressing and Reporting System (ACARS), Special Sensor Microwave Imager (SSM/I), surface, cloud track winds, Defense Meteorological Satellite Program (DMSP) and NOAA satellites. This data is interpolated to 16 pressure levels from 1000 to 10 mb on a full or incremental update cycle. Following this step the model is initialized ensuring that the perturbation pressure gradient is in hydrostatic balance with the buoyancy term to prevent spurious high frequency oscillations (Hodur 1997).

Recent experimental studies have verified COAMPS usefulness as a mesoscale model. Doyle (1997) concluded that COAMPS is capable of successfully simulating and

predicting topographically forced complex flows in littoral zones. Thompson et al. (1997) also commented that the COAMPS model performed well reproducing the dynamics of boundary layer coastally trapped waves along the California coast.

B. WINDS OVER CRITICAL STREAMLINE SURFACES

Winds Over Critical Streamline Surfaces (WOCSS) is a diagnostic model that interpolates observed or model wind and temperature parameters to produce three dimensional, mass-conserving wind fields adjusted to local topography. The concept is based on a wind-energy model of Bhumralkar et al. (1980) using a variational calculus numerical scheme. Endlich (1984) replaced the variational calculus numerical scheme for removal of divergence with a iterative technique developed earlier (Endlich 1967). He also applied a special coordinate system that intersects the terrain because normal sigma (σ) coordinates have failed to reproduce the flow around topography simulated in field studies.

Ludwig et al. (1991) also used the principle of critical dividing streamlines to develop his flow surfaces. The critical dividing streamlines approach assumes that the height an air parcel is displaced vertically, in complex terrain, is a balance between the original kinetic energy of the flow and the buoyant restoring force (Sheppard 1956; Hunt and Snyder 1980; McNider et al. 1984). Using this approach, Ludwig employed the following relationship to generate the maximum slopes possible in the flow surfaces near terrain in WOCSS:

$$Z_{\max} - z_o = V_o \left(\frac{d\theta}{dz} \frac{g}{\overline{T}} \right)^{-1/2} \qquad (1)$$

where $Z_{\max}$ is the greatest height that air at height z_o can be lifted, given local wind speed (V_o), against the local potential temperature gradient $d\theta/dz$. The mean temperature of the layer is represented by $\overline{T}$ and the gravitational constant is g.

These surfaces, illustrated in Figure 3, are meant to approximate the flow in complex terrain in WOCSS. This relationship assumes that $d\theta/dz$ > 0 and atmospheric processes are quasi-adiabatic. WOCSS uses a critical dividing streamline concept to simplify the three dimensional wind field solution by treating it as several two dimensional problems (surfaces). Figure 3 shows how the flow surfaces are not σ or z surfaces, but more like a hybrid between the two. The flow surfaces intersect the terrain where the flow does not have enough energy to overcome the obstacle and vertical stability. Separation of these flow surfaces (Δz) are variable from place to place in the model, therefore the mass fluxes must be adjusted to nondivergence. Endlich et al. (1982), used mass flux variables represented in equation:

$$u' = u\Delta z$$

$$v' = v\Delta z \qquad (2)$$

to replace the horizontal wind component variables in the continuity equation:

$$\frac{du'}{dx} + \frac{dv'}{dy} = 0 \qquad (3)$$

The divergence is set to zero at terrain intersections and the iterative scheme mentioned earlier adjusts the flow toward two-dimensional nondivergence to satisfy Equation (3) and force flow around the obstacle.

A WOCSS verification study conducted in the summer and fall of 1987 using observational data from the Southern California Air Quality Study (SCAQS) revealed some weaknesses in the WOCSS model performance. Ludwig et al. (1991) discovered that the terrain-following treatment of flow in WOCSS for neutral and unstable conditions was not realistic. Another weakness was the residual divergence that remained in the model analysis. This becomes a problem for representing mesoscale features that recirculate such as sea breeze fronts. Thykier-Nielsen et al. (1990) also performed experiments with WOCSS at Vandenberg Air Force Base that showed WOCSS did not perform as well during neutral and unstable lapse rates as it did with stable lapse rates. This study did report that overall WOCSS did outperform the Troen and de Baas (1986) model that used spectral solution of linearized equations of motion.

Ludwig and Sinton (2000) evaluated WOCSS against long-term surface observations in the San Francisco Bay area from 1996. The results showed root mean square errors (RMSE) of less than 45° for wind direction and 2.5 m/s for wind speed. These findings were encouraging, but several weaknesses were discovered. WOCSS tended to underestimate maximum wind events and gap flows. The model also had problems reproducing the split flow that occurs in San Francisco Bay. Mohammed (2000), using model gridded data

for initialization of WOCSS as opposed to actual observations, also found that WOCSS exhibited a low wind speed bias compared both to observations and to the mesoscale model providing the initial gridded data.

Recently, Ludwig (personal communications) has included output from the vertical momentum component (Equation 4) in his most recent version of the WOCSS code.

$$w = v \bullet \nabla z_{sfc} \tag{4}$$

Ludwig et al.(1991) and Ludwig and Sinton (2000) address several changes that could be made to possibly improve WOCSS performance. The first recommendation was to adjust the model upper boundary according to the height of the elevated inversion in order to capture damping effects of the inversion near terrain. The second recommendation was to adjust compression of the flow surfaces according to vertical stability. A parameter in WOCSS, known as the compression factor, can be adjusted to best represent flow during different stability conditions. The compression factor can best be described as the maximum fraction by which the initial separation between two surfaces can be reduced in a less stable lower layer (Ludwig and Sinton 2000). This value falls between zero, representing a very stable lower layer (terrain following flow), and one, which represents the case of an unstable lower layer (flow over terrain). The model default for compression factor is 0.1. Figure 3 gives an illustration of the changes to the flow surfaces for a given compression factor.

The final recommendation discussed removing residual divergence from the model that tended to misrepresent mesoscale features that recirculate through the model

(Ludwig et al. 1991). The removal of divergence by the model is performed through the Endlich (1984) iterative scheme and the default is currently set to 20 iterations. Removal of the residual divergence may also improve WOCSS's low wind bias and gap flow. This study will address all of these recommendations and well as explore other model configurations in an attempt to improve WOCSS wind solutions.

THIS PAGE INTENTIONALLY LEFT BLANK

IV. METHODS

A. CASE STUDY COLLECTION

There were thirteen case studies collected between November 28, 2001 and May 9, 2002 of significant wind (mean wind speed >5 m/s averaged over forecast period) events on the Central Coast. Four of the thirteen cases were selected for verification purposes based on two criteria: 1) the ability of the large area model to capture the synoptic situation and 2) completeness of model and observation data collected. The first two cases (11/28/01 and 12/20/01) are frontal cases with high spatial and temporal variability in wind, temperature and stability. The last two cases (03/13/02 and 05/09/02) are non-frontal gradient winds with lower spatial and temporal variability in these parameters. A complete discussion of synoptic and mesoscale forcing mechanisms involved in each of these case studies are presented in Chapter V.

There are two different types of data to be collected for model verification studies. The first one is model data to provide initial and lateral boundary conditions for the internally nested domains (model nesting is explained in the next section). It is important that the outer nest model capture the synoptic situation as accurately as possible, so three large area models, NOGAPS (1 degree), ETA (22 km), and AVN (2.5 degree) were collected for each case. The ETA model verified the best for each of the four case studies and was the model used to provide outer nest and initial condition information to the COAMPS inner domains.

The second type of data to be collected is available observations, both surface and boundary layer. The surface, profiler and sounding data were collected from the agencies mentioned in Chapter II C via dial-up or FTP connection and automated scripts. Irregularities in reporting times, particularly CDF observations, by some of the agencies created errors or missing data. This missing data was retrieved through the Mesowest Archive website. This website collects observation data from 65 different agencies and disseminates it to the public domain via the web. This data is provided in near real-time and can also provide archive data from as far back as 1997. Horel et al. (2002) provides an in depth overview of the MesoWest collection, quality control and dissemination process. Retrieval of surface data from the MesoWest Archives increased data completeness by 20%. The remaining missing data was simply unavailable.

B. MODELING METHODOLOGY

The model nesting technique is used to provide information from the large area model (ETA in this case) to the inner nests of COAMPS at 81km, 27km, 9km and 3km horizontal resolutions. Figure 4 shows the domain coverage and nesting arrangement for each of the COAMPS resolutions. This arrangement can be set up into two-way or one-way nesting. The one-way method allows synoptic features in the large area model to influence mesoscale features in the smaller area mesoscale models. The two-way method allows one-way processes as well as allowing interactions in the inner nest mesoscale models to influence synoptic features

in the large area model. This study uses the one-way nesting technique.

The inner model nest can be initialized in one of two ways, warm or cold start. Warm start uses the mesoscale model forecast grid fields (F03, F06, etc.) of the limited area model to initialize and update lateral boundary conditions. The advantage of this is nested mesoscale models do not have to “spin-up” mesoscale features because they are already present in the first guess data. The disadvantage of this method is errors present in the first guess fields are propagated through the mesoscale forecast if there are insufficient observations to correct for these errors (Monterrosa 1999).

Cold start uses the large area model (F00) fields to initialize the mesoscale model instead of the warm start method of using mesoscale model forecast fields. The advantage of this approach is the elimination of any errors associated with mesoscale features from a previous model forecasts. The disadvantage of this method involves the early forecast period spin-up that can take up to 6 hours to complete in the mesoscale models.

The study uses a modified cold start method for a 36-hour forecast. The modification is the blending of observation data into the ETA analysis used to initialize the inner nests of COAMPS. The blended analysis is then used to initialize the COAMPS 81, 27, 9, 3 kilometer domains using 2-D multiquadric interpolation (Nuss and Titley 1994). The lateral boundary conditions are updated from ETA model analysis fields every 6 hours. This is done to minimize errors discussed by Kuypers (2000) associated

with synoptic feature propagation entering the boundaries of the inner nests. Mesoscale features developed in the COAMPS 81 km domain are updated to the 27, 9, 3 km domains and 27 km mesoscale features are updated to the 9 and 3 km and so on.

The WOCSS model was initialized from the COAMPS 81, 27 and 9 km forecast grids using the following technique. The COAMPS model forecast "observations" are input into WOCSS at COAMPS grid point locations. The flow is then adjusted by WOCSS to reflect local changes in terrain elevation and force the winds toward horizontal non-divergence and output on the WOCSS grid.

C. DATA ANALYSIS

To evaluate the performance of the various model configurations involved in this study, statistical tools were enlisted to rate model skill. These tools were used to compare COAMPS/WOCSS 3 kilometer winds, bilinearly interpolated to observation locations. COAMPS wind forecasts for all four nested grids were also compared to observations to determine how COAMPS/WOCSS performed against COAMPS alone.

The mean of the data represents the total average magnitude or direction of the entire data set and is defined as:

$$\bar{x} = \frac{1}{n}\sum_{i=1}^{n} x_i = \frac{x_1 + x_2 + \ldots + x_n}{n} \qquad (5)$$

where $x_1 + x_2 + \ldots + x_n$ represents the sum of n observations. The mean is useful in determining the prevailing wind direction

over the domain as well as the general strength of the atmospheric forcing.

The second statistical tool is the standard deviation (STD) which measures the variability of the data around the mean. The standard deviation represents the range over which approximately 68% of the data falls within. The following equation is used to calculate the standard deviation:

$$x = \sqrt{\frac{1}{n}\sum_{i=1}^{n}(x_i - \bar{x})^2} \tag{6}$$

where x_i is each observation and $\bar{x}$ is the mean of all the observations.

Root mean square error (RMSE) is simply the mean positive difference between the simulated and observed result. The RMSE parameter is represented mathematically as:

$$RMSE = \sqrt{\frac{1}{n}\sum_{i=1}^{n}(x_{m,i} - x_{o,i})^2} \tag{7}$$

where, for this study, $x_{m,i}$ represents model data and $x_{o,i}$ is observation data.

The final statistical measure is the bias. The bias can best be described as the average difference between the model and observation. This tool is useful in determining if the model over-forecasted (positive), or under-forecasted (negative) a parameter. The bias is represented as:

$$Bias = \frac{1}{n}\sum_{i=1}^{n}(x_{m,i} - x_{o,i}) \tag{8}$$

where $x_{m,i}$ and $x_{o,i}$ represent model and observation parameters respectively.

V. SYNOPTIC DISCUSSION

The following discussion describes the synoptic conditions during the time of the case studies to provide the reader with an understanding of the weather elements involved. Figures used to illustrate the conditions were retrieved from the ETA model fields displayed in the Gempak Analysis Rendering Program (GARP). The date and time were consolidated to save space in the following format, ddmmmyy hhZ (i.e. 28NOV01 00Z). The ETA analysis was used for the figures to be discussed, except for the 21DEC01 00Z time period because the analysis was not available. The 6-hour forecast from the 20DEC01 18Z analysis was used in its place.

The case studies were divided into two categories; frontal and non-frontal. The 28NOV01 and the 20DEC01 cases are considered frontal cases and present the greatest challenge to numerical forecasting. This challenge is due in part to the requirement of the model to correctly capture the frontal propagation speed. The 13MAR02 and 09MAY02 cases are the non-frontal cases. These cases are less challenging than the frontal cases but still present thermally induced mesoscale processes that are difficult to model.

A. 28 NOVEMBER 2001 CASE STUDY

This case study is the first of the frontal cases presented in this study and covers the 28NOV01 00Z to 29NOV01 12Z time period. Figure 5 shows meridional flow over California in the 500mb height fields for 28NOV01 00Z.

Central California is under the influence of an upper-level ridge with a strong long-wave trough approaching from the Northern Pacific. The trough has two absolute vorticity maxima associated with it, one is located over the interior of the nearly closed 5400 meters contour and the other is located near the base of the trough. A strong 160 knots (plus) jet streak at 300 mb exists (not shown) from the base of 500 mb trough to the top of the ridge located downstream.

A 986 mb surface low pressure system, seen in Figure 6, is located beneath the left front exit region of the 300 mb jet streak helping develop that system. The surface low has a well organized frontal system seen by the strong packing of the 850 mb equivalent potential temperature (ThetaE) gradients contoured on Figure 6. Cold and warm frontal placement is on the warm sides of the 850 mb ThetaE packing. The front is occluded from the center of the low pressure southeast to 45N 135W. Central California is located in a Col area during this time providing weak and variable surface winds. Data from Figure 7 of the Oakland sounding shows an unstable boundary layer up to 500 meters, neutral from 500-1500 meters sealed by a weak inversion at 1500 meters.

Twenty-four hours later, 29NOV01 00Z, the 500mb trough is now located off the Pacific Northwest coast maintaining two distinct absolute vorticity maxima (Figure 8). The jet streak has weakened considerably (<120 knots) but the surface low, now located off the Washington Coast, has deepened to 978 mb. The surface low pressure has receded further into the cold air and the occlusion now stretches

from the center of the low southward to Central California (Figure 9). Strong prefrontal winds now dominate the Central Coast as the frontal systems makes landfall. Observed winds vary between less than 5 knots and variable at 28NOV01 00Z, to 15-35 knots and southerly from 29NOV01 00Z to 29NOV01 06Z and back to moderate and southwesterly at 29NOV01 12Z. This case varies widely in wind magnitude and direction over the 36-h period. The Oakland sounding for this time period shows a conditionally unstable boundary layer up to 1500 meters and a warm frontal inversion above 1500 meters (Figure 10).

B. 20 DECEMBER 2001 CASE STUDY

This case is the second of the two frontal case studies covering the time between 20DEC01 00Z to 21DEC01 12Z. This situation shows Central California under the influence of moderate prefrontal southwest flow. Figure 11 illustrates the position of the front and surface low pressure. Figure 12 displays the large absolute vorticity maximum in the center of the 5400 meters contour. The Polar Jet, at approximately 300 mb (not shown), has begun to split into a northerly and southerly branch around the 500 mb trough. The symmetry of the 500 mb vorticity maximum, the collocation of the surface and 500 mb lows, and the branching of the Polar Jet indicate that the low pressure system is becoming barotropic in structure. The Central Coast sounding from Oakland for this time period (see Figure 13) shows a neutral boundary layer to 1000 meters capped by a moderate inversion.

The next 24 hours indicates that the low pressure system has cut-off and lost most of its frontal structure by 21DEC01 00Z (see ThetaE packing in Figure 14). The upper-level low, seen in Figure 15, and the surface low pressure systems are stacked vertically and the low has filled to 1002 mb. This low passes directly over the inner model domain of WOCSS and supplies 10-20 knot winds from the south by 21DEC01 00Z. The last 12 hours of the forecast period (21DEC01 00Z-12Z) has a large amount of variability in space and time as the low pressure system moves through the inner model domain. Easterly flow is observed in the northern portions of the domain and southwesterly flow in the southern portions. Figure 16 is the Oakland sounding at 21DEC01 00Z and shows neutral to conditionally unstable conditions beneath 2500 meters and a moist atmosphere.

C. 13 MARCH 2002 CASE STUDY

This case is the first of two non-frontal cases where the wind direction and magnitude tend to vary less than frontal cases and it covers the weather conditions from 12Z 13MAR02 to 00Z 15MAR02. The synoptic situation at 12Z 13MAR02 is dominated by two features, one is the EASTPAC High Pressure and the other is low pressure on the lee of the Sierra Nevada mountain range. An unseasonably strong ridge over the eastern Pacific supports a 1040 mb EASTPAC high pressure circulation (See Figures 17 and 18). The 500 mb trough located over Northern California supports a 1008 mb low over Southern Nevada which creates a strong gradient over Central California. The winds at 12Z are 5-10 knots

out of the north-northwest but increase to 10-25 knots through the day of the 13th. The 12Z sounding (Figure 19) shows a dry adiabatic lapse rate in the boundary layer during this time.

The 12Z 14MAR02 charts show the 500 mb trough now covers the entire western U.S. and the surface low pressure system has intensified on the lee side of the Rockies and has deepened to 993 mb (Figure 20 and 21). A short-wave trough in the Northern Pacific has intensified the downstream ridge moving the EASTPAC High closer to West Coast. The combination of the intensifying low and the eastward movement of the EASTPAC High provides continued sustained 10-20 knot northwesterly winds for the remainder of the forecast period. The Oakland sounding once again shows a dry adiabatic lapse rate in the boundary layer due to mixing, and the intrusion of the 500 mb ridge (Figure 22).

D. 9 MAY 2002 CASE STUDY

The final case study is also a non-frontal case and covers the time period from 00Z 09MAY02 to 12Z 10MAY02. The 500 mb analysis at 09MAY02 00Z shows the Pacific ridge extending all the way up into the Gulf of Alaska and is part of a persistent blocking pattern (Figure 23). A cut-off low located beneath the ridge has been stationary or regressing westward over the past several days. Figure 23 also shows a short-wave trough entering the Pacific Northwest and is supporting an inverted trough seen in the sea level pressure fields along the Sierra Nevada and Cascade Mountain Ranges (Figure 24). The orientation of

the inverted trough and the position of the EASTPAC High Pressure system produce northwest winds at 10-20 knots along the Central Coast. The 00Z Skew-T from Oakland shows a dry stable boundary layer (Figure 25).

The 00Z 10MAY02 charts show the 500 mb short-wave dropping down into Northern California supporting a developing low pressure system in Southern Nevada (Figure 26 and 27). The inverted trough gives way to a closed cyclonic circulation with the Central Coast wedged between the Nevada Low and the EASTPAC High. This pressure gradient orientation allows 10-20 knot winds from the northwest to continue similar to the earlier forecast hours. The Oakland sounding during this analysis period shows a very unstable surface and adiabatic boundary layer capped by a strong subsidence inversion at 500 m from the EASTPAC High (Figure 28).

VI. RESULTS

A. MODEL PERFORMANCE - CONTROL

This section addresses the overall performance of the WOCSS (control settings) and COAMPS models verses wind observations, as well as, significant biases and trends in the data. COAMPS was cold-started for all cases therefore all data comparisons prior to the 6-hr forecast are deleted to allow the model to spin-up mesoscale structures. Wind direction observations associated with wind speeds less than 2.5 m/s were removed due to the variability in wind direction during these conditions. The COAMPS 3km, 9km, 27km and 81km domains will be referred to as coa3k, coa9k, coa27k and coa81k, respectively. The COAMPS(9km)/WOCSS, COAMPS(27km)/WOCSS and COAMPS(81km)/WOCSS combinations will be referred to hereafter as wox9k, wox27k and wox81k. All of the COAMPS/WOCSS combinations involve 3 km horizontal resolution WOCSS wind outputs. The postscripts 9k, 27k and 81k on the end of the wox abbreviation only indicates the corresponding parent COAMPS model used to initialize WOCSS (i.e., coa9k is the parent model of wox9k). The control settings for WOCSS are listed in Table 6. This section contains only the data from the 58 surface observations. The vertical data is discussed in a section later in this chapter. Case Studies 28NOV01, 20DEC01, 13MAR02 and 09MAY02 will be referred to as CASE I, II, III and IV, respectively.

Figure 29 combines all surface data from all case studies comparing the overall RMSE performance of WOCSS vs. COAMPS. Recall that WOCSS is run at 3km horizontal

resolution and being compared to COAMPS at the same resolution. The performance of the COAMPS parent models, that provided initialization information to WOCSS, is also displayed. This is done to investigate whether WOCSS is outperforming the coarser grid COAMPS fields from which WOCSS was initialized.

From Figure 29 it can be seen that wox9k outperformed the other COAMPS/WOCSS combinations as expected for wind speed, but performed about the same as COAMPS at 3 and 9km (coa3k and coa9k). The wox81k had the highest RMSE and the wox27k, wox9k and coa3k performed nearly the same for wind direction, but not as well as coa9k and coa27k, although the difference is not large. The first glance synopsis of Figure 29 shows that wox9k is performing about the same as coa3k, but wox9k is not outperforming the initialization model coa9k.

To investigate the strengths and weaknesses of the COAMPS/WOCSS methodology as a function of synoptic-scale weather regime, the data was separated into Frontal (CASE I and CASE II) and Non-frontal (CASE III and CASE IV) categories. Figure 30 shows the Frontal results. Wind speed RMSE results for wox9k, coa9k and coa3k are similar, but the wind direction RMSE for wox9k is nearly 4° higher than coa9k and 3° higher than coa3k.

Figure 31 contains the Non-frontal RMSE values and shows a significant improvement in the COAMPS/WOCSS winds, particularly the wox9k. The wox9k wind speed RMSE is 0.1 m/s better than coa3k and the wox9k wind direction RMSE is 3.2° better! Not only did wox9k outperform coa3k, but wox9k also outperformed coa9k (which it had not done in the

frontal cases). Non-frontal situations show significant improvements over frontal situations for wox9k compared to the surface observations.

The next set of figures examine the comparisons even further by investigating the hour by hour variations. The hourly comparisons between coa3k, wox9k, wox27k and wox81k are displayed for each case study in Figures 32-39. The top panel is the RMSE errors of the various models with the standard deviation of the observations plotted (dashed line), as well. The bottom panel is the mean over the study domain of the various models along with the mean of the observations (dashed line). Figures 32 and 33 are the CASE I 36-hour forecast winds. They demonstrate that all models are following the mean wind parameters well and RMSE values fall below the standard deviation of the observations (dashed line) beyond the 15-hr forecast (except for wox81k wind speed). CASE I was by far the best forecast of the two frontal cases. The black arrows on figures 32-33 show when frontal passage occurred. The coa3k results show a 0.1 m/s and 1° RMSE improvement over wox9k which is the next best model. The parent COAMPS models had an overall high wind bias for this case, particularly around frontal passage (27-33Z). This high bias is passed down to the WOCSS model, but the WOCSS - COAMPS (parent model) wind speed difference (shown in Table 7) was negative for CASE I. The WOCSS - COAMPS difference, referred to in Table 7, represents reduction or increase of wind parameters compared to the parent COAMPS model. For instance, if the wox9k - coa9k were negative, this may indicate that WOCSS reduces overall flow received from the parent model. The WOCSS - COAMPS difference values

presented in Table 7 represents the average WOCSS - COAMPS difference for all model combinations. The COAMPS Bias in Table 7 refers to the under- or overestimation of COAMPS winds compared to actual observations. The negative WOCSS - COAMPS difference demonstrated in CASE I is important because WOCSS offsets the wind speed error associated with the high bias of COAMPS. Nevertheless, the WOCSS parent models always outperformed the corresponding WOCSS model. The ~5° wind direction difference in WOCSS-COAMPS (Table. 7) did not appear to affect WOCSS wind direction results. Here again the parent COAMPS model always outperformed the corresponding WOCSS model, except for wox27k which had a RMSE ~0.5° better (not significant) than coa27k.

Figures 34 and 35 show the second frontal case statistics for the CASE II 36-hr forecast. This case was the most difficult forecast situation of the four cases. The wind speed errors for wox9k and coa3k are nearly the same, but wox81k outperforms both models by nearly 0.2 m/s. WOCSS outperforms the parent model (COAMPS) in each of the wind speed comparisons (not shown), but for the wrong reason. COAMPS did not handle the weakening structure of the land falling low-pressure system well and, therefore, over-forecasted pre-frontal winds (Figure. 34 21-27Z forecasts). The WOCSS – COAMPS wind speed difference for this particular case was –0.83 m/s (Table. 7). This helped offset the COAMPS high wind speed bias (Table. 7).

Forecast skill remains good between 6-27Z, but at 30Z the low-pressure system makes land-fall right over the center of the domain. COAMPS fails to capture this difficult forecast situation. The black arrow on Figures

34 and 35 show when this occurs and mean forecast and observation directions diverge. Overall, all models in this case had higher average wind direction RMSE (figure 35) than the standard deviation of the observations which by our standards constitutes no forecast skill. Removal of the 30-36Z data from this case lowered the overall RMSE values well below the standard deviation of the observations but relative performance between models remains the same with wox81k having the lowest RMSE.

The wox81k model provided lower RMSE results for both wind speed and direction than any model combination. This happens because interpolation of surface observations for 81 km grids smoothes out many of the details. This decreases error magnitudes in coarser grid models more, due to incorrect phase speed forecasts, than for higher resolution grids in frontal situations.

The third case and the first of the non-frontal cases is the CASE III 36-hr forecast displayed in Figures 36 and 37. The standard deviation of the wind speeds are fairly high for this case and vary according to the strength and location of the inland low and EASTPAC High Pressure systems. Wind speed errors were ~0.2 m/s lower for wox9k and wox27k compared to coa3k and about the same for wox81k and coa3k. All model total RMSE falls below the overall standard deviation of the observations. The WOCSS models performed slightly better than the parent COAMPS models, except for the wox81k which performed slightly worse. Table 7 exhibits a negative WOCSS-COAMPS difference (~-0.25 m/s) that probably aided the WOCSS RMSE since the COAMPS

models had a high wind speed bias compared to the observations.

The wind direction standard deviation of the observations is considerably lower with a prevailing northwesterly flow between the two pressure systems. Figure 37 shows wind direction RMSE results and, once again, the WOCSS model combinations outperform coa3k with wox27k RMSE 4° lower and wox9k RMSE 3° lower. The WOCSS models perform equally as well as their respective parent models for this case for both wind speed and direction.

The last case and the second non-frontal case is the CASE IV 36-hr forecast shown in Figures 38 and 39. This case was the best forecast of the two non-frontal cases judging from the difference between RMSE values and the standard deviation of the observations for all model forecast beyond 06Z (except for wox81k). Wind speed variations for this case are higher than any other case due, once again, to the large changes in EASTPAC High and inland low pressure position and strength. The coa3k model wind speeds outperformed all the WOCSS combinations but only 0.07 m/s better than wox9k (Figure. 38). All of the WOCSS model combinations performed as well or better than the parent model, wox9k had a 0.1 m/s improvement over coa9k. This case also revealed a slightly positive difference between wox9k and its parent model which was not observed in the previous case studies (Table. 7). The other two WOCSS combinations (wox27k and wox81k) showed no significant bias which also differs from the WOCSS usual low bias. Figure 39 shows only one model RMSE less than the standard deviation of wind direction observations for

all hours, wox9k. Although the variation in the wind direction is periodically high, the prevailing flow is almost directly out of the west-northwest for the entire period (bottom panel Figure 39). The wox9k model is the only WOCSS model to outperform coa3k and does so by ~3.6°. The wox9k model outperforms the parent COAMPS model by nearly 6°. This is a stark contrast to the previous cases where WOCSS usually performed as well or slightly worse than the parent model. The only difference between this case and the others is a strong low-level subsidence inversion seen previously on Figure 28.

Next, we will discuss different biases separated into wind speed, frontal vs. non-frontal, and overall categories. Table 7 list all the wind speed and direction COAMPS biases and WOCSS - COAMPS differences for each of these categories. The last column displays the total number of observations used to produce this statistic. The COAMPS bias values are the combined average of coa9k, coa27k and coa81k. The WOCSS - COAMPS difference values are the combined average of wox9k, wox27k and wox81k. There are times when the wox9k - coa9k difference greatly exceeds the wox27k - coa27k and wox81k - coa81k differences. When these situations occur it will be clearly noted in the results discussion.

Overall WOCSS appears to have a ~-0.25 m/s (-0.5 knots) low wind speed difference compared to the parent model. If this total bias is broken down into Frontal and Non-frontal cases, it is clear that the majority of this error comes from the Frontal cases (See Table 7 – Frontal and Non-frontal WOCSS-COAMPS difference column). CASE IV

is the only case with a positive WOCSS-COAMPS wind speed difference on Table 7.

Wind speed is also divided into less than and greater than 5 m/s to identify any significant COAMPS biases or WOCSS - COAMPS differences based on speed. Table 7 shows that the WOCSS - COAMPS difference is nearly the same for either situation overall. Frontal wind speeds over 5 m/s have the highest negative wind speed difference but only vary from the overall frontal difference by 0.1 m/s. The Non-frontal WOCSS - COAMPS wind speed difference for observations greater than 5 m/s shows a positive difference but, as before, only about 0.1 m/s from the Overall Non-frontal difference. WOCSS - COAMPS differences related to wind speed are not significant.

The COAMPS wind speed biases overall from Table 7 demonstrate a tendency of the model to underestimate flow during high wind speed (> 5 m/s) situations. The reverse is true for low wind speeds (< 5 m/s) where the bias is over 2 m/s.

Figures 40 and 41 show the wox9k isotachs (in knots) with parent model (COAMPS 9km) 10 meter winds barbs overlaid. The circled areas show regions of the domain where significant differences between the WOCSS and the parent model wind speed magnitude occur (possible source of negative WOCSS - COAMPS difference). These shadow zones occur regularly in the isotach fields of WOCSS. The shadow zone near Monterey Bay makes physical sense because this region is the convergence zone blocked by terrain, between the Santa Clara Valley outflow and the Monterey Bay inflow causing more vertical than horizontal motion in this

region. The shadow zone on the west side of the Diablo Range may also make sense because of the wake effect in the lee of the range. The shadow region up to the Northeast portion of the domain is the most consistent feature and the least understood since no significant topographic feature resides in this area. These areas may actually exist but observation density deficiencies do not allow us to confirm their existence.

Wind Direction COAMPS biases and WOCSS - COAMPS differences are also listed in Table 7 in the same category format. Overall, there is a ~6.5° positive wind direction WOCSS - COAMPS difference. Non-frontal cases have higher differences than frontal cases. Wind speed variation does not affect the difference more than a degree or two either way. The Non-frontal wind speeds less than 5 m/s have the highest speed variable difference at 9.12°. Case by case the wind direction WOCSS - COAMPS difference remains around 5° until the final case (09MAY02) when the difference increases to almost 12°. The wox9k model showed differences significantly higher than the other two WOCSS models for all cases and tended to average around 10°. Figures 42 and 43 show examples of wox9k wind fields (small wind barbs) and coa9k parent model wind fields (larger wind barbs) with contours of terrain elevation. The circled areas show areas where wox9k wind directions are advanced (positive WOCSS - COAMPS difference) compared to coa9k parent model winds, in the absence of significant topographic features.

B. MODEL PERFORMANCE - EXPERIMENTS

There were several different experiments conducted to test the COAMPS/WOCSS approach in different configurations and possibly make improvements.

1. Compression Factor

The compression factor ranges in value from 0 to 1. Compression values near 0 allow more flow surfaces to intersect the topography allowing the flow to be more terrain following. This type of flow is representative of a stable boundary layer. Compression values near 1 are the reverse, allowing fewer flow surfaces to intersect the terrain causing more of the flow to pass over the topography instead of around. This situation is more representative of neutral or unstable flow. Figure 3 provides an illustration of the effects of changing compression. Three different compression factors are tested, 0.01, 0.4 and 0.8. The control is set to 0.1 and does not currently vary according to stability. The purpose of this experiment is to identify whether or not the compression factor should vary according to different stability regimes. Changing the compression factor does not increase computation time.

Changes resulting from the compression factor experiments were insignificant overall. Frontal or non-frontal data RMSE results differed by no more than 0.06 m/s for wind speed and 0.5° for wind direction. Changes in the WOCSS - COAMPS differences were no more than 0.1 m/s wind speed and 1.0° for wind direction. Ludwig and Sinton (2000) also noticed little change in the verification results when

changing the compression value for WOCSS using surface observations in the objective analysis. The purpose of this experiment was to test WOCSS sensitivity to compression changes using model "observations" in the objective analysis.

2. Number of Iterations

This experiment also deals with changing a model parameter, the number of iterations (NIT) performed to remove divergence. This parameter is explained in more detail in section III B. WOCSS was tested with NIT equal to 10, 100, and 1000. The control value is set to 20. The purpose of this experiment is to determine if more iterations produce a better forecast. If true, an important issue is whether or not this increased performance is worth the extra computation time involved with increasing NIT. The compression factor will remain at the control value (0.1) for each of the iteration experiments.

The overall changes in RMSE between the control and NIT = 10 varied very little, as expected, only .02 m/s wind speed and 0.2° direction changes. Changing NIT = 100 resulted in an increase in RMSE of 0.02 m/s in wind speed and 0.8° in wind direction. Finally the NIT = 1000 experiment yielded increases in the RMSE of 0.04 m/s and as high as 1.8° in wind direction. Increasing the number of iterations resulted in slightly decreased forecast skill. Figure 44 gives a visual display of these RMSE values compared to the control. Changes in NIT do not affect the overall statistics significantly. The data will now be

separated into frontal and non-frontal to isolate the increasing RMSE.

Frontal results of NIT = 10 displayed a 0.04 m/s increase in RMSE and 0.5° decrease in wind direction RMSE. The NIT = 100 RMSE remained steady for wind speed but increased for wind direction (~2.0°). The RMSE for NIT = 1000 increased to nearly 0.1 m/s for wind speed and from 2-4° (wox9k at 4°) for wind direction. The results suggest that increasing iterations in a frontal situation increases wind parameter RMSE, particularly wind direction. Figure 45 gives a visual display of the RMSE performance. The wox9k model was twice as sensitive (for the worse) to NIT changes than the other two domains. The increased wind speed RMSE may be due to a lower WOCSS-COAMPS difference, which previously made the statistics appear better (lower RMSE, but due to offsetting biases).

The non-frontal cases for NIT = 10 showed virtually no change in wind speed error and the reverse of frontal results for wind direction with RMSE increasing between 0.4 – 0.6 degrees. The NIT = 100 experiment once again displayed very little wind speed changes, but a decrease in RMSE in wind direction of 0.5 – 0.8 degrees, once again a reverse from the frontal cases. The RMSE for NIT = 1000 had a decrease of 0.02 m/s in wox9k and an increase 0.02 m/s for wox27k and wox81k. The wind direction RMSE improved by 0.4 – 0.9 degrees. Figure 46 gives a visual display of WOCSS forecast RMSE vs. Control for non-frontal cases. These improvements are not dramatic, but from this data there is trend between frontal and non-frontal situations. Non-frontal situations, increasing NIT shows

slightly increased forecast skill. Increasing NIT for the frontal situations decreases forecast skill significantly.

Figure 47 was included to show how the WOCSS – COAMPS difference decreases with increasing iterations in both frontal and non-frontal situations. The difference actually becomes positive for the non-frontal cases (difference was only slightly negative to begin with). The wox9k model is more sensitive to these changes than the other two model combinations. Increasing the number of iterations removes more residual divergence and increases the overall flow (Ludwig and Sinton 2000). Figure 48 shows the WOCSS 10 m wind isotachs for NIT = 10, 100 and 1000 to illustrate how increasing iterations changes the flow in the model. Increasing iterations smoothes through the objective analysis “dots” (seen on the NIT = 10 plot) and provides a visually more realistic flow pattern. The shadow zones (areas of unusually low wind speeds) also disappear with increasing NIT value. Increasing iterations does improve the negative wind speed WOCSS - COAMPS difference, but the overall RMSE results degrade slightly. Table 8 shows the computation times involved with each experiment and clearly increasing NIT affects the time availability of the model. Increasing iterations from 20 to 1000 may take 2 times (wox9k) or 12 times (wox81k) longer for WOCSS to compute a three-dimensional flow field.

3. Maximum Adjustment Near Observations (ADJMAX)

This model parameter controls how much the observations input into WOCSS will influence the model wind fields for that particular point. The control setting is

zero which allows no adjustment to occur (model observation is exactly the same as WOCSS model output for that particular point). The experiment was to change this parameter to one. This would allow WOCSS to adjust the model observation from COAMPS to the terrain. The results of the experiment yielded almost no change, only 0.01 m/s in wind speed and 0.01° in direction for RMSE compared to the control. This was unexpected, particularly in the wox9k model where 736 COAMPS model soundings are input into WOCSS. Many of these points fall on complex terrain and adjustment by the WOCSS model physics in these areas were expected to make changes to the results. Coarse verification observation density may have contributed to the absence of a noticeable change in the results.

4. Height Adjustment of Highest Flow Surface (AVTHK)

The AVTHK parameter in WOCSS adjusts the highest level in WOCSS (Sigma = 1). The control AVTHK is 5000 meters; the experiment changed AVTHK to 3000, 4000 and 5000 meters for each case. This experiment used only the wox9k combination. Table 9 shows the control sigma levels as well as corresponding control and experimental heights above ground level for WOCSS, as well as, COAMPS vertical levels. This experiment examined the effects of redistribution of WOCSS vertical levels (WOCSS vertical resolution) on performance. The overall, frontal, and non-frontal data plot (not shown) did not fully explain the results of this experiment so results are displayed case-by-case in Figures 49-56. All experiments are plotted together with the control, coa3k, and observations (obs),

with the observed standard deviation time trace (dashed line) shown in the top panel and the observed mean time trace (dashed line) is shown in the bottom panel.

The AVTHK = 3000 and 4000 meters had very similar results and will be discussed together first. Wind speed RMSE errors increased by ~0.75 m/s for each of the first three cases and by over 1.0 m/s for the last case (Figures 49-52 top panel). Wind speed RMSE is well above the standard deviation of the observations (except for the CASE IV case). The bottom panels of Figures 49-52 show that the mean model wind speed is low and that the WOCSS-COAMPS difference is significantly negative, more than 1.0 m/s more negative than the control difference across all cases. Wind direction errors increased 44-51° for each of the two frontal cases (Figure 50-52 top panel). CASE III (non-frontal) increased wind direction RMSE only ~18° (Figure 54 top panel). CASE IV only increased by ~6° and also managed to be the only case that stayed under the standard deviation of the observations (Figure 56 top panel). The wind direction WOCSS - COAMPS difference increased by 6° overall, but the first two frontal cases alone contributed a 35° positive wind direction difference while the final two non-frontal cases had a -26° difference.

The final AVTHK experiment was run at 6000 meters. The wind speed RMSE value was only 0.08 m/s higher for CASE I while CASE II actually improved by 0.05 m/s. CASE III changed very little from the control RMSE wind speed and CASE IV improved by 0.13 m/s (Figures 49-52). The WOCSS - COAMPS difference changed very little from the control

values. Wind direction RMSE increased for CASE I by 0.5°, CASE II by 0.25° and CASE III by 1° from the control wind direction RMSE (Figures 53-56). The final case did not change significantly. The wind direction WOCSS - COAMPS difference remained nearly the same as the control biases. CASE IV appeared to not be as sensitive to AVTHK changes as the other cases. Cases I and II were extremely sensitive to changes while CASE III was somewhere between the frontal and CASE IV sensitivity.

5. Distance To Weight (DTWT)

This parameter is the weighting factor for the objective analysis of model observations into WOCSS. The control setting is 2.0 which results in a parabolic weighting away from the observation point (1/Distance**DTWT). The DTWT parameter was changed to 1.0 to provide a linear weighting to the equally spaced model observations. The results showed a slight decrease in the RMSE for Cases I and II and an even more negative WOCSS - COAMPS wind speed difference (by 0.15 m/s). The RMSE improvement was probably due to the decrease in the wind speed WOCSS - COAMPS difference since COAMPS was over estimating wind speeds for these cases. CASE III showed virtually no change at all even though the WOCSS - COAMPS difference decreased by 0.08 m/s. The final case had an increase in RMSE and a decrease in wind speed WOCSS - COAMPS difference. The models were running a little low for the wind speed on CASE IV and the lower wind speed difference (by ~0.13 m/s) probably increased the RMSE.

The linear weighting function appeared to decrease high wind speeds and increase lower wind speeds, as seen in the isotach comparison in Figure 57. Overall the WOCSS - COAMPS difference decreased to -0.37 m/s which is 0.11 m/s more negative than the control difference. Apparently the decreases to the higher wind speeds were higher in magnitude than the increases in low wind speed creating an even lower WOCSS - COAMPS difference.

6. Roughness Length (ZZERO)

The roughness length determines the amount of forcing the surface will impart on the lower layer flows due to friction. The control value is 0.05 meters, the experiment changed the value to 0.55 meters which represents more frictional forcing (typical of higher vegetation growth). The results were similar to that of the compression factor changes, insensitive to large variations in roughness length. The wind speed changes for RMSE were less than 0.05 m/s and the wind direction changes for RMSE were less than 0.5° compared to control. The WOCSS - COAMPS differences changed, from the control, by less than 0.08 m/s for speed and less than 0.9° for wind direction.

7. WOCSS 1KM Grid Spacing

The final experiment reduced the WOCSS horizontal grid spacing for wox9k from 3 km to 1km. CASE I wind speed RMSE increased by 0.2 m/s (Figure 58) but this was due to the decrease in the WOCSS - COAMPS wind speed difference from –0.47 to –0.11 m/s. Wind direction RMSE decreased by 0.7°

(Figure 59) and the WOCSS – COAMPS difference decreased from 4.87 to 2.61 degrees.

CASE II showed a decrease in RMSE from the control of ~.1 m/s (Figure 60) for wind speed, but the improvement is due to the increase in the WOCSS – COAMPS difference from –0.58 (control) to –0.71 m/s. The wind direction RMSE also decreased ~1.5° (Figure 61) while once again the WOCSS – COAMPS wind direction difference decreased from 10.16 (control) to 5.90 degrees.

CASE III increased wind speed RMSE by 0.07 m/s (Figure 62) and the WOCSS - COAMPS wind speed difference improved from –0.23 to –0.09 m/s. Wind direction RMSE improved by 0.8° (Figure 63) and the WOCSS – COAMPS wind direction difference decreased from 4.56 to 3.33 degrees.

CASE IV increased RMSE wind speed by 0.14 m/s (Figure 64) while the WOCSS – COAMPS difference changed from 0.13 to –0.08 m/s. The wind direction RMSE increased by 1.6° while the WOCSS – COAMPS difference remained near the control increasing the positive difference by only 0.6°.

The 1 km grid spacing experiment did not change the results significantly and the overall performance was slightly worse. The only consistent pattern was a slight decrease in the wind direction WOCSS – COAMPS difference. The wind speed WOCSS – COAMPS difference increased for the first three cases and decreased for the final case (opposite of control trend). The true value of the 1 km experiment cannot be determined from the observation network comparisons completely, because the observation network cannot sample the WOCSS 1km horizontal grid

properly. Figure 66 focuses on 1 km WOCSS (wox9k) flow through complex topography (Northern Diablo Range). The flow appears to be following the terrain obstacles in most cases but the lack of observations in these areas makes verification difficult. Figure 67 compares wox9k(3km) to wox9k(1km) over the Santa Cruz Mountains. The added value of the 1km model can be seen by the flow deflection around peaks then through high passes. Figure 68 shows wox9k 1 km isotachs (10 m) and once again the flow looks very realistic but the observation density in complex terrain does not allow for verification. Computation times for the 1km WOCSS product are reasonable and are shown in Table 8. Comparable COAMPS products would require a considerably longer time to produce.

C. DATA QUALITY

To examine the effects of including data from several different agencies we decided to re-evaluate the data after removing the California Department of Forestry observations. These observations were chosen because they have a less stringent maintenance schedule (every two years), lower wind measurement height (20 ft. instead of 33 ft.), lower reporting wind direction resolution (10° instead of 1°), longer averaging time (10 min. compared to 2 min.) and are monitored less than government agency observations. Removal of this data decreases the number of observations by 35% and nearly eliminates the higher elevation (> 200 m) observations.

Figure 69 shows the overall performance of all cases minus CDF data compared to parent models and the original

control RMSE values. The wind speed RMSE values are considerably lower than the control and well below the parent COAMPS models. Wind direction RMSE for both WOCSS and COAMPS are 5° lower overall (lower panel Figure 69). Overall WOCSS direction RMSE is slightly worse than the parent COAMPS models but better relative to the control difference.

For frontal cases (Figure 70), one can see the WOCSS wind speeds are outperforming the parent models but wind direction RMSE is still much higher than the parent model (particularly for wox9k). The non-frontal cases (Figure 71) show significant improvement in the wox9k and wox27k wind speeds and wox9k wind direction RMSE relative to the respective parent models. The conclusions derived from the control data do not change because of these results, but the RMSE of the COAMPS parent models do change relative to each other significantly.

Figure 72 breaks down each data agency group for each model and the results show a consistent high RMSE for CDF data compared to the total collection. The NOAA data significantly outperforms all other agencies with BAMI (without CDF) data coming in second and slightly below the overall combined data. The CDF data significantly raises the overall RMSE for both speed and direction.

To summarize the removal of the CDF observations from the data set, the wind direction RMSE results decrease by nearly 6° overall, but the model results remain the same relative to each other compared to the all inclusive data set. The wind speed results show that the removal of the CDF data has improved the WOCSS RMSE more than the COAMPS

parent models (Top panel Figure 69). The major reason for this is the degradation of the high resolution COAMPS models during non-frontal cases, illustrated in Figure 71 (top panel). This suggest that WOCSS wind speeds perform better than the corresponding COAMPS models at the lower elevations where non-CDF observations were concentrated, particularly in non-frontal situations. Figure 72 supports this conclusion based on the consistent decrease in wind speed RMSE between WOCSS and its respective parent model for both the NOAA and BAMI (without CDF) data sets. The NOAA dataset has an average elevation of 23.55 meter and the BAMI dataset, without CDF data, has an average elevation of 81.88 meters. The reverse is true for the higher elevation CDF dataset alone. Figure 72 shows that the RMSE increases for WOCSS compared to each respective COAMPS parent model. The average elevation of CDF data is 433.47 meters. This suggests that the COAMPS parent models outperform WOCSS at higher elevations. This last statement is made with caution due to the higher errors observed with the CDF dataset.

D. VERTICAL DATA RESULTS

The vertical data was divided into the Oakland sounding and the four vertical wind profilers. The results from this section are not as statistically relevant as the surface data because far fewer observations were collected.

Data was used from the Oakland sounding for each case study to evaluate the performance of WOCSS and COAMPS in the lower atmosphere. Between 15 and 25 data points were

chosen between 0 and 2500 meters for each case study sounding, except for CASE III where data was unavailable.

The wind speed RMSE values for CASE I are displayed for each sounding in Figure 73. The line labeled “observations” is the actual Oakland sounding. High RMSE values can be seen in the 12Z 28NOV01 sounding (Figure 73) above 2000 meters due to a higher observed pressure gradient at 700 mb that was not simulated by the models. The overall RMSE values for WOCSS and COAMPS showed the wox81k outperforming the other models by ~0.5 m/s. This value is similar to the parent model (coa81k) statistics and the lower RMSE could be due to smoothing advantages 81 kilometer models have over finer resolution models in frontal situations. The coa3k outperforms the other models in wind direction error over the next best model (wox9k) by ~3.0° (Figure 74). Figures 75 and 76 display wind speed and direction errors for CASE II. CASE II has fairly strong winds through the first 24 hours of the forecast. The overall RMSE for each of the four soundings once again shows wox81k outperforming the other models, but also has the highest bias of any model. Wind direction comparisons look well simulated until the 21DEC01 12Z sounding where the forecast models completely lose forecast skill due to land-falling low pressure system mentioned earlier. The coa3k wind direction RMSE overall has the best result once again. CASE IV (Figures 77 and 78) shows that, wox81k has the overall best wind speed RMSE and the best bias. Both wox9k and wox27k outperform coa3k in wind direction.

The overall performance comparisons of WOCSS verses COAMPS for the Oakland sounding show that WOCSS generally

performs very similarly to the parent model. The coa3k model will occasionally display significantly different (better or worse depending on case) results in the lower levels. This is to be expected since coa3k better resolves low level thermal properties and mesoscale features associated with the surface.

The vertical wind profiler data was combined for all four stations and for all 13 forecast periods for each case to produce wind speed and direction RMSE plots (Figures 79 and 80). The dashed line labeled “STD Obs.” is the standard deviation of the observations. The same large wind speed RMSE errors show up in the 28NOV01 profiler data (Figure 79 - upper left corner) at the upper levels that appeared in the Oakland sounding data. This indicated that the upper-level (above 1200 meters) flow was not properly simulated by any of the models for CASE I. The wind speed RMSE for any model does not remain below the standard deviation of the observations, particularly at higher levels. This happens for two reasons, one, the winds do not vary at higher levels as much as they do at lower levels lowering the standard deviation, and two there are only about 18-25 observations per layer per case which increases the variability of the RMSE (decreasing reliability). The wind direction results (Figure. 80) once again show RMSE results higher than the standard deviation of the observations, except in CASE III. The frontal cases (Cases I and II) wox81k appears to perform better for all wind parameters. CASE III all models perform equally, but for CASE IV coa3k handles the 300 – 1500 meter layer better than the WOCSS models.

Table 10 provides the RMSE and WOCSS – COAMPS differences for all cases combined for each layer. The overall statistics reveal that WOCSS does not perform that much differently than the parent COAMPS model at levels above the ground. Virtually none of the model RMSE values fall below the standard deviation of the observations due mainly to the low number of comparisons (observations). The wox81k and coa81k performed better for wind speed for all layers. The coa27k performed better for wind direction for layers 1-3 with wox81k better at layer 4. There was no consistent wind speed WOCSS – COAMPS difference in WOCSS, but some evidence supporting a positive WOCSS – COAMPS wind direction difference (as with surface obs. results) for WOCSS up to but not including layer 4.

VII. SUMMARY

A. WOCSS PERFORMANCE

This study attempted to answer the question “Can a mesoscale model (COAMPS) and high horizontal resolution simple diagnostic model (WOCSS) combination provide as good or better short range mesoscale wind forecast as a high resolution mesoscale model alone?” The COAMPS/WOCSS methodology was run with COAMPS at 81, 27 and 9 kilometers and WOCSS at 3km (experimented at 1km) compared to COAMPS at 3km over various weather regimes.

The results show that over the four case studies presented here wox9k performed as well as coa3k (Figure 29). Further inspection of frontal vs. non-frontal weather regimes showed that the COAMPS/WOCSS combination performed notably different for each regime. The wox9k combination for non-frontal situations proved to be far superior to coa3k and the parent model coa9k (Figure 31). The frontal results showed that the COAMPS/WOCSS methodology was not superior to coa3k or each of the respective parent models (Figure 30).

The wox9k results were particularly poor for wind direction. The frontal results displayed a reverse trend in forecast skill with coa81k performing better than the higher resolution COAMPS or WOCSS models. The phase errors associated with frontal/low pressure situations in the models presents a mesoscale model verification problem. These situations have complex wind fields where the wind direction can change as much as 70° and wind speeds as much as 5 m/s in an area less than 100 km (pre-frontal/post-

frontal). High resolution models may only have a 75 km error in frontal position but, due to the higher horizontal resolution the forecast winds, may be southerly and strong when the observations are westerly and weak or vice-versa. The coarser grid models tend to smooth through these errors since direction and speed is interpolated for surface comparison points between grids points, therefore forecast winds are southwesterly and moderate, lowering overall forecast error. Figure 81 gives an example of this situation and may explain the shape of the curve in Figure 30. The top panel of Figure 81 shows the coa81k wind barbs and the position of the model low (label L_{model}) and the position the actual low pressure system (label L). The position error is 150 km too far to the north-northwest. The four circled model wind barbs represent the model winds used in the interpolation to the circled observation location. The same is done for coa9k in the lower panel. The increased grid spacing of the 81 km COAMPS allows two of the interpolation points to be located over land where increased roughness length over land turns winds more into the low. The increased grid spacing also places the model winds used for interpolation further into the southeast portion of the low where winds are more southerly. The high resolution of the 9 km COAMPS grid uses model winds closer to the proximity of the observation. These effects allow coarser grid models to perform better in difficult forecast situations such as fronts and land-falling low pressure systems.

The greatest success of COAMPS/WOCSS occurred in CASE IV, which was the only case dominated by a strong subsidence inversion. The COAMPS/WOCSS combinations had

failed to significantly outperform its parent model until CASE IV when wox9k had a RMSE 6° lower than coa9k. This improvement indicated that the WOCSS model had taken on its own identity and provided a flow much different than the parent model.

A negative WOCSS – COAMPS difference in wind speed was found of approximately -0.25 m/s overall. The first three cases all had negative wind speed differences with the frontal cases having nearly double the overall average wind speed negative difference suggesting that WOCSS does not handle mass flow in frontal situations as well. Mohammed (2000) also observed low wind speed biases in his studies. Though WOCSS was originally designed for low wind speed applications, the wind speed differences for both low and high winds were nearly identical, while Ludwig and Sinton (2000) only observed underestimation of high wind speeds. The wind direction difference between WOCSS and the parent model was consistently positive across all cases and always more drastic between wox9k and coa9k. Mohammed (2000) noticed a positive wind direction bias in warm situations with a negative bias during cold situations (diurnal cold and warm periods). Although the bias was not divided into diurnal cold and warm periods, this study did show an increase in positive wind direction WOCSS – COAMPS difference for the warmer non-frontal situations with less of a positive wind direction difference during colder frontal situations. Ludwig and Sinton (2000) did not notice any significant wind direction bias using actual observations in the WOCSS objective analysis.

Evaluation of vertical profiles from the Oakland sounding and the four profilers did not provide reliable results because of the small size of the dataset. Model verification for small network coverage in the vertical needs to be conducted over a much longer period of time to collect more statistically significant comparisons.

B. EXPERIMENTS

Ludwig and Sinton (2000) mentioned in their conclusions the lack of sensitivity to changes in WOCSS model configuration. This study using the COAMPS/WOCSS methodology also noticed the same insensitivity to changes in model parameters with some exceptions. Changes in the compression factor, adjustment near observations, and roughness length changed the overall results very little. Although increasing the number of iterations decreased the observed low wind speed difference between WOCSS and the parent model, the improvements and changes in the results were also minimal.

Reducing WOCSS horizontal resolution from 3 to 1 kilometer also proved to change the statistics modestly, but an argument can be made that this result is due to the verification method. The domain for this study covered over 75,000 km^2 and the mean distance between surface observations was 36 km. Even though this is considered a relatively dense observation network, verification of 3 and 1 kilometer models using traditional comparisons may be misrepresentative.

The AVTHK experiment, which adjusted the height of the top surface in WOCSS (adjust the vertical distribution of

flow surfaces essentially), yielded the most dramatic results. The experiments adjusting AVTHK to 3,000, 4000 and 6,000 meters decreased forecast skill, but for the first time a significant change in the forecast results occurred. Changes in AVTHK affected the frontal cases much more than the non-frontal cases. The adjustment of the vertical distribution of flow surfaces could be a key factor in improving WOCSS performance in frontal and non-inversion type regimes.

C. DATA QUALITY

There are several advantages to combining observation network agencies, such as, increasing data density and providing observation data at various elevations. There are several disadvantages as well which were observed during this study. Although the California Department of Forestry RAWS observation sites were strategically placed in data scarce high elevation locations, the reliability of this data is suspect. The results from Figure 72 show how one observation network (CDF in this case) can drastically increase RMSE. The good news is that increase in RMSE by the CDF data did not change the overall conclusions about the COAMPS/WOCSS methodology dramatically. The only modifications to the original conclusions are wox9k and wox27k for non-frontal cases outperformed coa3k and the parent models even more than the all inclusive dataset, particularly in wind speed (Figure 71).

Another concern about observation data is the accuracy of the published observation positions. Verification of models with 10 km plus horizontal resolution using a

position accuracy of 0.01 degrees latitude/longitude was fine since position errors were much less than the resolution of the model. A position accuracy of 0.01 degrees could result in position errors that are just over 1 kilometer. This position accuracy is not sufficient for verification of 3 and, particularly, 1 km models. A position accuracy of 0.001 degrees produces errors just over 100 meters and would be sufficient for high resolution verification. Just under 40% of the data used for this study is at three digit accuracy, the rest is two digit (Listed in Tables 1, 2 and 3).

D. FUTURE WORK

The COAMPS/WOCSS control configuration appears to perform well in stable, non-frontal and low level subsidence inversion situations. Frontal situations display less forecast skill for the COAMPS/WOCSS method, but this may be simply a result of the verification problems discussed in Figure 81. The other explanation is that the performance of WOCSS is degraded during frontal situations. The adjustment of the vertical levels (AVTHK) in the WOCSS configuration may provide a solution to this problem since none of the other parameters affect flow significantly. The lower performance of WOCSS at higher elevation observations (CDF) compared to the COAMPS parent model, observed in figure 72, could also be investigated with AVTHK experiments.

Another area of future work is the evaluation of COAMPS/WOCSS methodology over other areas of complex terrain, such as central continents and eastern coastlines.

Most of the WOCSS evaluations have been conducted in Central and Southern California. These domains are typically under the influence of a subsidence inversion and stable air.

Figure 82 addresses an issue concerning the model soundings used in the COAMPS/WOCSS method. The top figure represents the actual Oakland sounding while the bottom figure represents the COAMPS 9km model sounding used in the wox9k objective analysis over the Oakland position. The circled areas show how the model sounding smoothes the low level subsidence inversion observed in the Oakland sounding. The inversion is much weaker (5° F compared to the 10° F observed) and elevated ~500 meters above the observed inversion. These differences can change the slope of the flow surfaces in WOCSS significantly. Future work experimenting with using actual soundings to represent the vertical temperature structure in WOCSS may prove useful.

The final area of work addresses the need for a product like COAMPS/WOCSS in an operational setting. The highest operational need of forecast mesoscale winds presently are in the dispersion modeling community. The COAMPS/WOCSS methodology may also become valuable in 4-D Cube Virtual Natural Environment (VNE) applications. This concept is under development to provide relevant three dimensional weather parameters, and their variations in time, to the warfighter using the latest information technology. One example of the COAMPS/WOCSS usefulness to the VNE database is the input of high resolution winds into weapons dropped at altitude. The COAMPS/WOCSS approach provides short-range forecast of high resolution mesoscale

winds in a fraction of the time of a full physics mesoscale model. Emergency response and VNE applications require fast accurate meteorological products. The portability of WOCSS is also operationally significant since the model can easily be run on a laptop (as opposed to supercomputers) or command center desktop. The ability of the COAMPS/WOCSS method to provide winds as accurate as similar resolution COAMPS models at a greatly reduced processing time could greatly enhance the ability of the Navy's Meteorology and Oceanography Community to serve operational needs.

The hypothesis of this thesis addressed the possibility of a mesoscale model (COAMPS) combined with a simple high horizontal resolution diagnostic model (WOCSS) could produce as good or better short-range mesoscale wind forecast as a high resolution mesoscale model. This study has shown that the COAMPS/WOCSS methodology at 3km horizontal resolution does indeed produce mesoscale wind forecast as good as COAMPS at 3km overall. The COAMPS/WOCSS method provides much improved results over COAMPS at 3km for non-frontal situations, particularly in wind direction, but frontal situations appear not to be as successful. This study has shown that it can be useful during certain conditions and further experimentation may expand this to all situations.

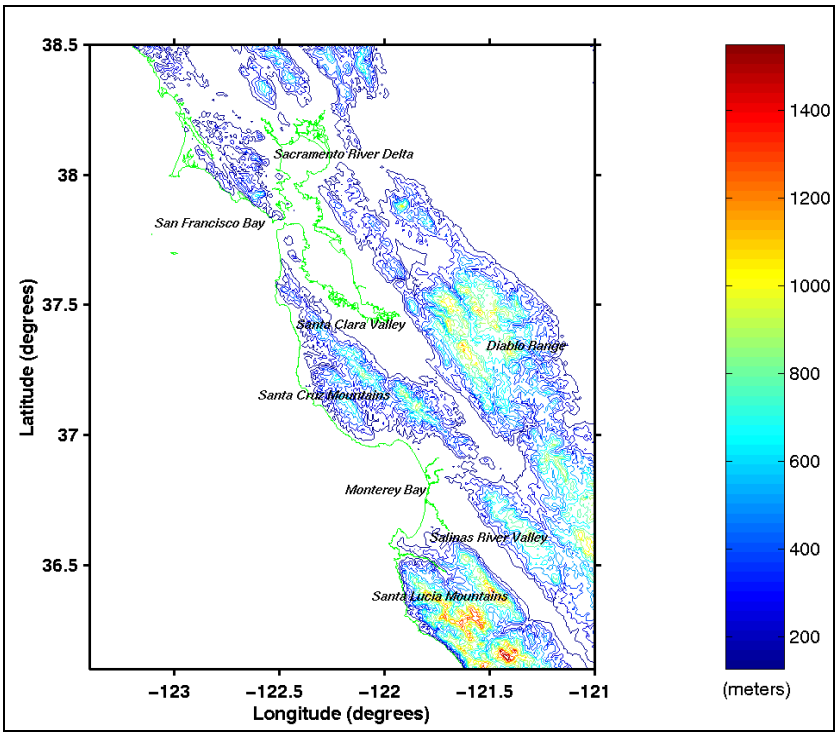

Figure 1. Domain of Study

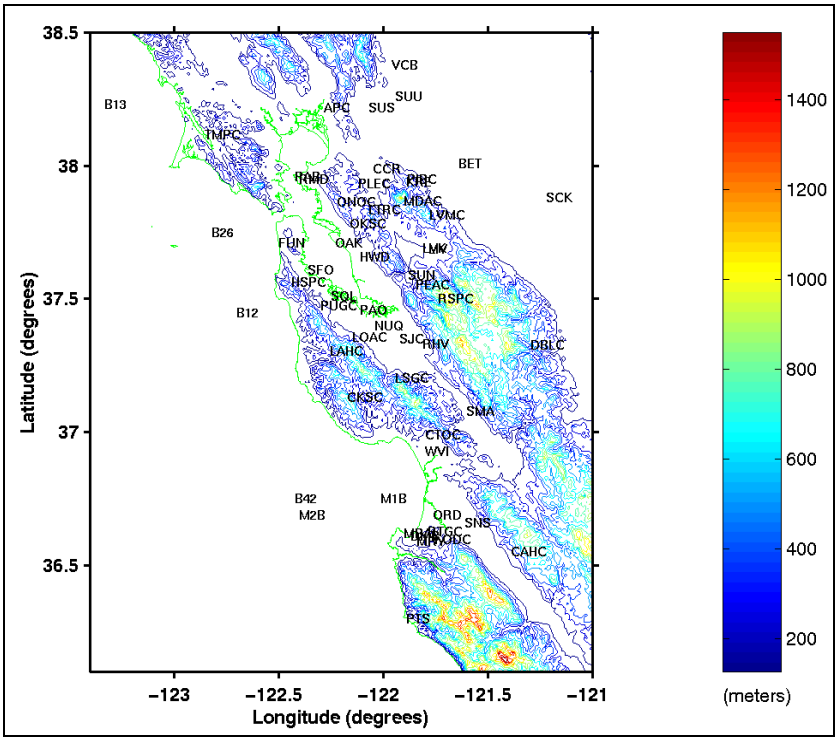

Figure 2. Station Locations

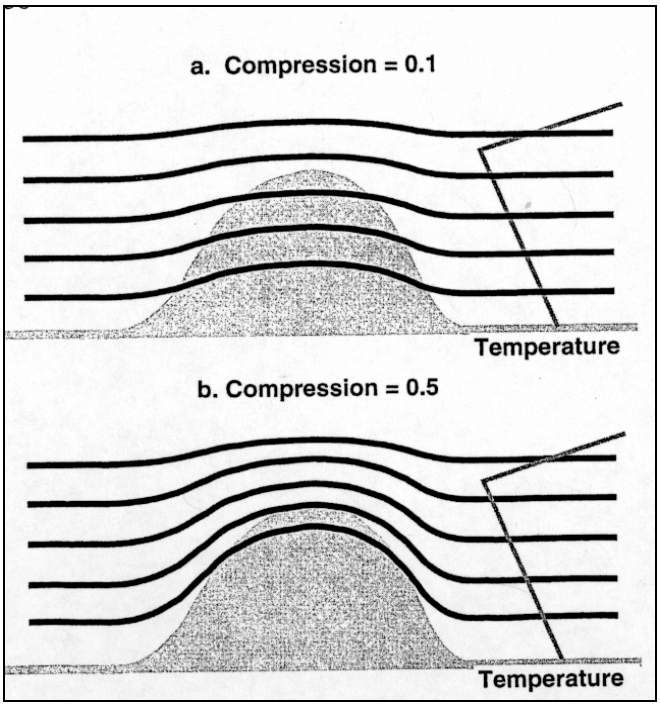

Figure 3. WOCSS Flow Surfaces (From: Ludwig et al. 1991)

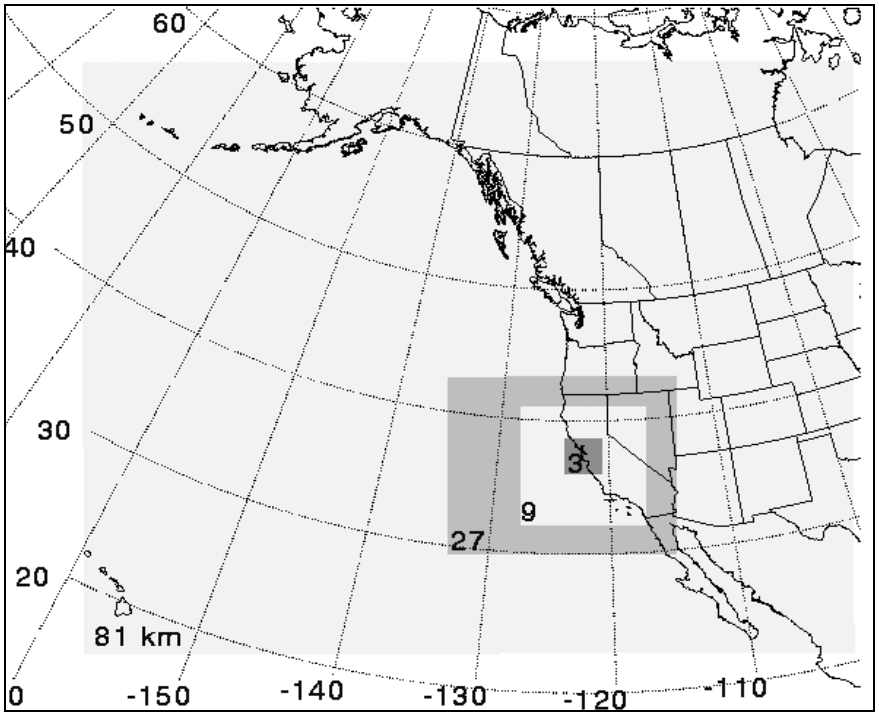

Figure 4. Nested Grids

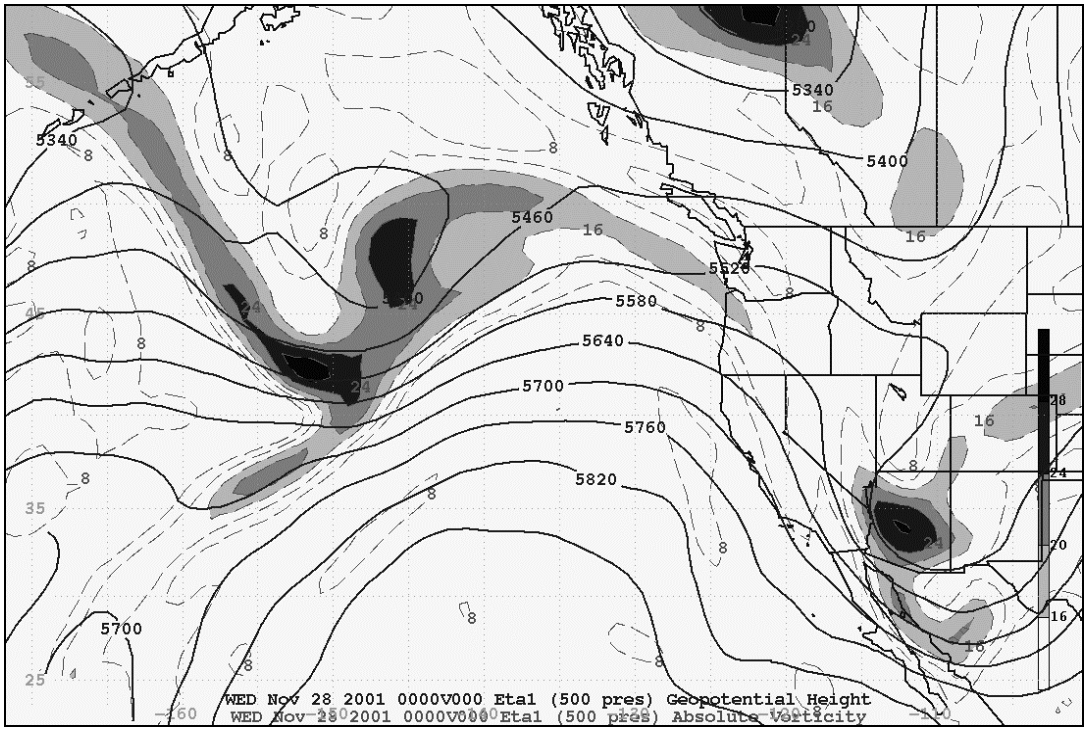

Figure 5. 28NOV01 00Z 500mb HGTS and Abs. Vorticity

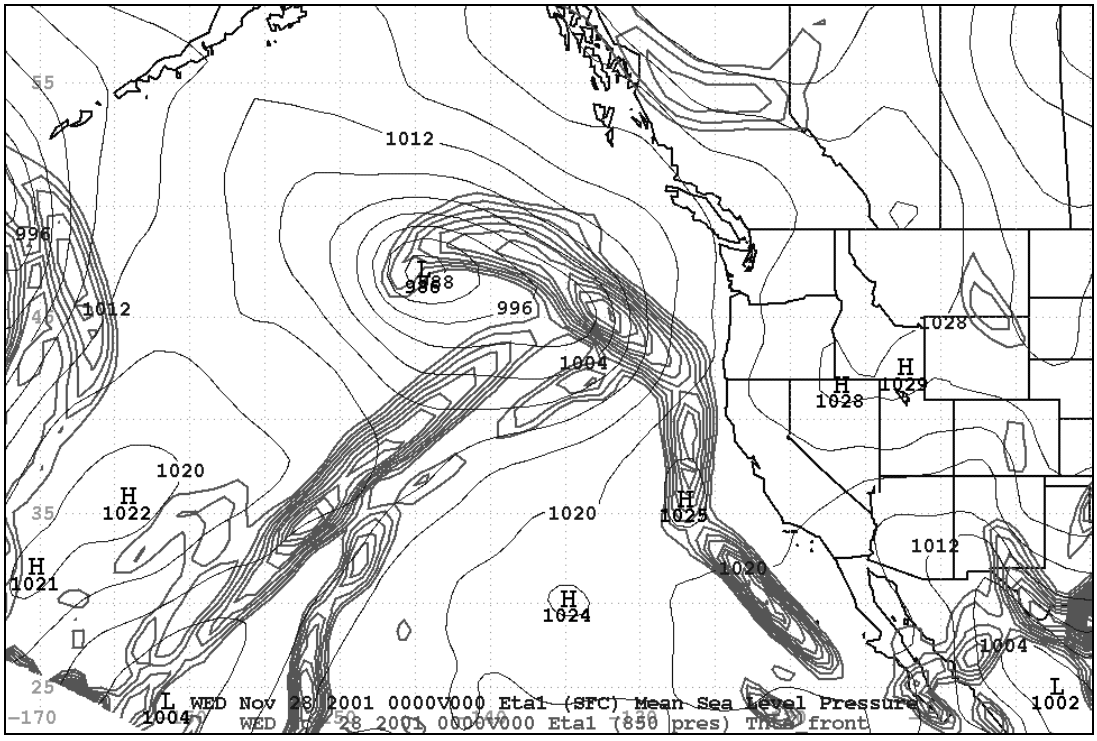

Figure 6. 28NOV01 00Z 850mb ThetaE Gradient and SLP

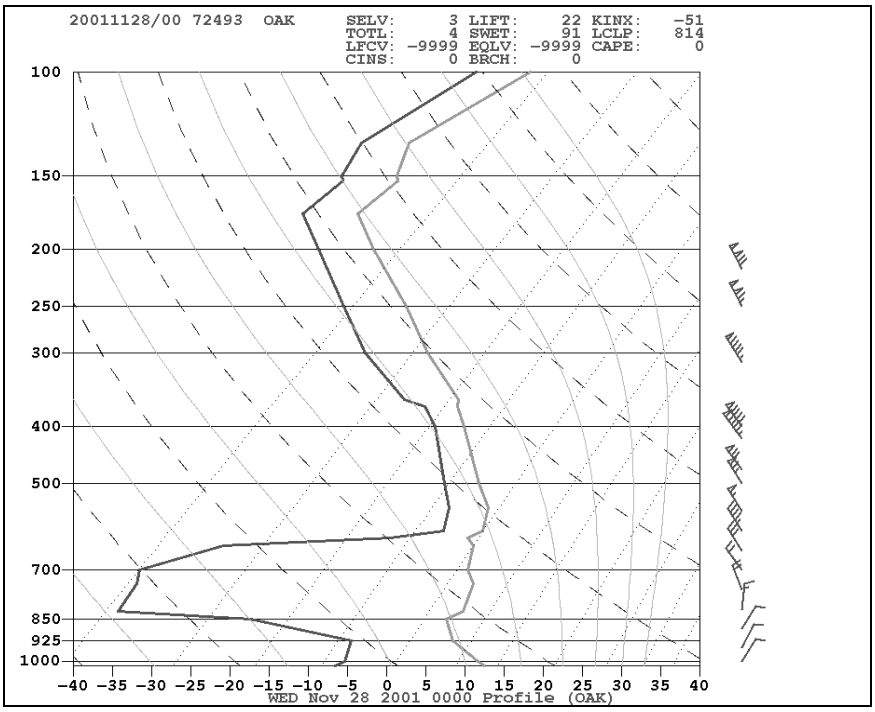

Figure 7. 28NOV01 00Z Oakland Skew-T

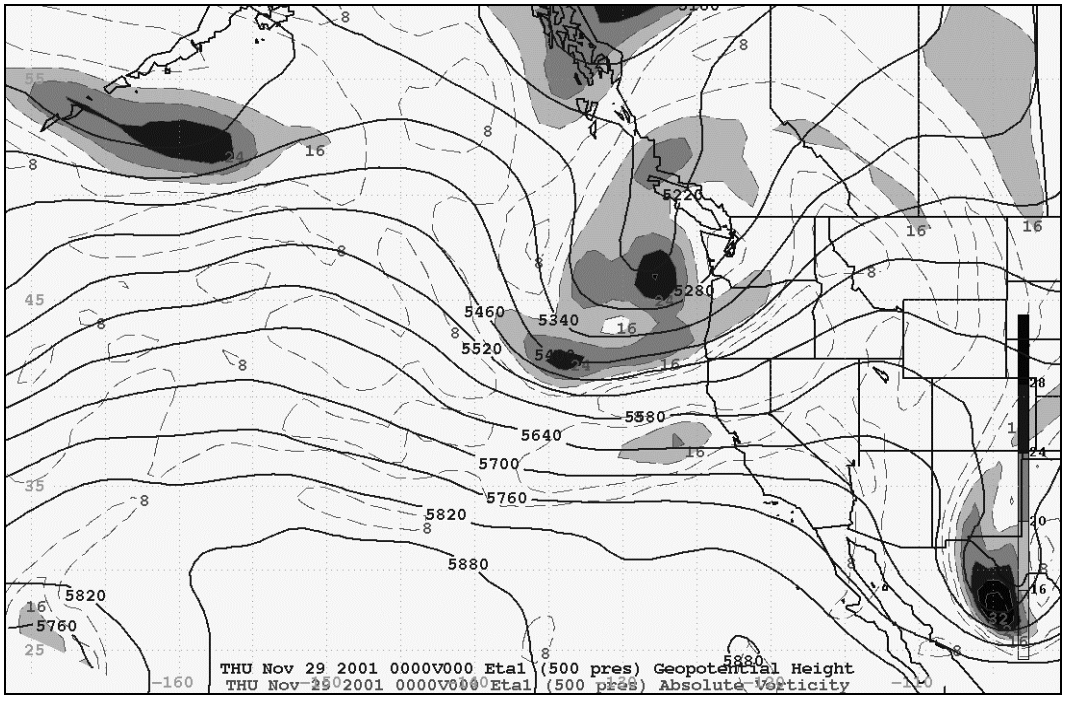

Figure 8. 29NOV01 00Z 500mb HGTS and Abs. Vorticity

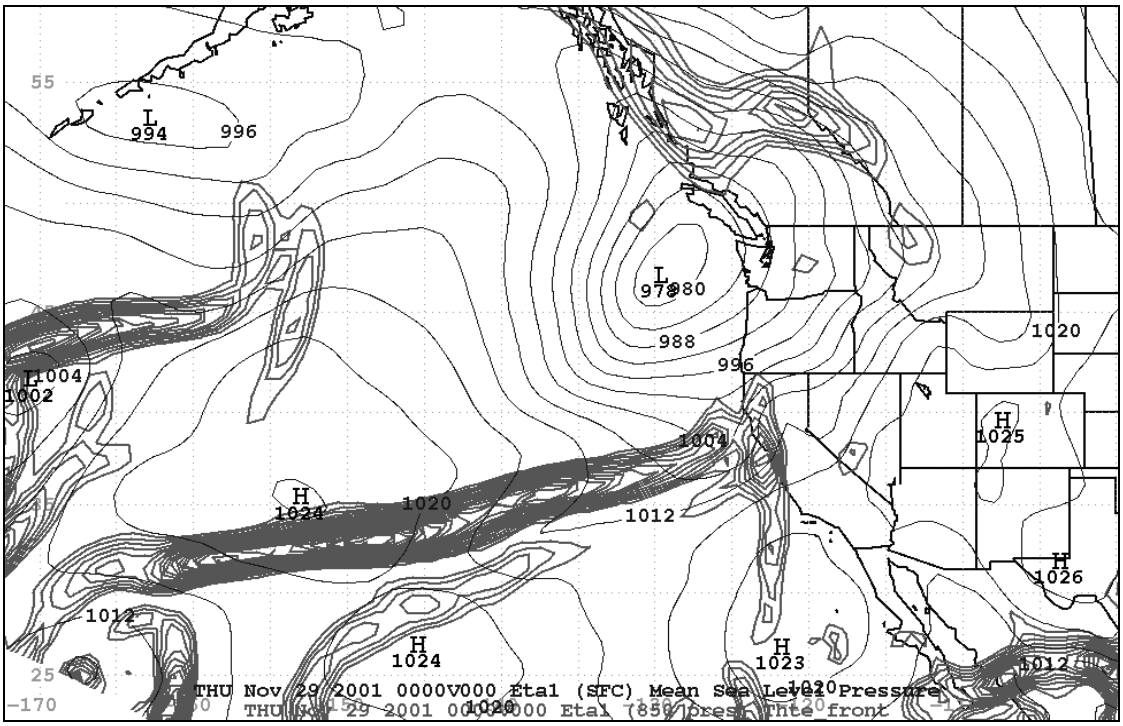

Figure 9. 29NOV01 00Z 850mb ThetaE Gradient and SLP

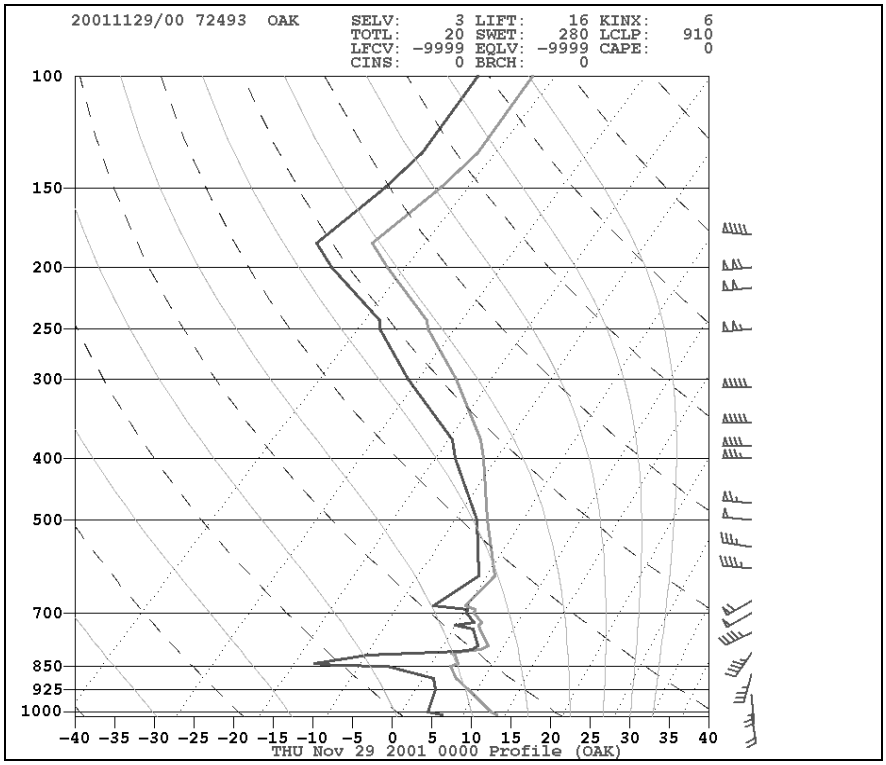

Figure 10. 29NOV01 00Z Oakland Skew-T

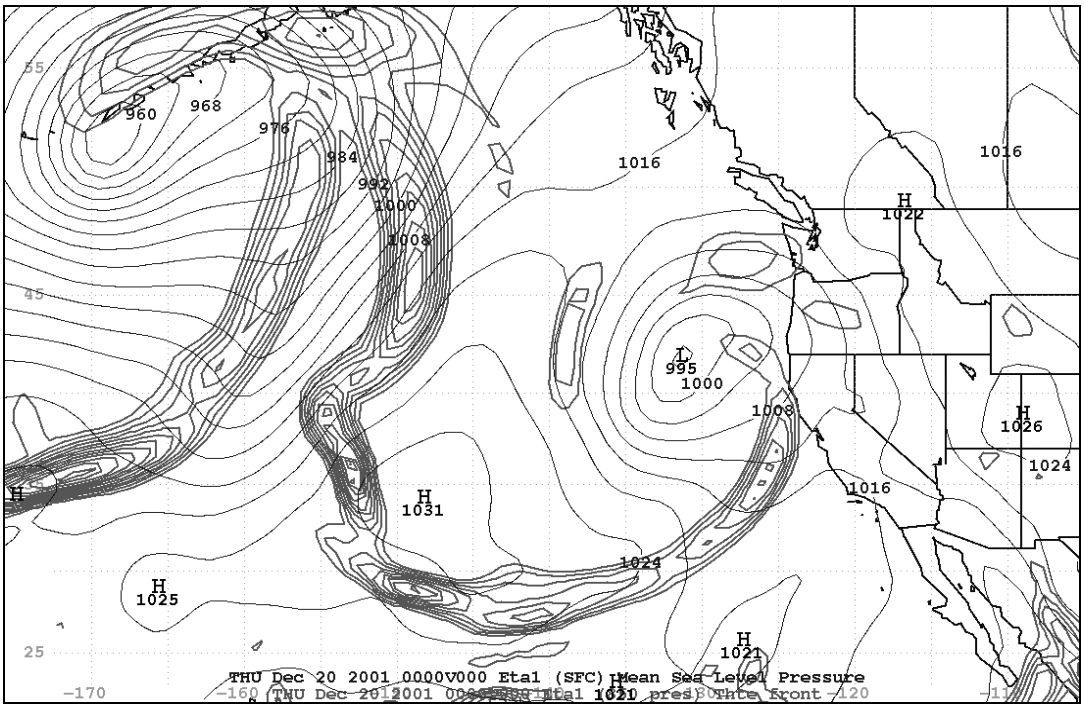

Figure 11. 20DEC01 00Z 850mb ThetaE Gradient and SLP

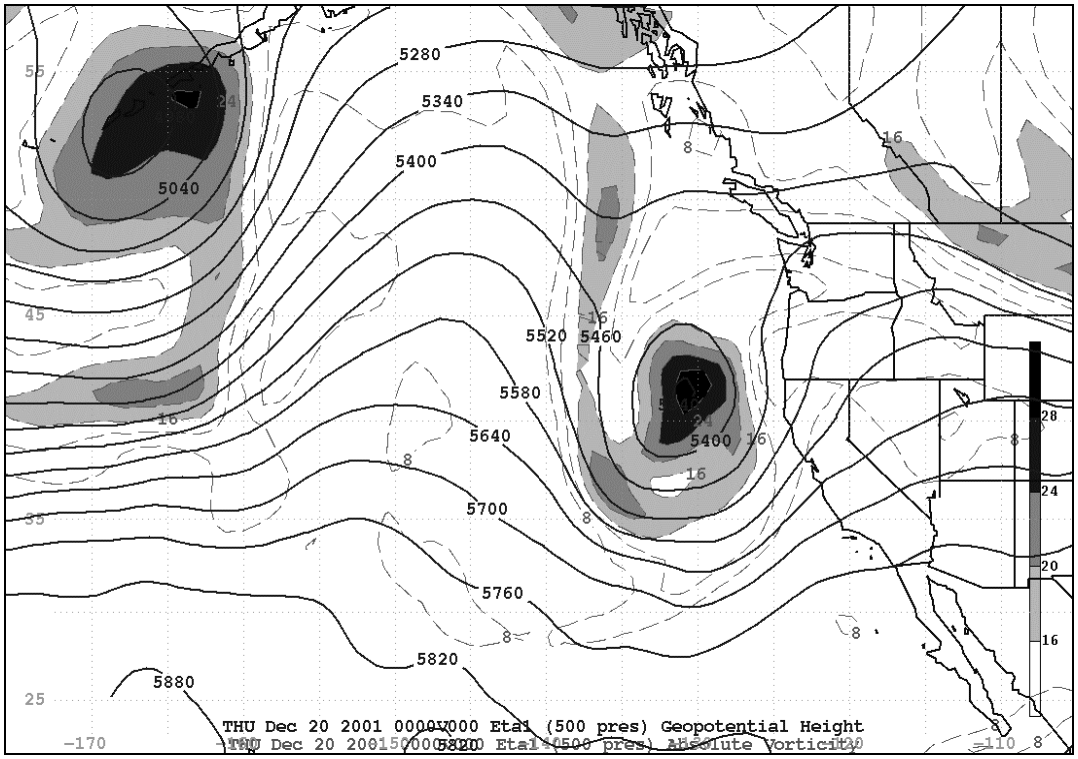

Figure 12. 20DEC01 00Z 500mb HGTS and Abs. Vorticity

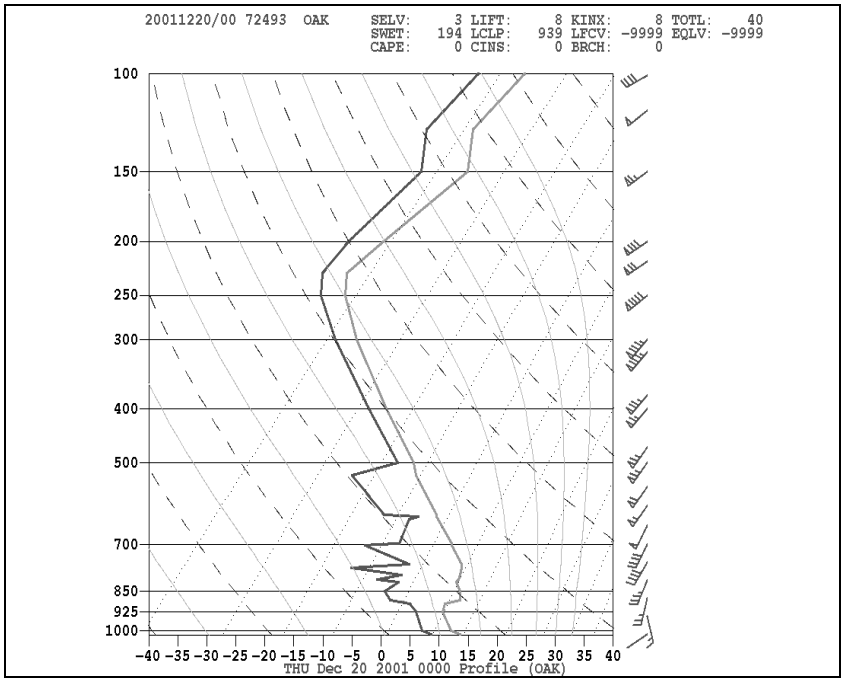

Figure 13. 20DEC01 00Z Oakland Skew-T

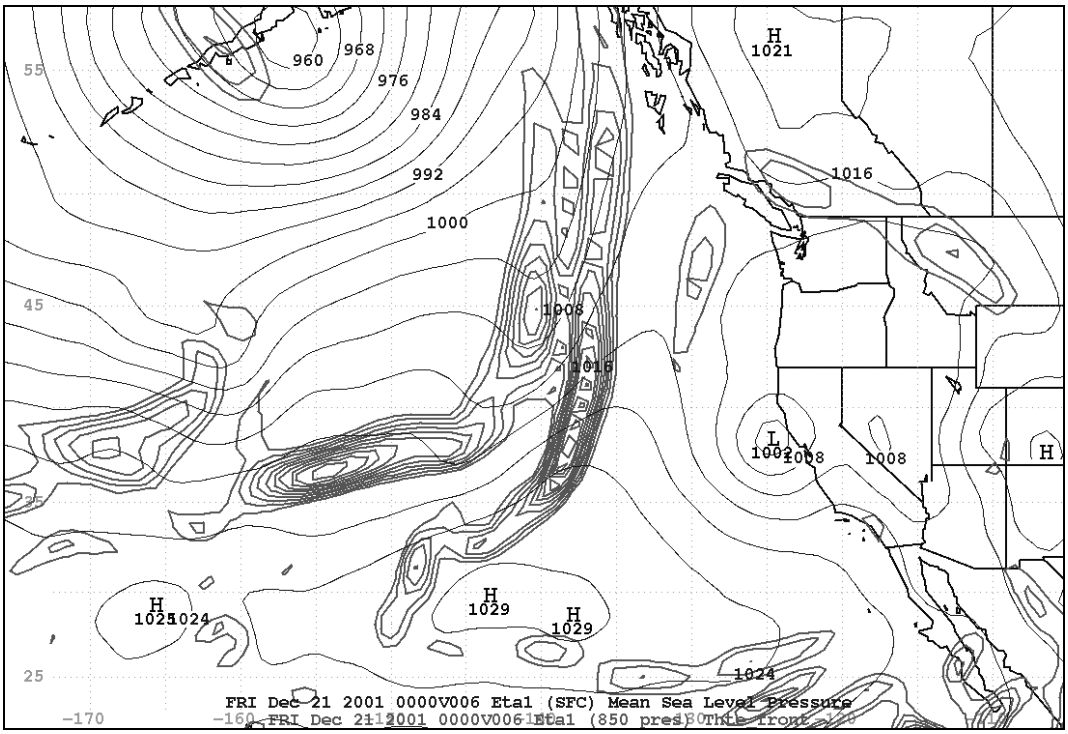

Figure 14. 21DEC01 00Z 850mb ThetaE Gradient and SLP

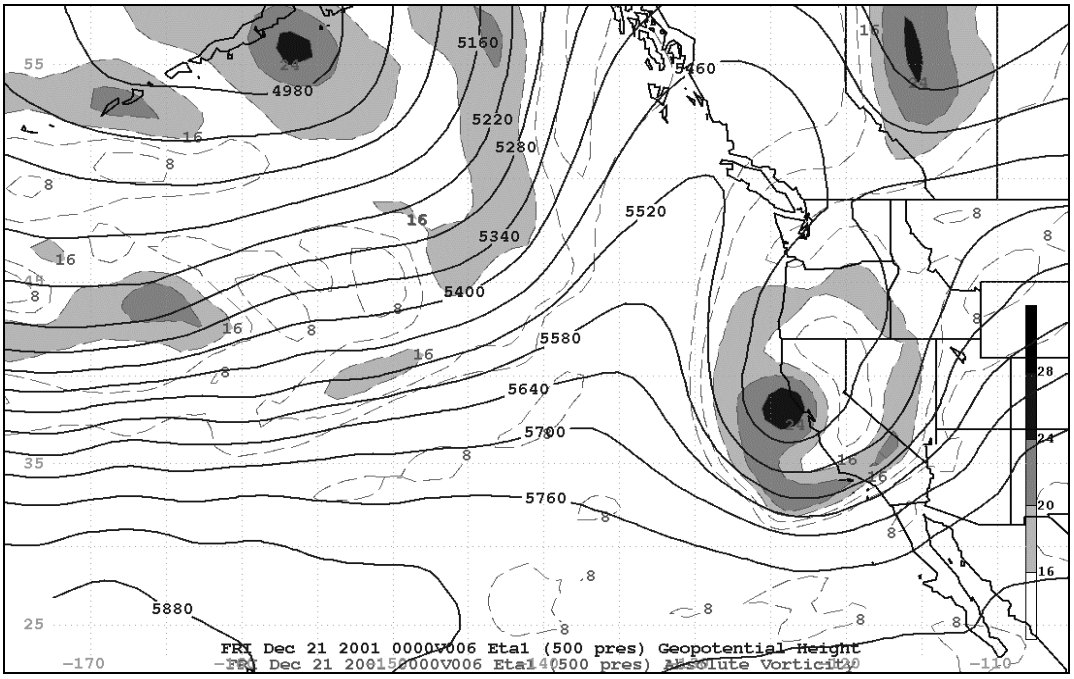

Figure 15. 21DEC01 00Z 500mb HGTS and Abs. Vorticity

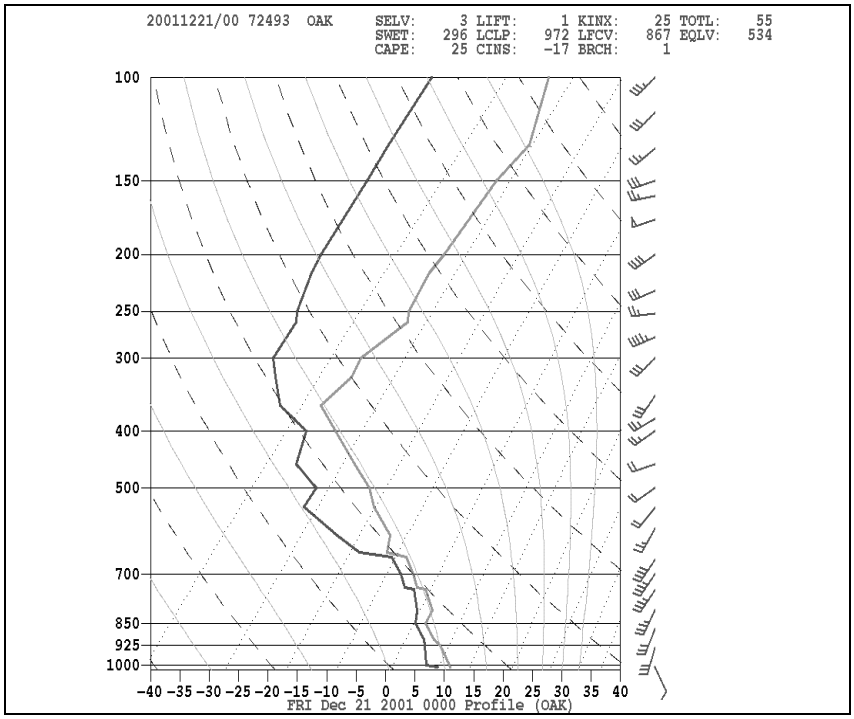

Figure 16. 21DEC01 00Z Oakland Skew-T

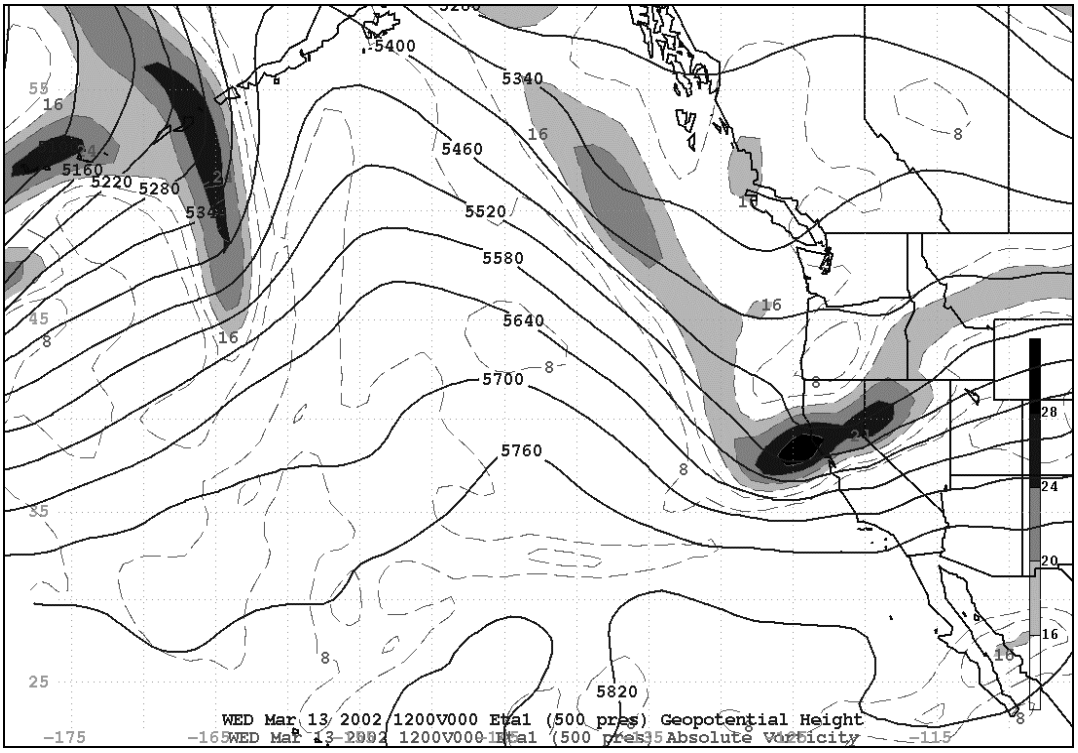

Figure 17. 13MAR02 12Z 500mb HGTS and Abs. Vorticity

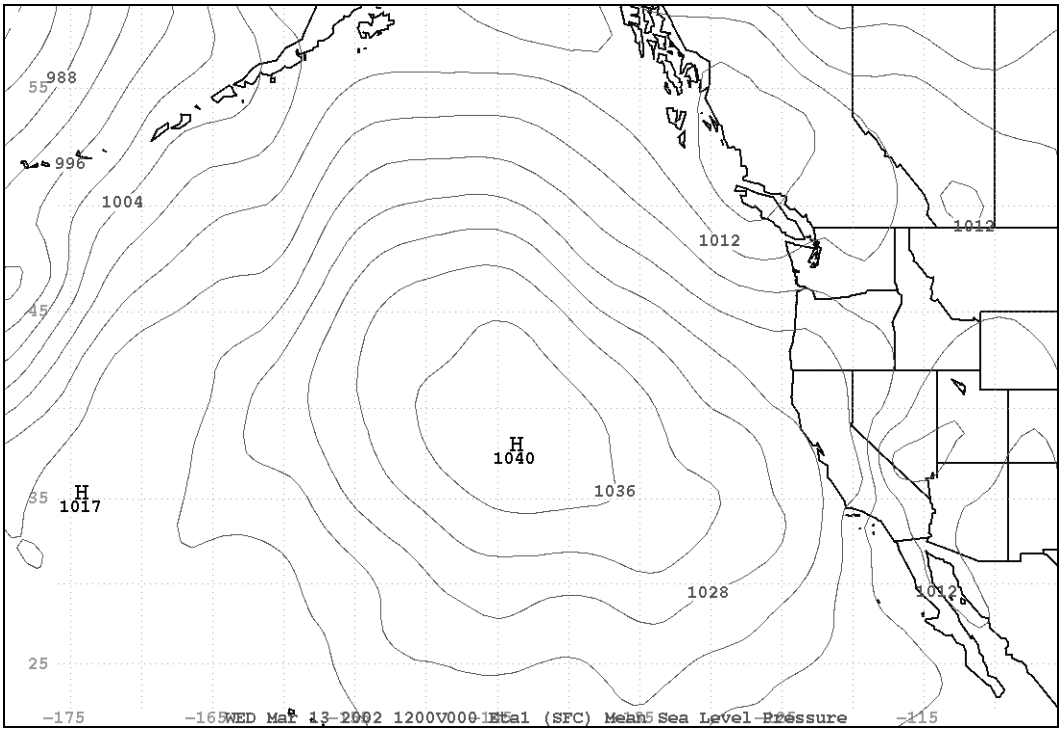

Figure 18. 13MAR01 12Z SLP

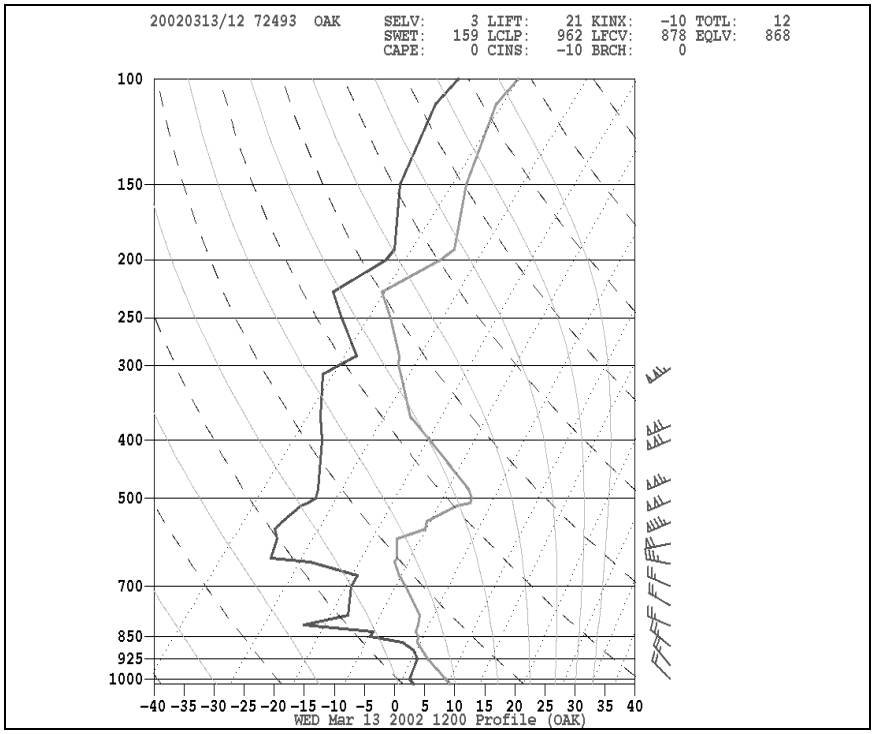

Figure 19. 13MAR02 12Z Oakland Skew-T

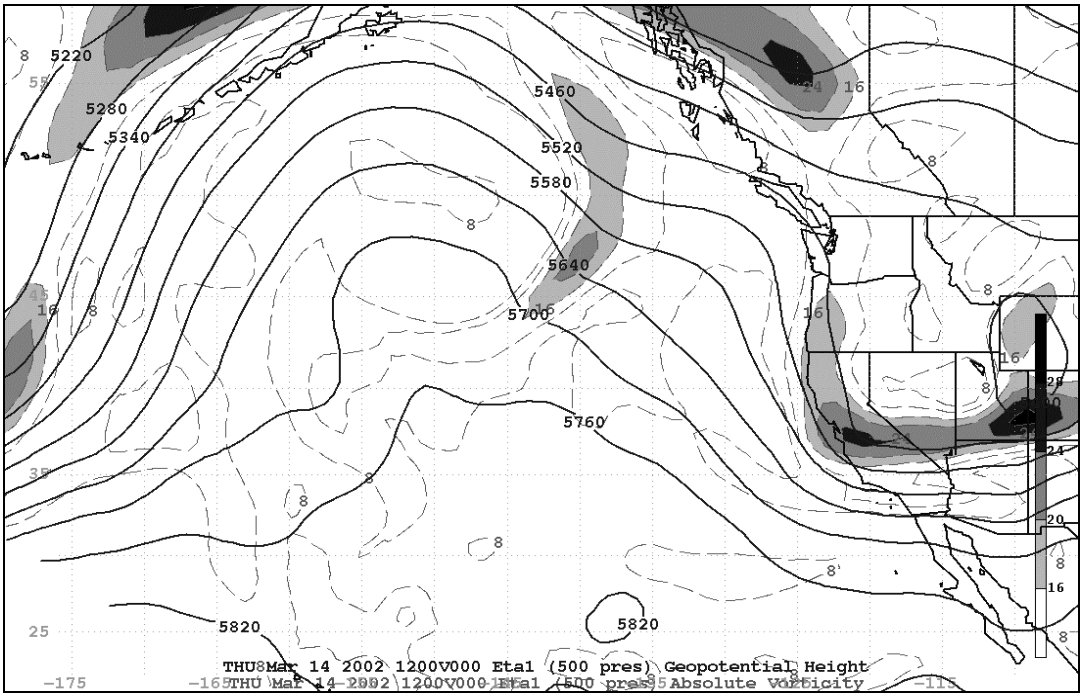

Figure 20. 14MAR02 12Z 500mb HGTS and Abs. Vorticity

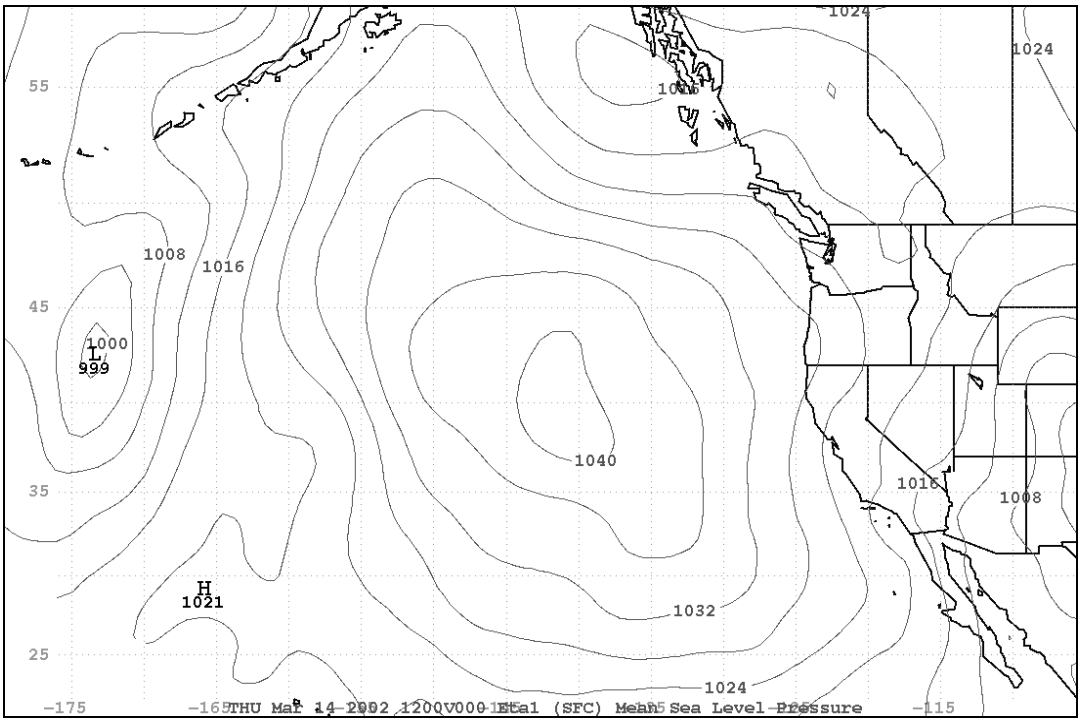

Figure 21. 14MAR01 12Z SLP

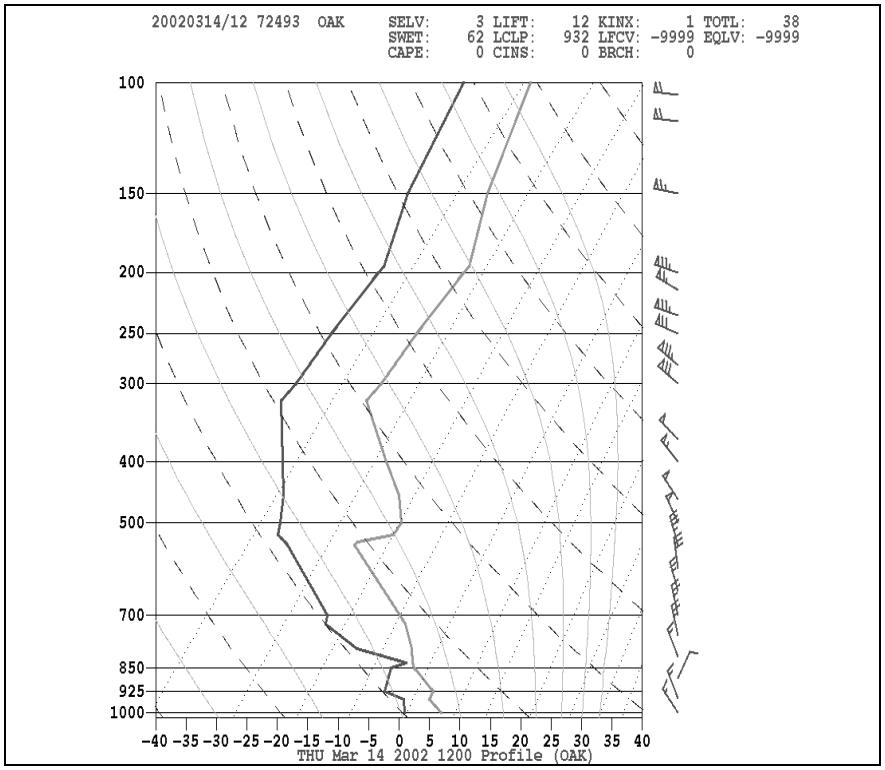

Figure 22. 14MAR02 12Z Oakland Skew-T

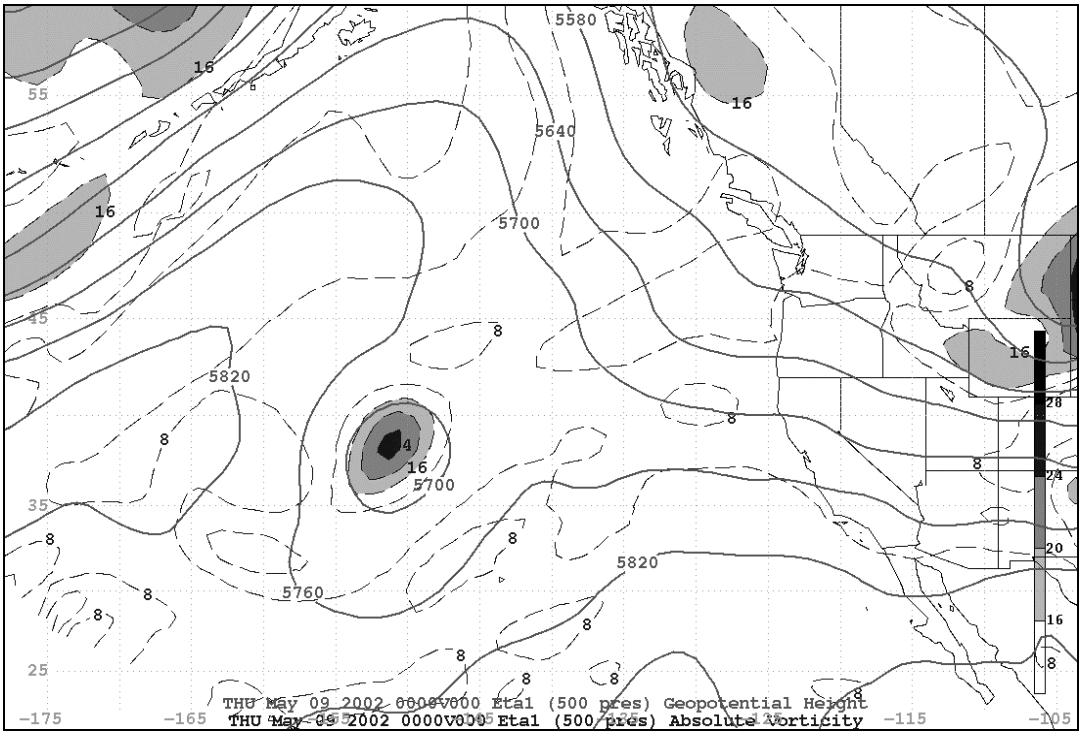

Figure 23. 09MAY02 00Z 500mb HGTS and Abs. Vorticity

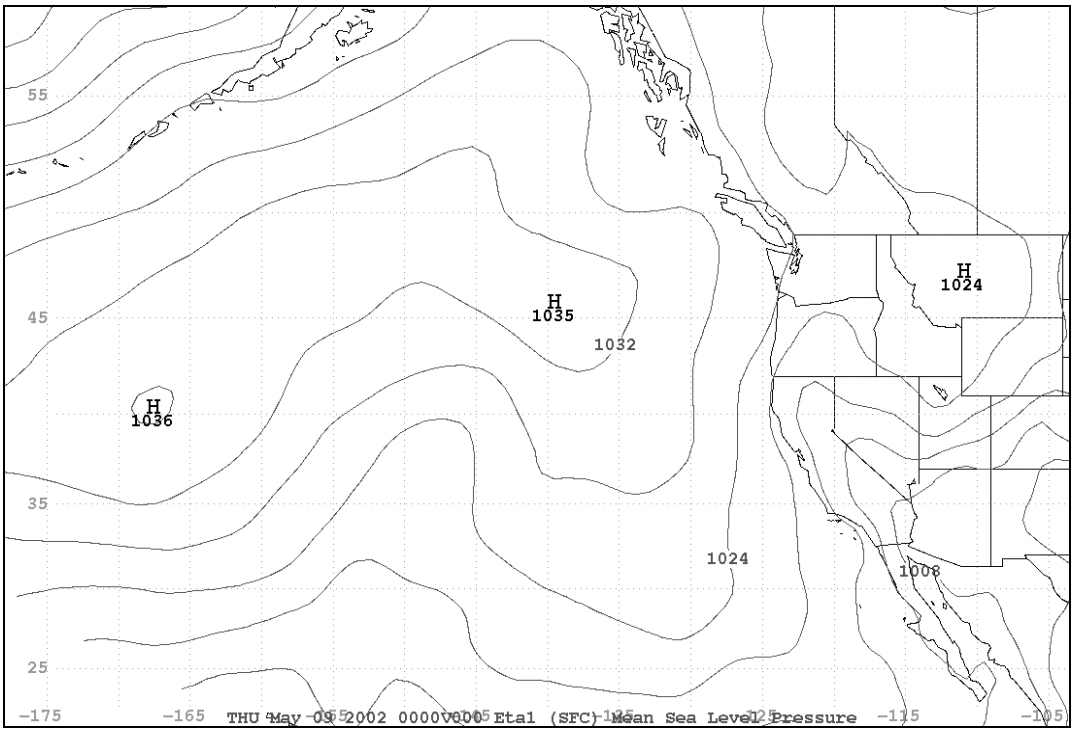

Figure 24. 09MAY02 00Z SLP

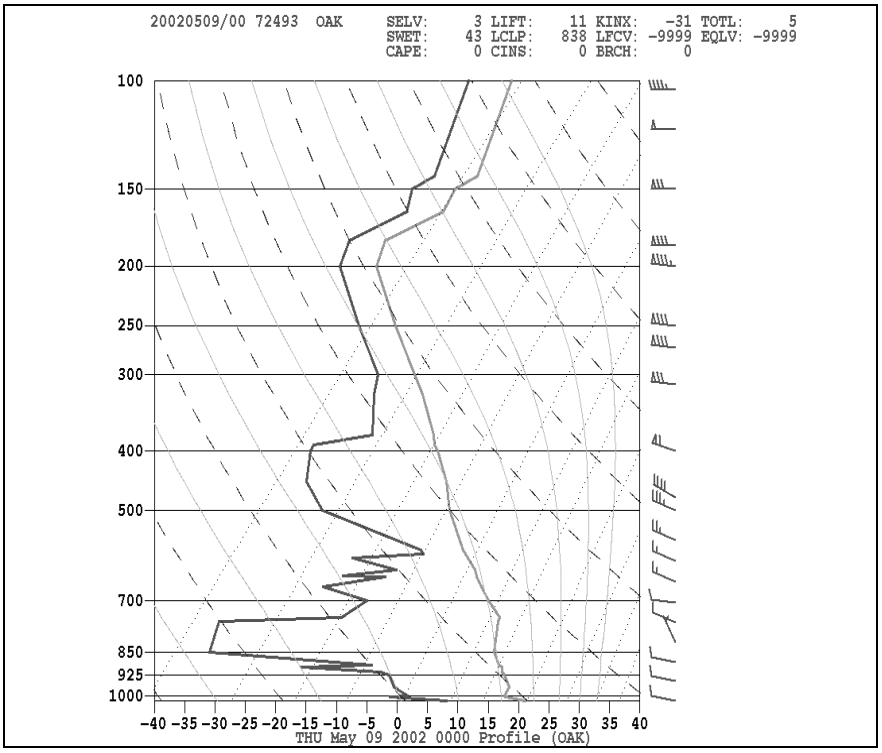

Figure 25. 09MAY02 00Z Oakland Skew-T

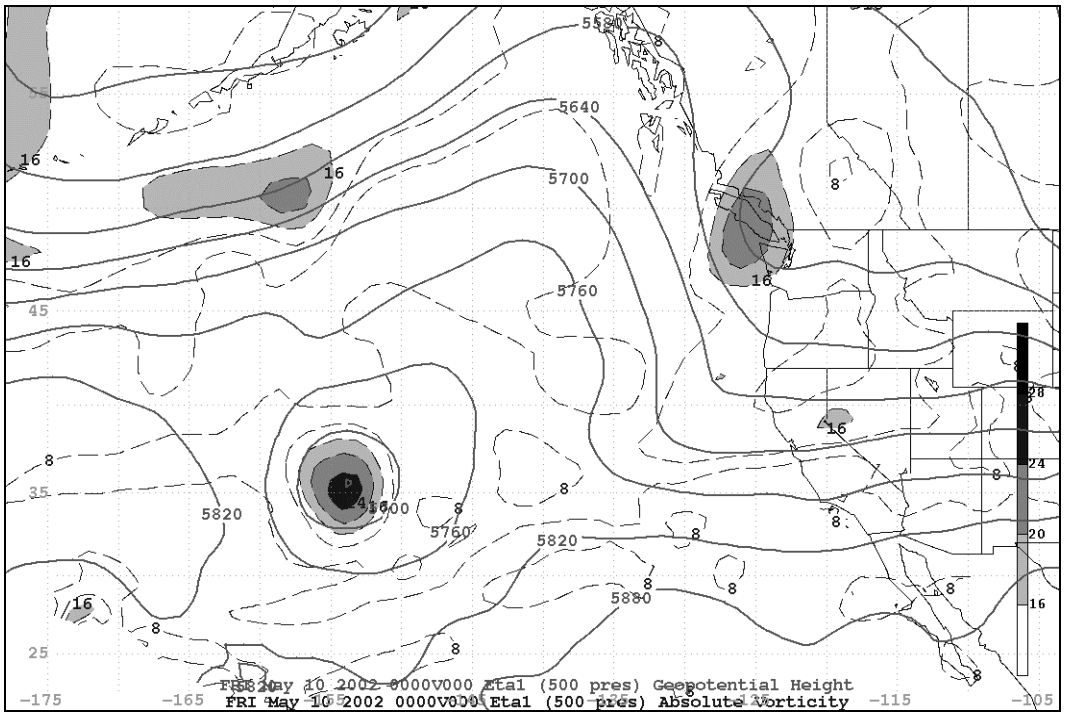

Figure 26. 10MAY02 00Z 500mb HGTS and Abs. Vorticity

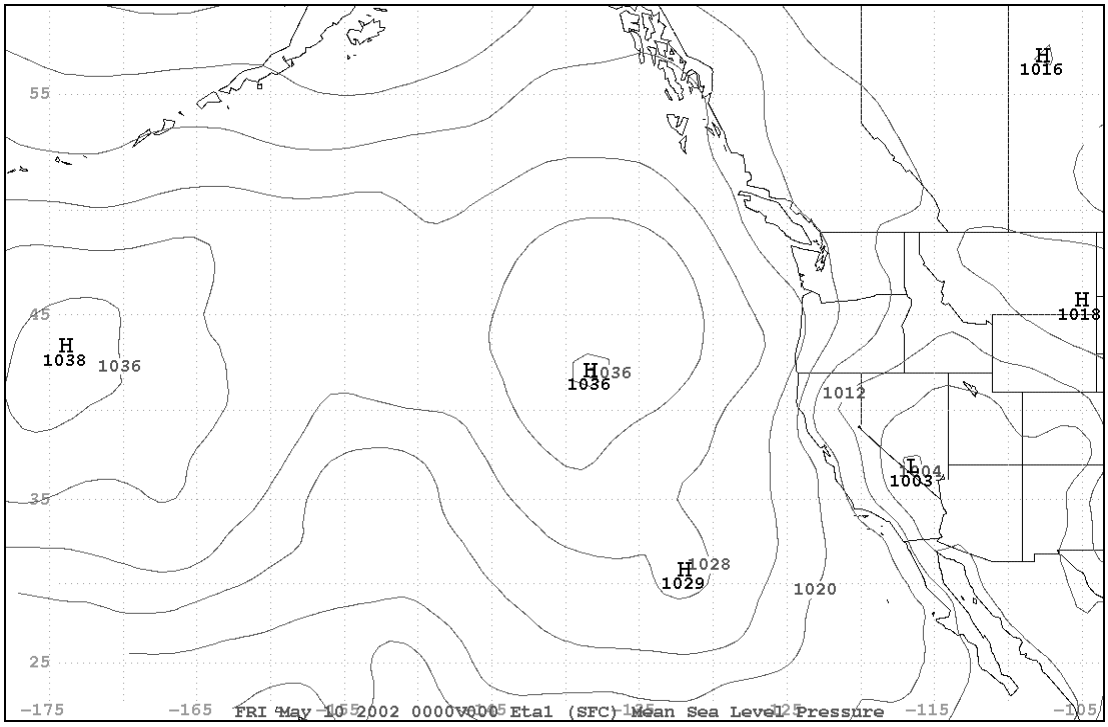

Figure 27. 10MAY02 00Z SLP

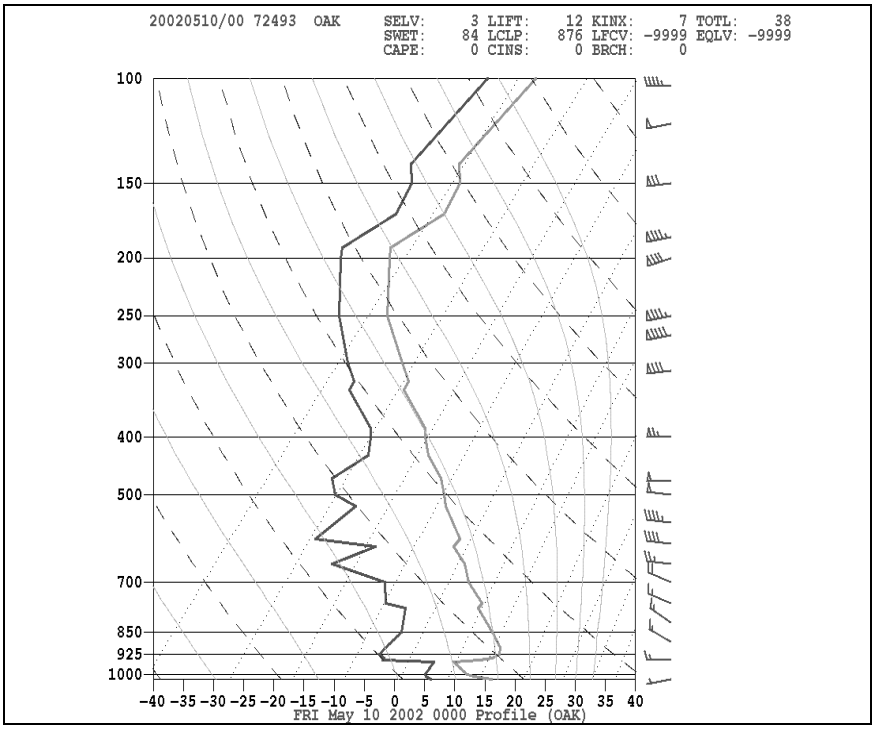

Figure 28. 10MAY02 00Z Oakland Skew-T

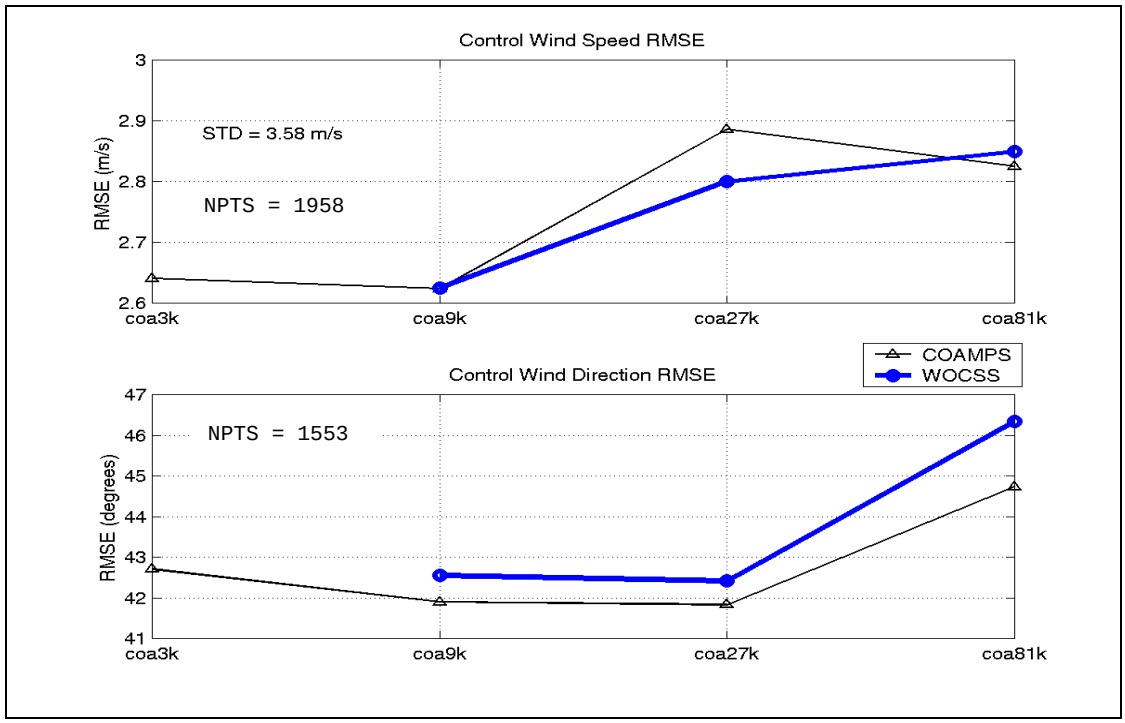

Figure 29. Overall Surface Obs. Control RMSE

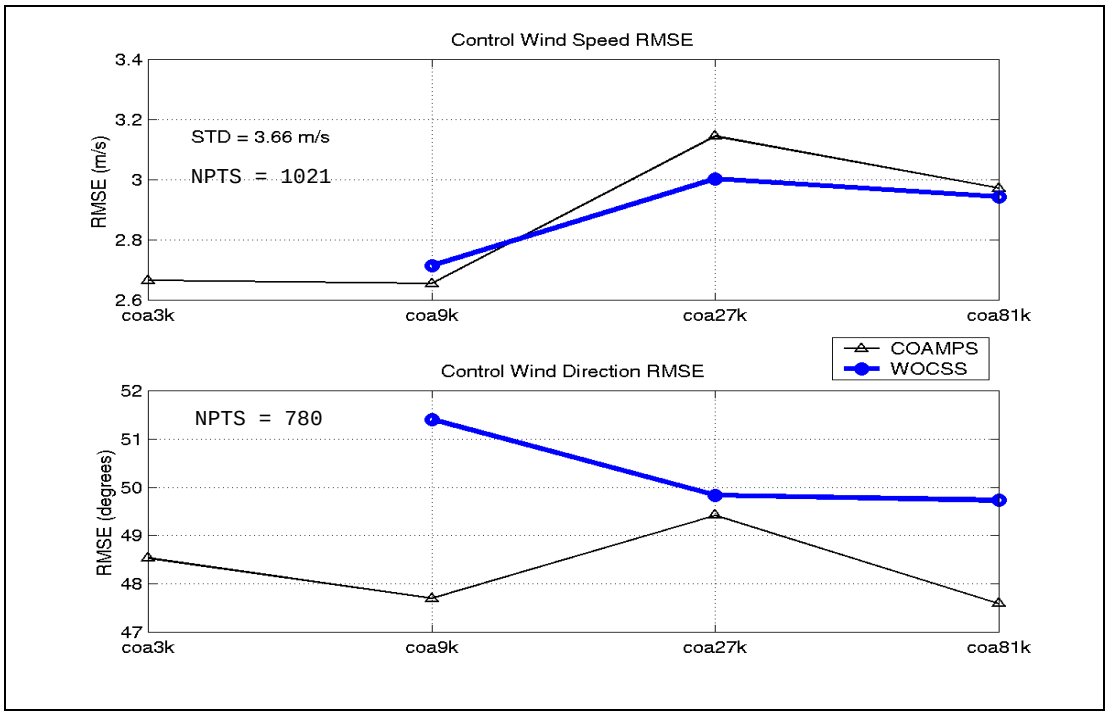

Figure 30. Frontal Surface Obs. Control RMSE

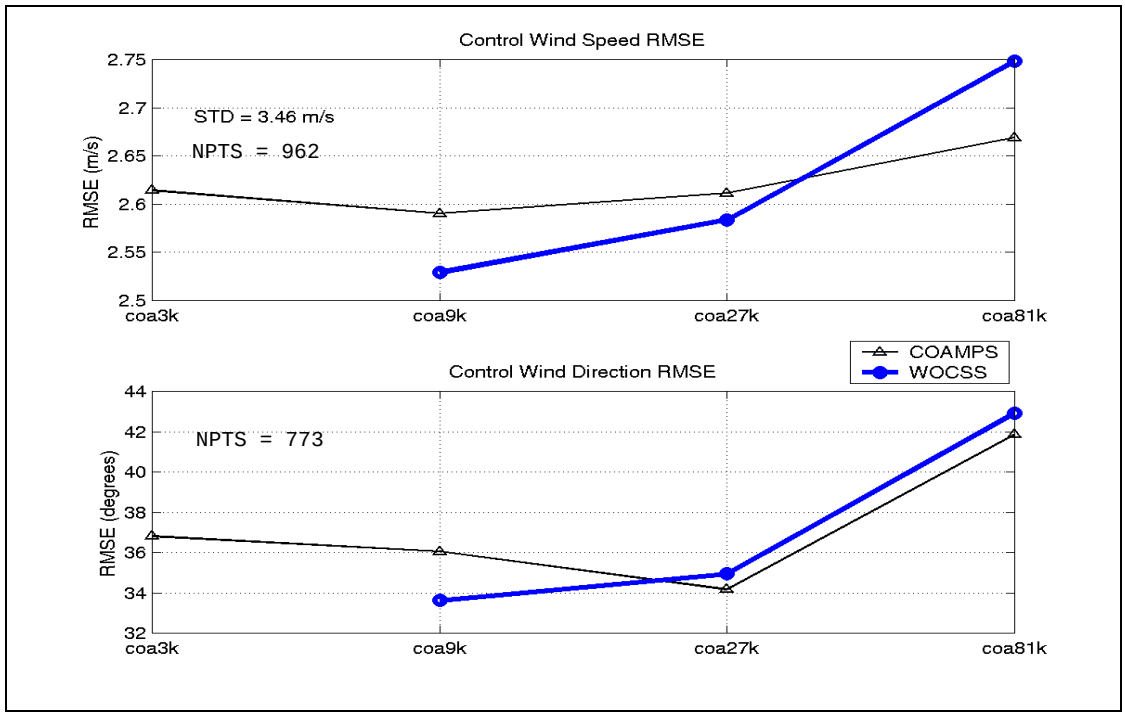

Figure 31. Non-frontal Surface Obs. Control RMSE

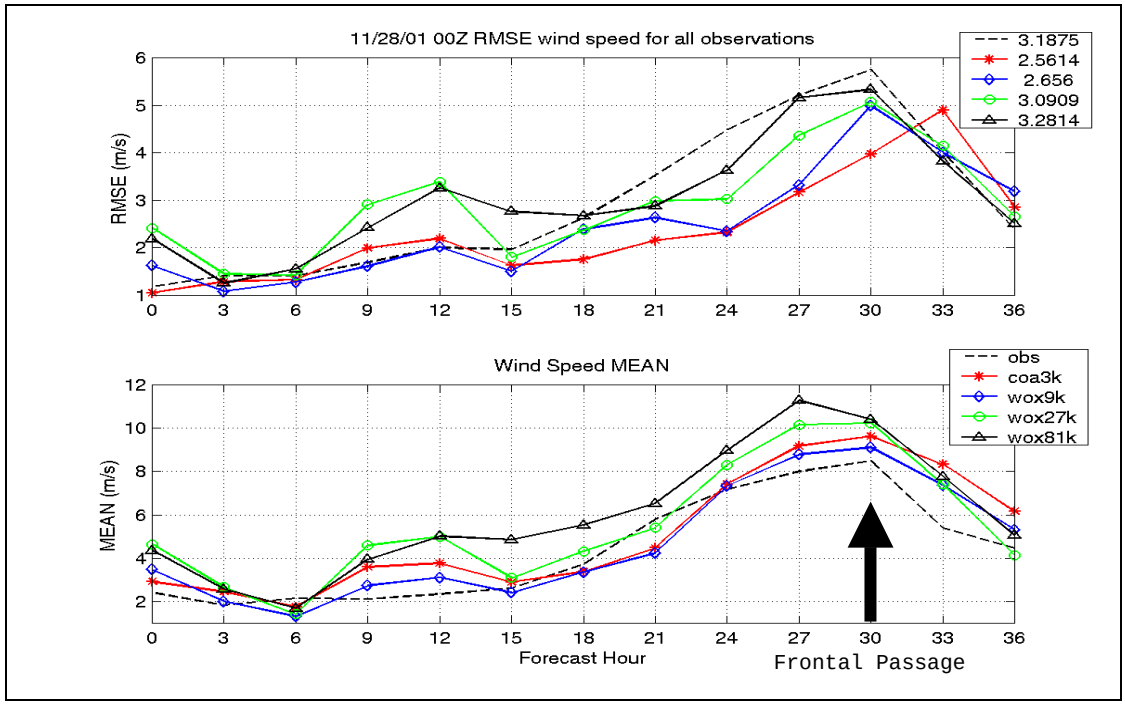

Figure 32. 28NOV01 Wind Speed RMSE and Mean

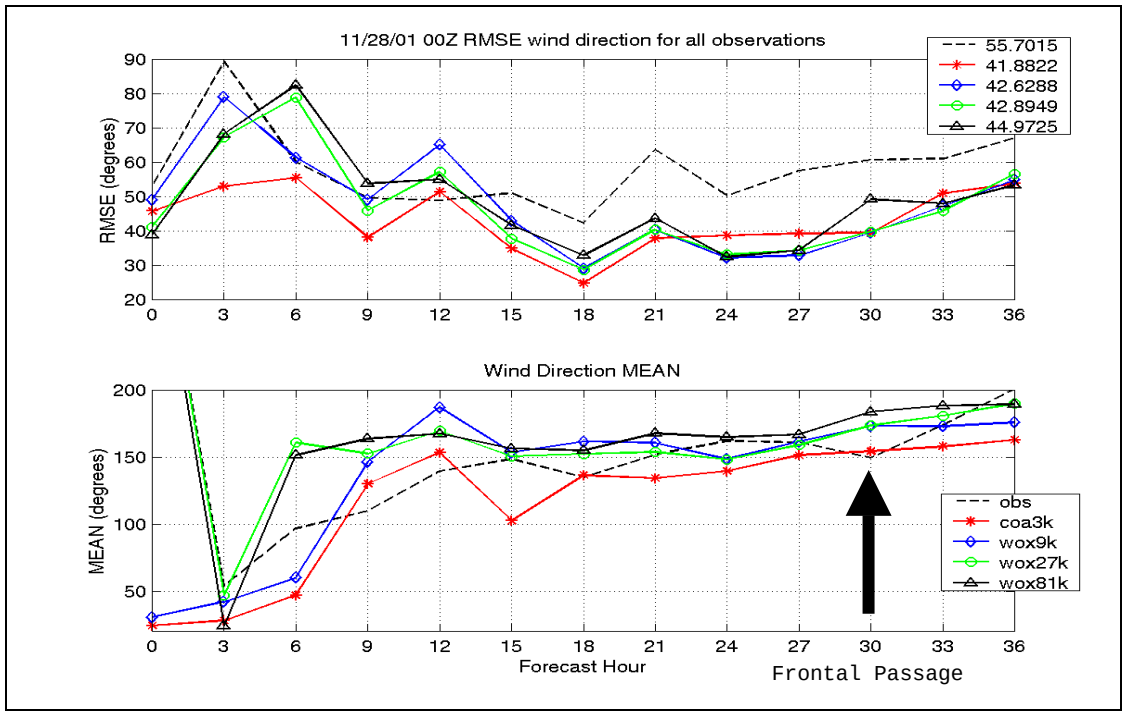

Figure 33. 28NOV01 Wind Direction RMSE and Mean

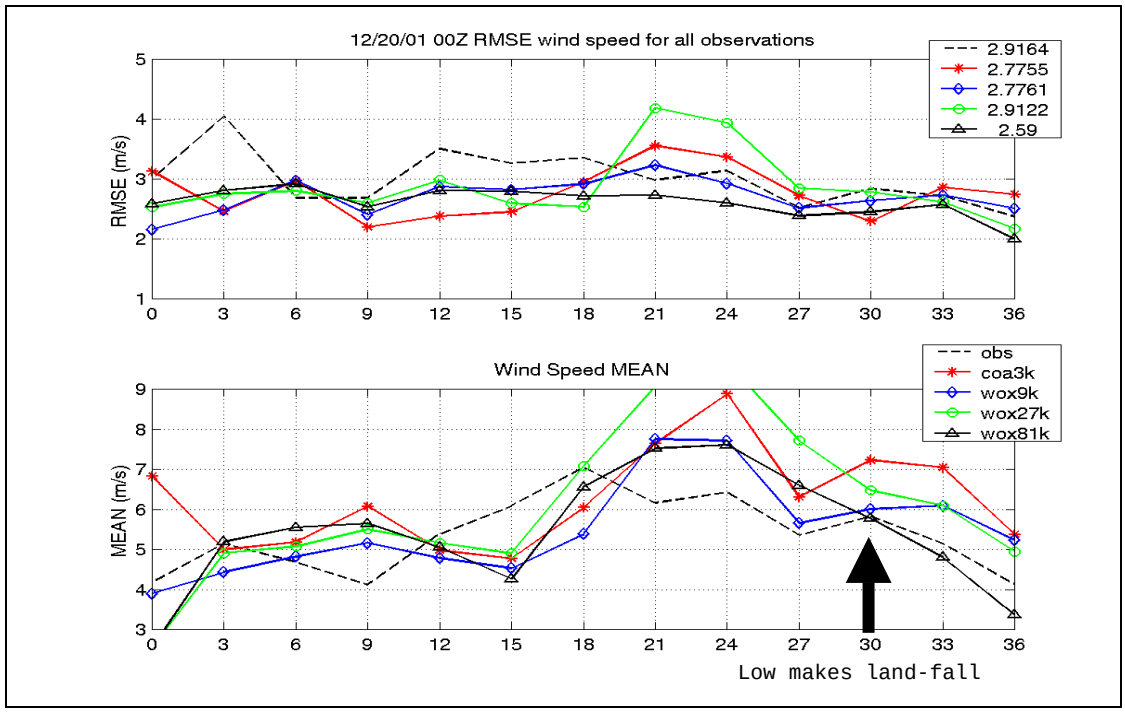

Figure 34. 20DEC01 Wind Speed RMSE and Mean

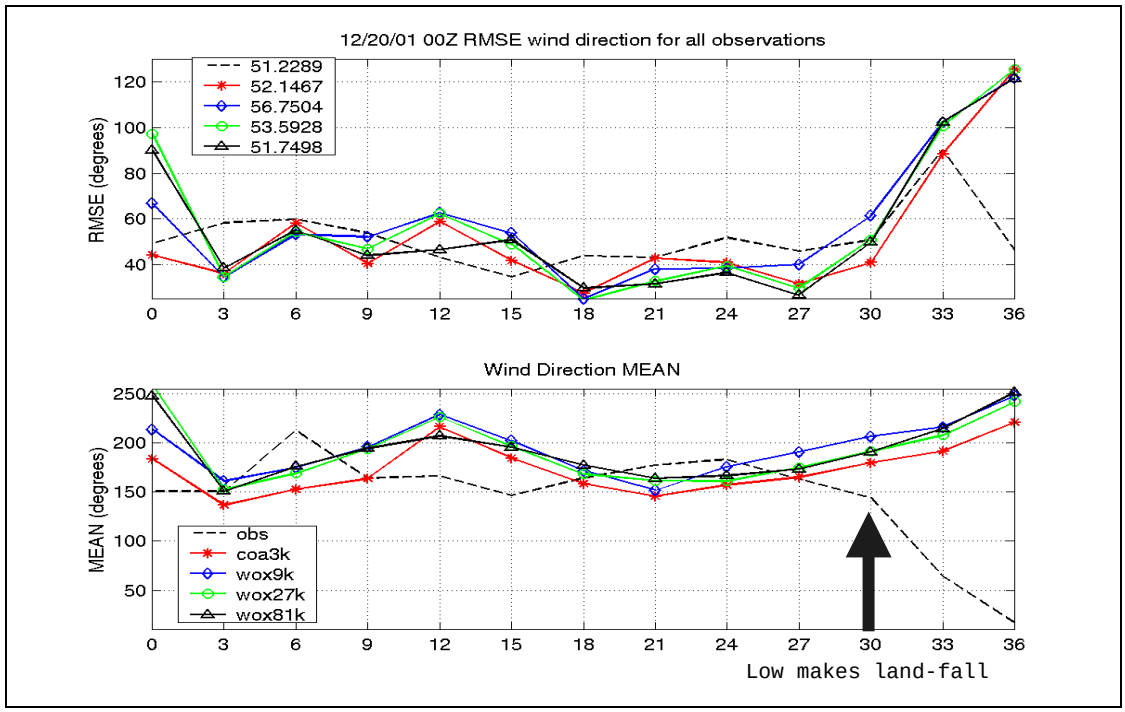

Figure 35. 20DEC01 Wind Direction RMSE and Mean

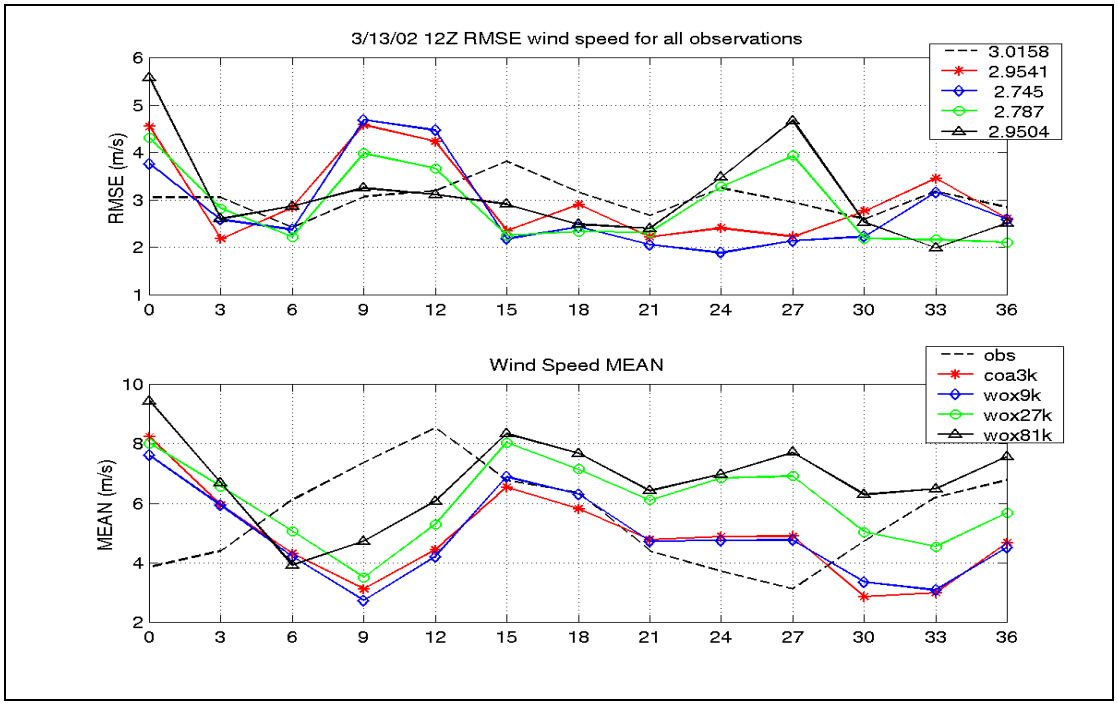

Figure 36. 13MAR02 Wind Speed RMSE and Mean

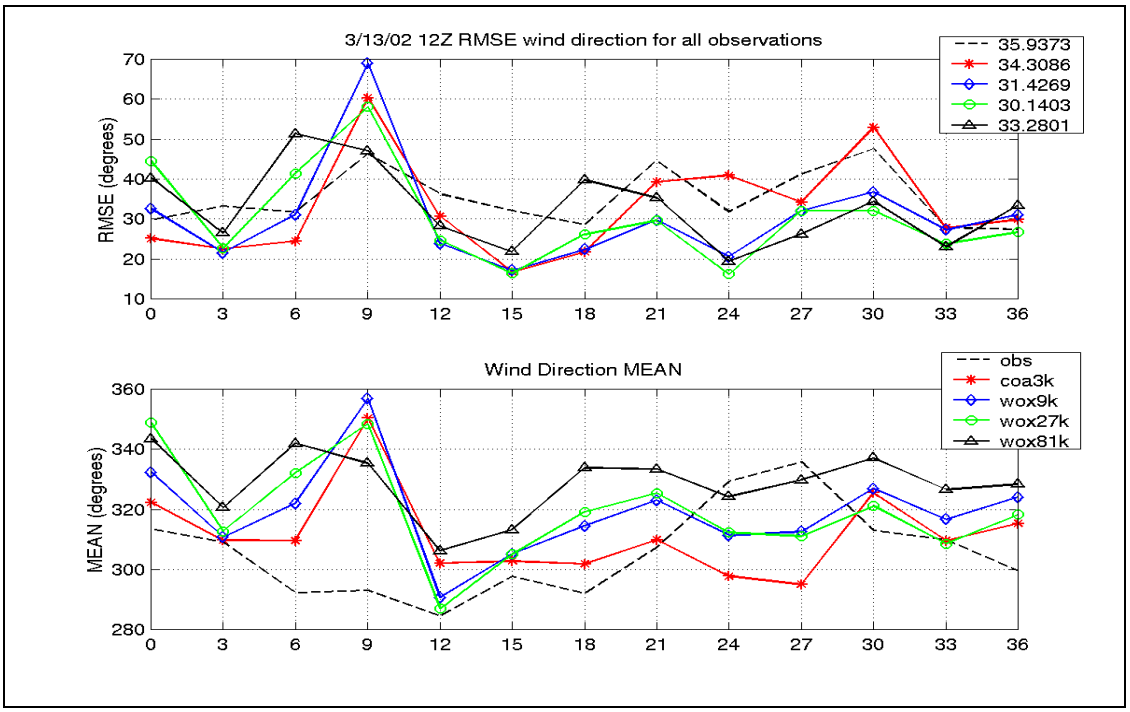

Figure 37. 13MAR02 Wind Direction RMSE and Mean

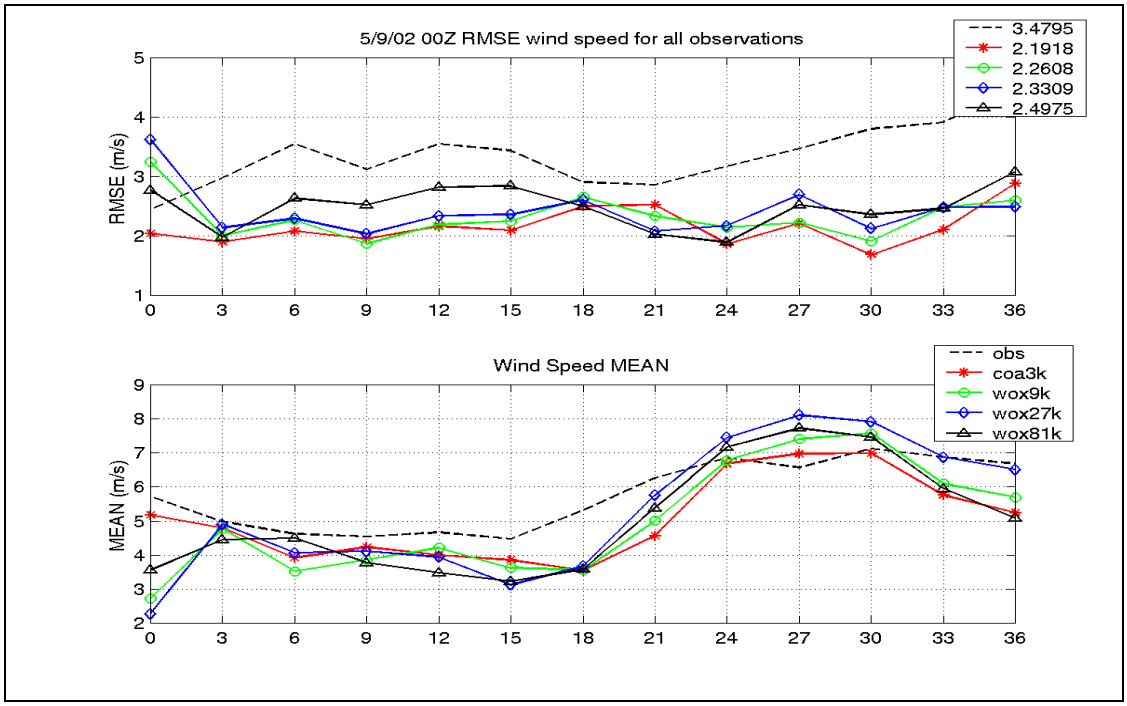

Figure 38. 09MAY02 Wind Speed RMSE and Mean

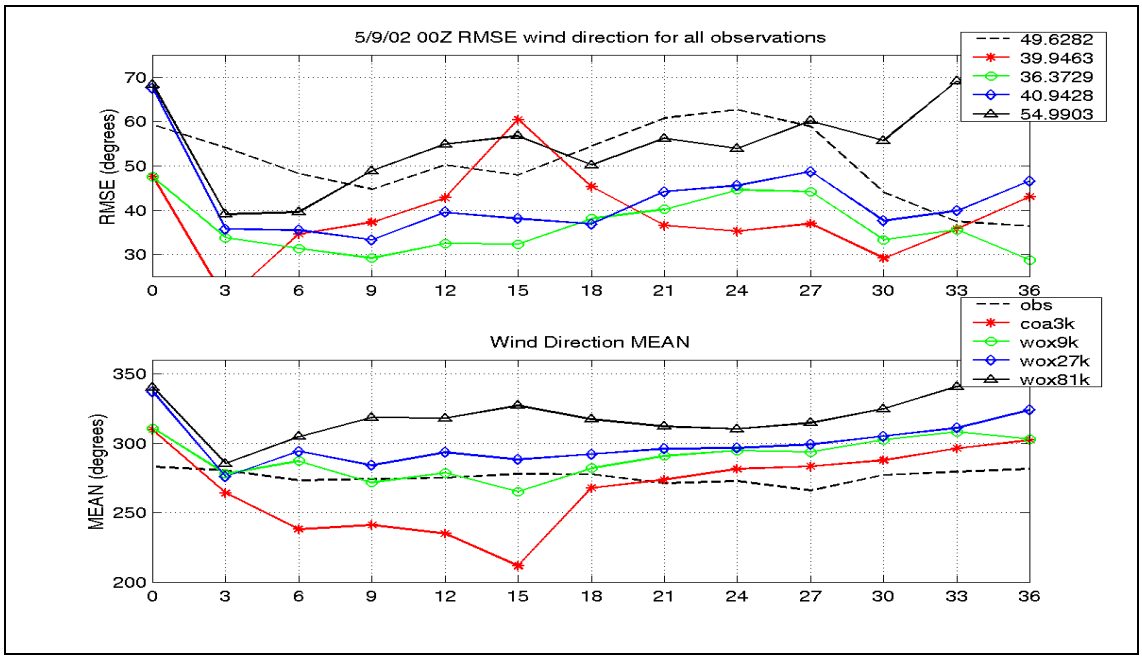

Figure 39. 09MAY02 Wind Direction RMSE and Mean

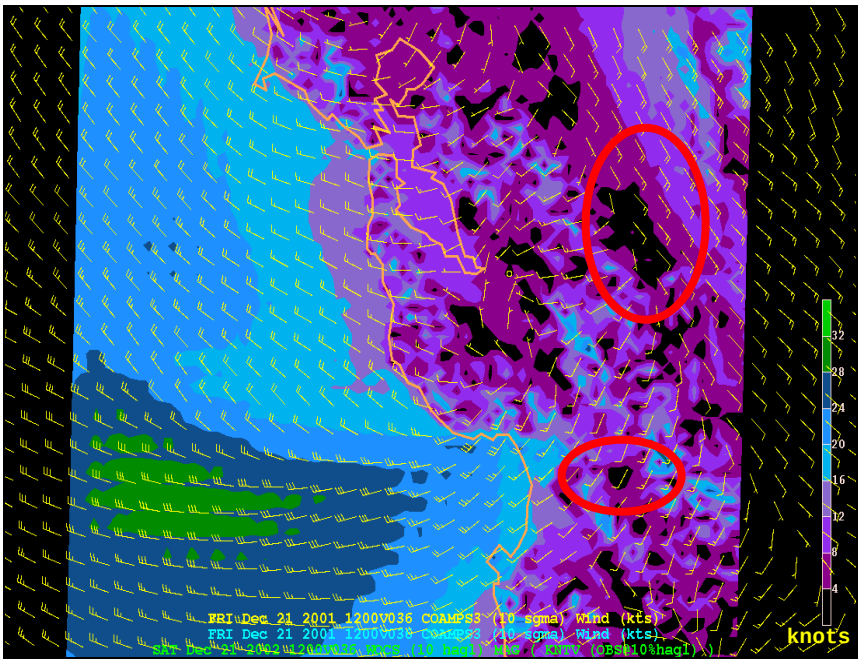

Figure 40. 21DEC01 12Z wox9k Isotachs and coa9k 10 m Winds

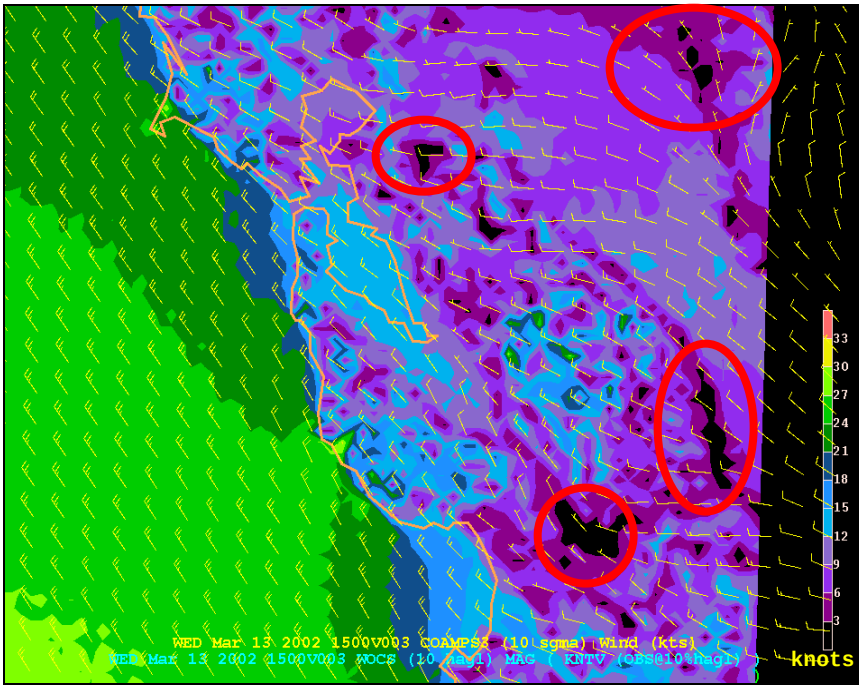

Figure 41. 13MAR02 15Z wox9k Isotachs and coa9k 10 m Winds

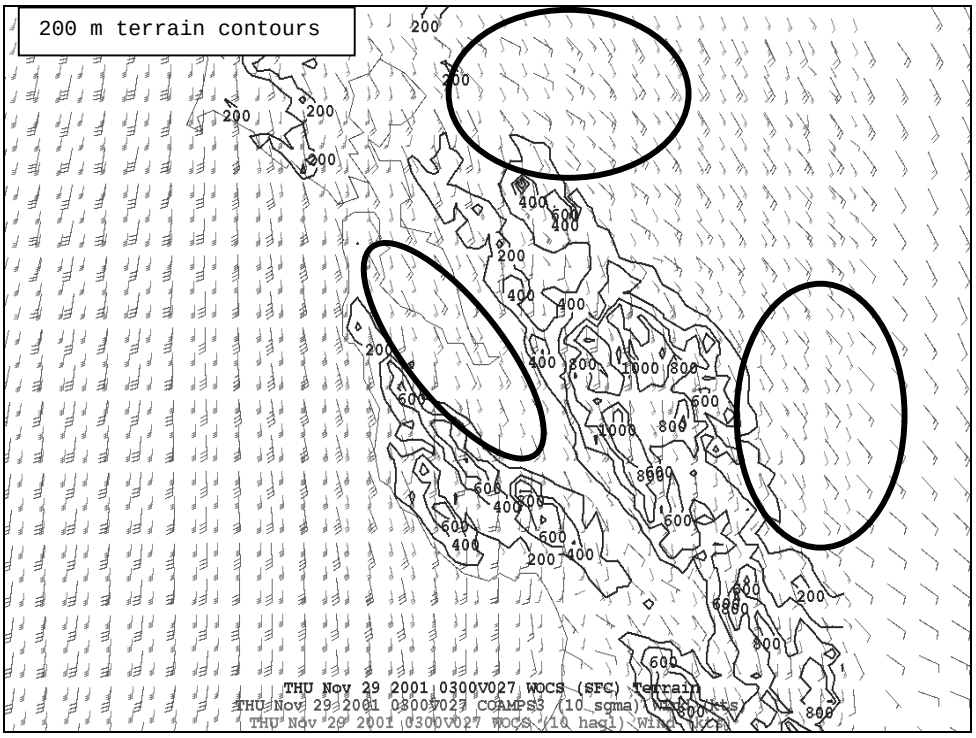

Figure 42. 29NOV01 03Z wox9k (Small Barbs) and coa9k (Large Barbs) 10 m Winds

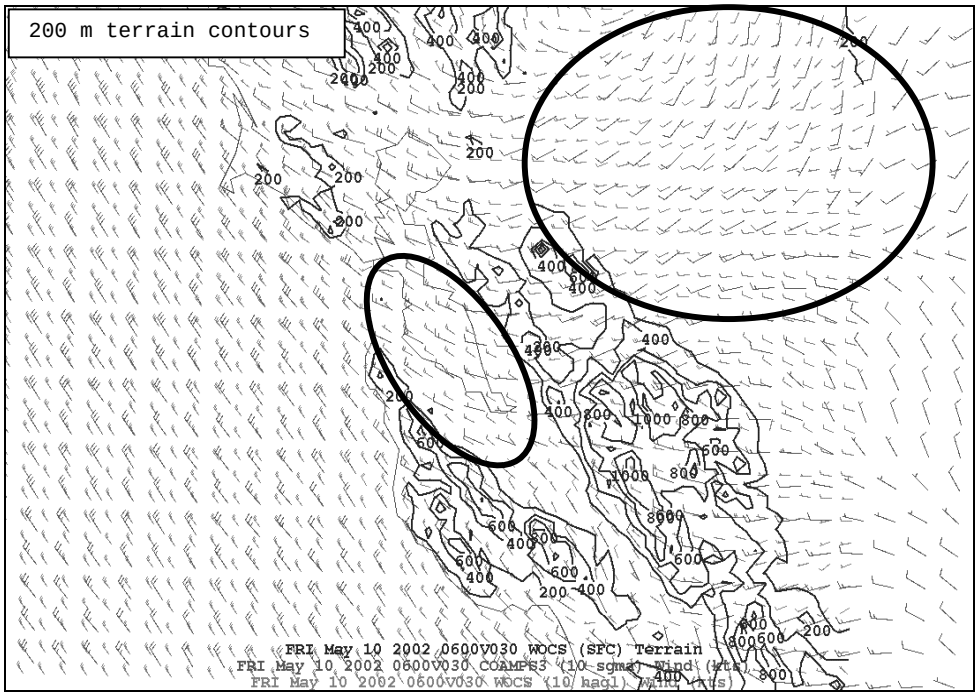

Figure 43. 09MAY02 wox9k (Small Barbs) and coa9k (Large Barbs) 10 m Winds

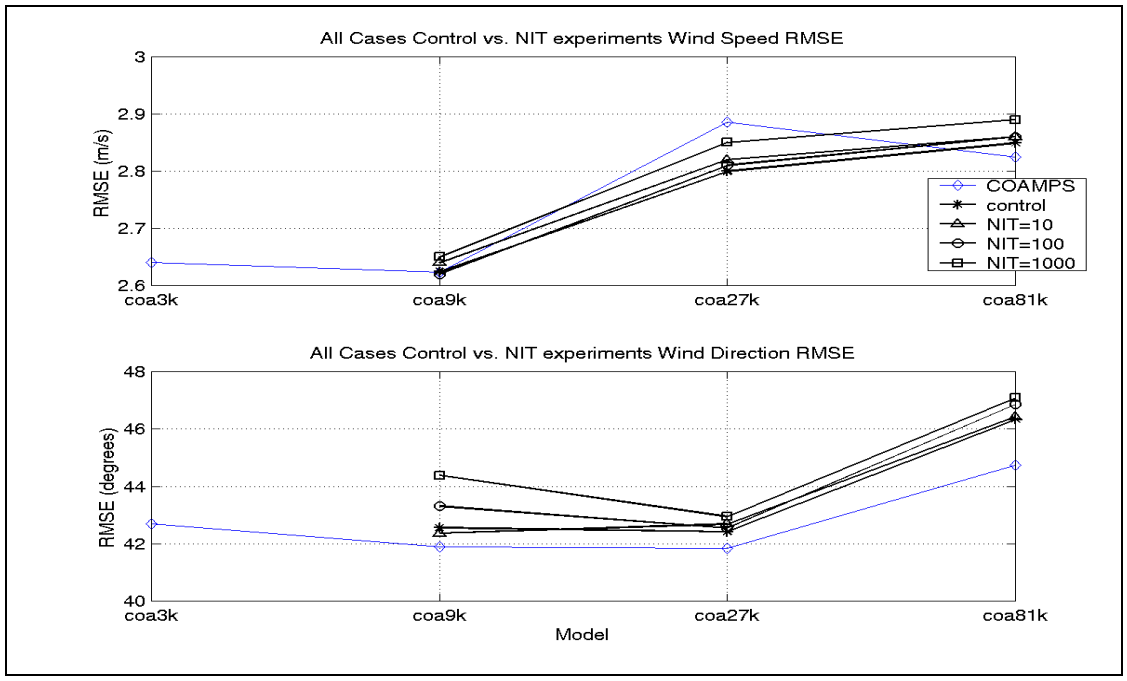

Figure 44. Overall RMSE for NIT = 10, 100, 1000

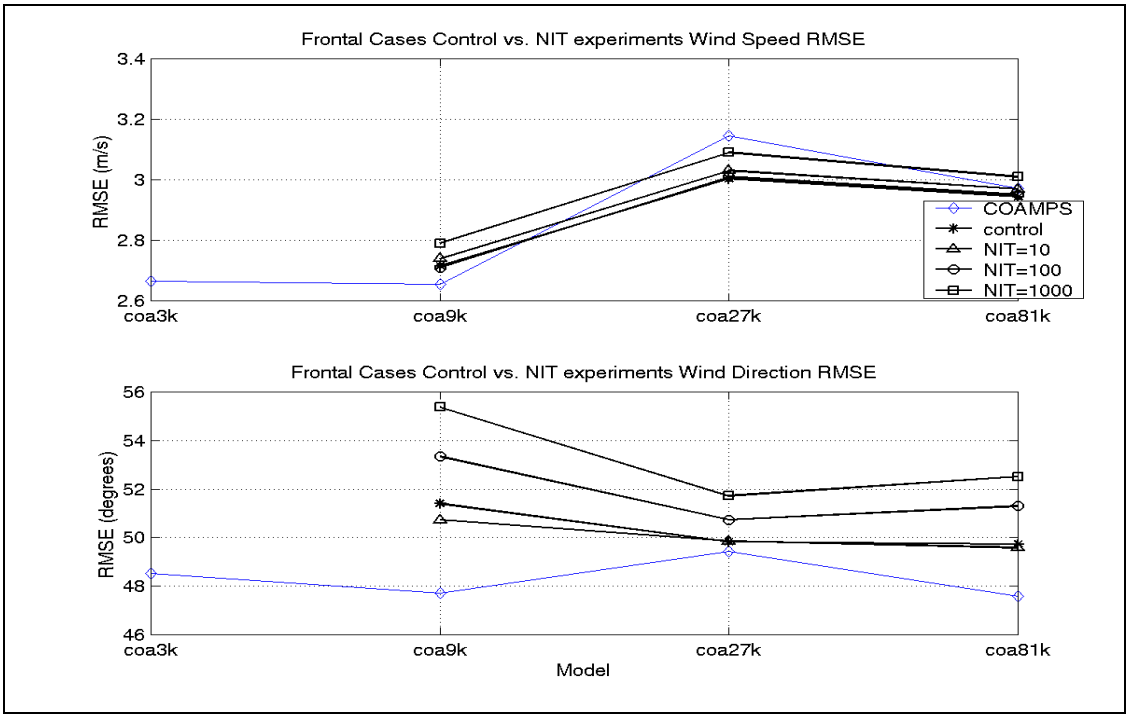

Figure 45. Frontal RMSE for NIT = 10, 100, 1000

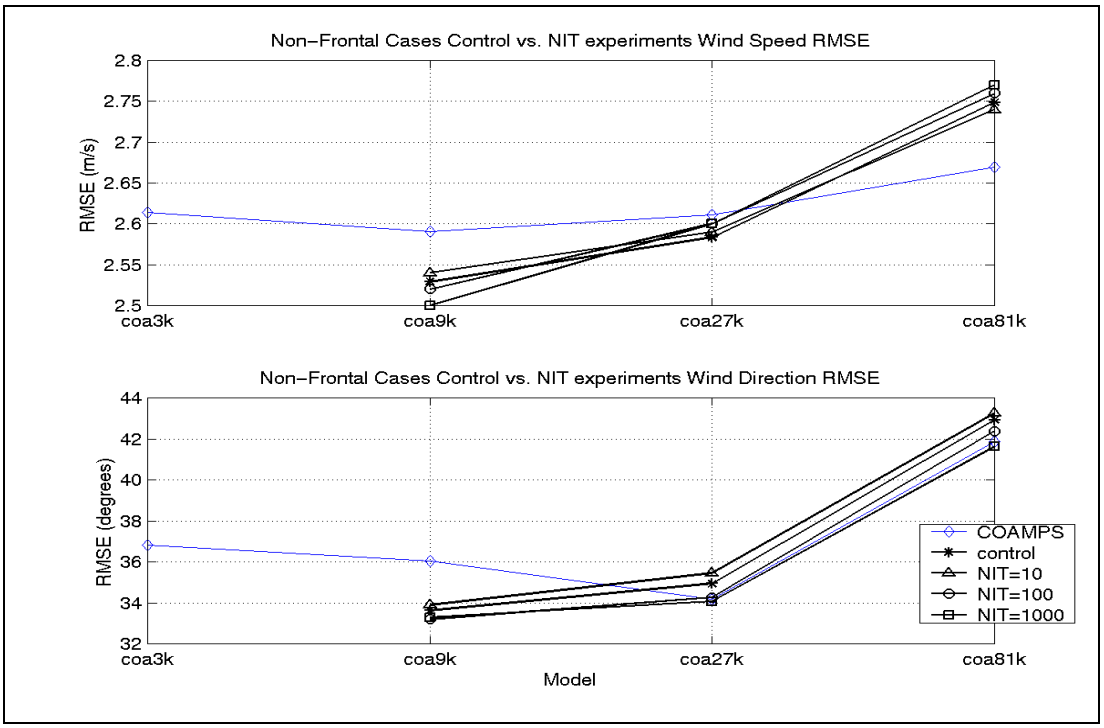

Figure 46. Non-frontal RMSE for NIT = 10, 100, 1000

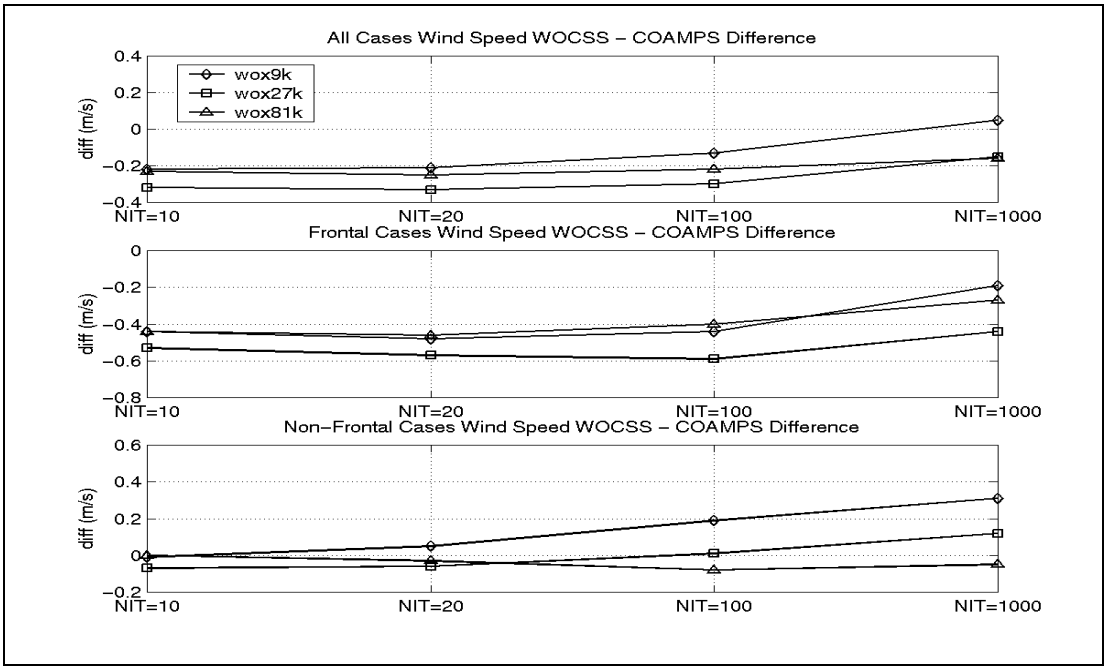

Figure 47. Difference (WOCSS-COAMPS) in Wind Speed for NIT = 10, 100, 1000

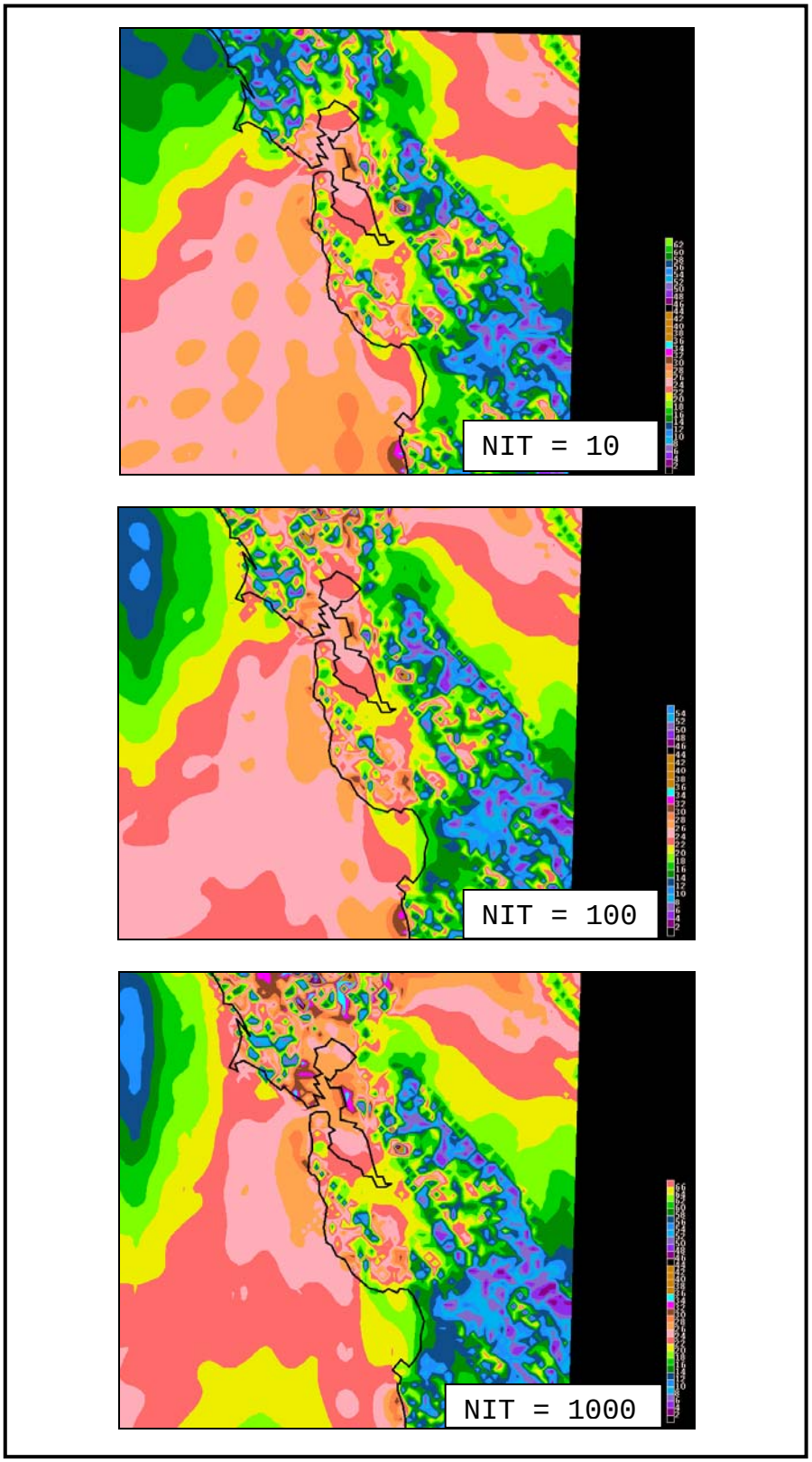

Figure 48. 29NOV01 06Z wox27k Isotachs at NIT = 10, 100, 1000

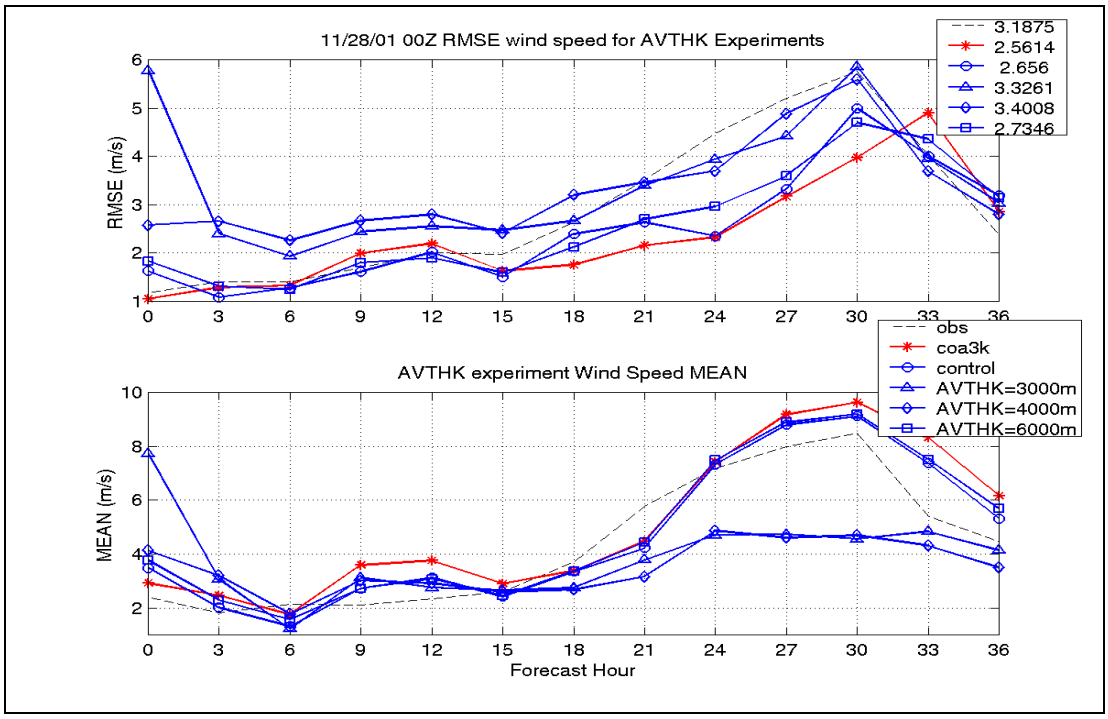

Figure 49. 28NOV01 00Z RMSE Wind Spd. AVTHK Experiments

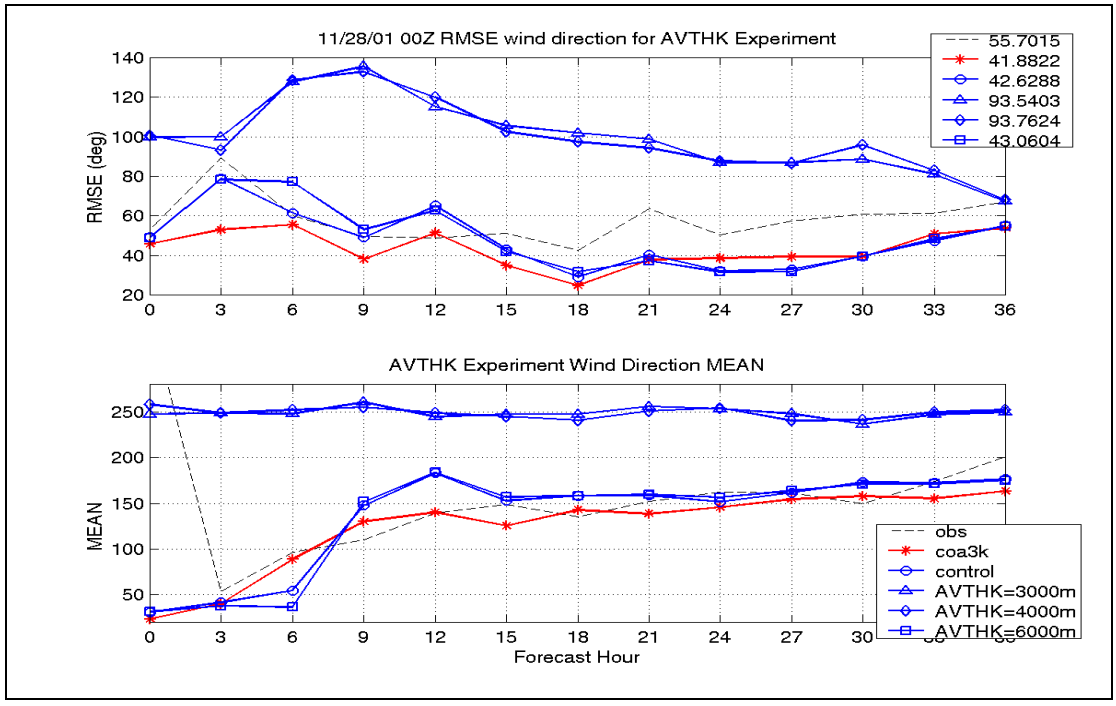

Figure 50. 28NOV01 00Z RMSE Wind Dir. AVTHK Experiments

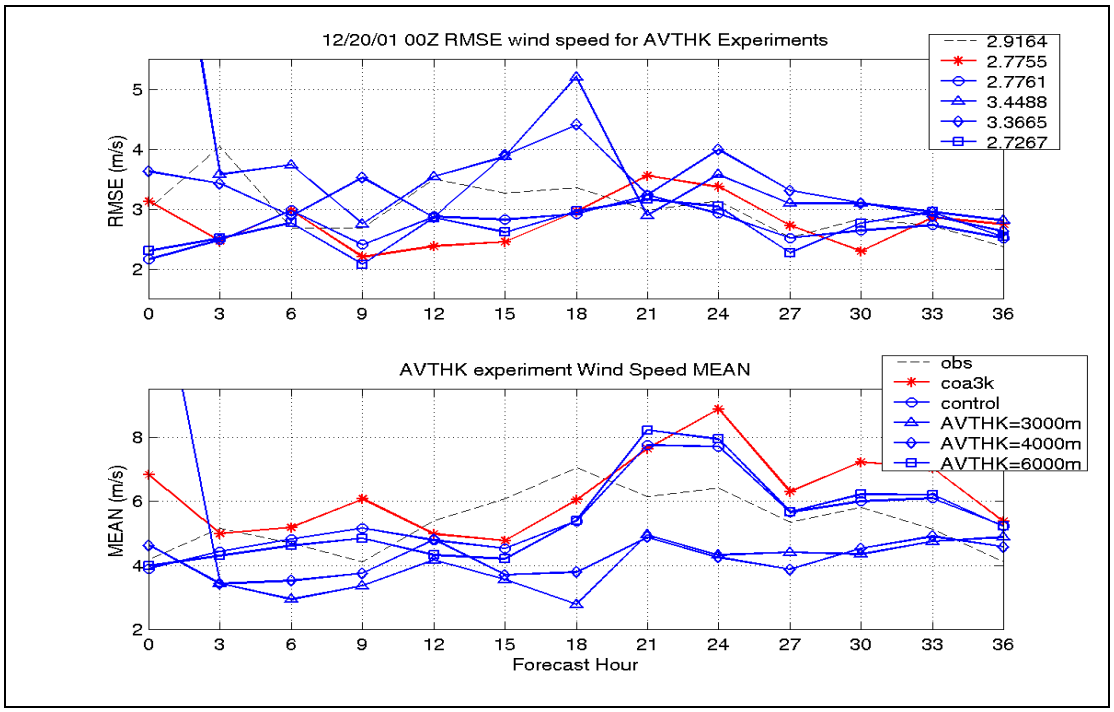

Figure 51. 20DEC01 00Z RMSE Wind Spd. AVTHK Experiments

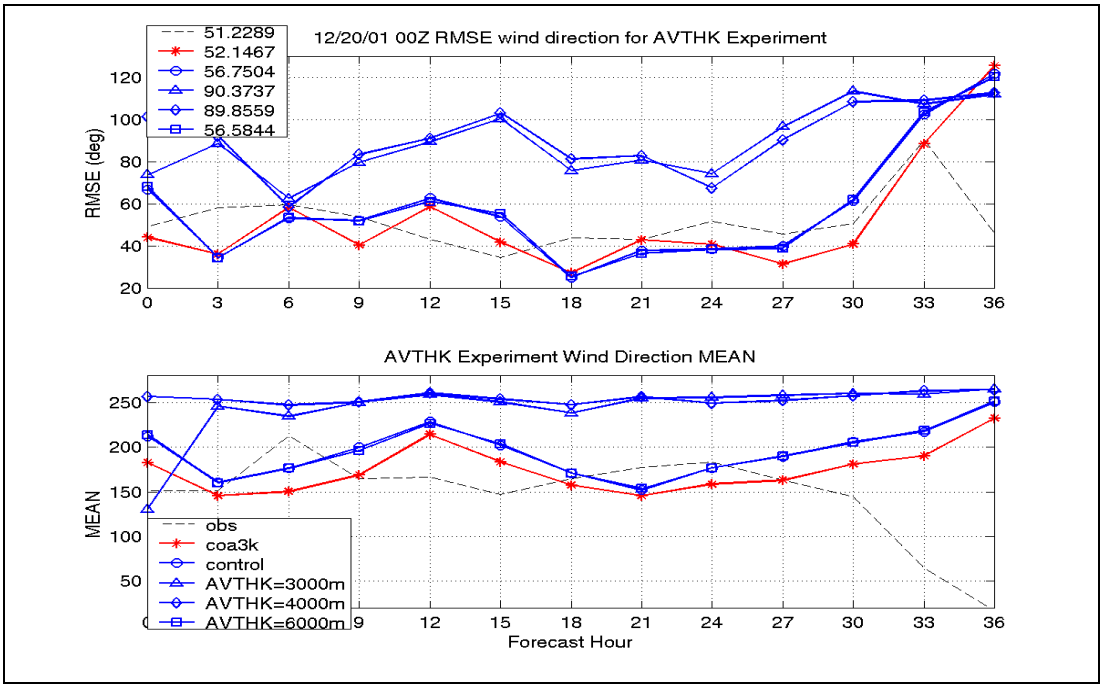

Figure 52. 20DEC01 00Z RMSE Wind Dir. AVTHK Experiments

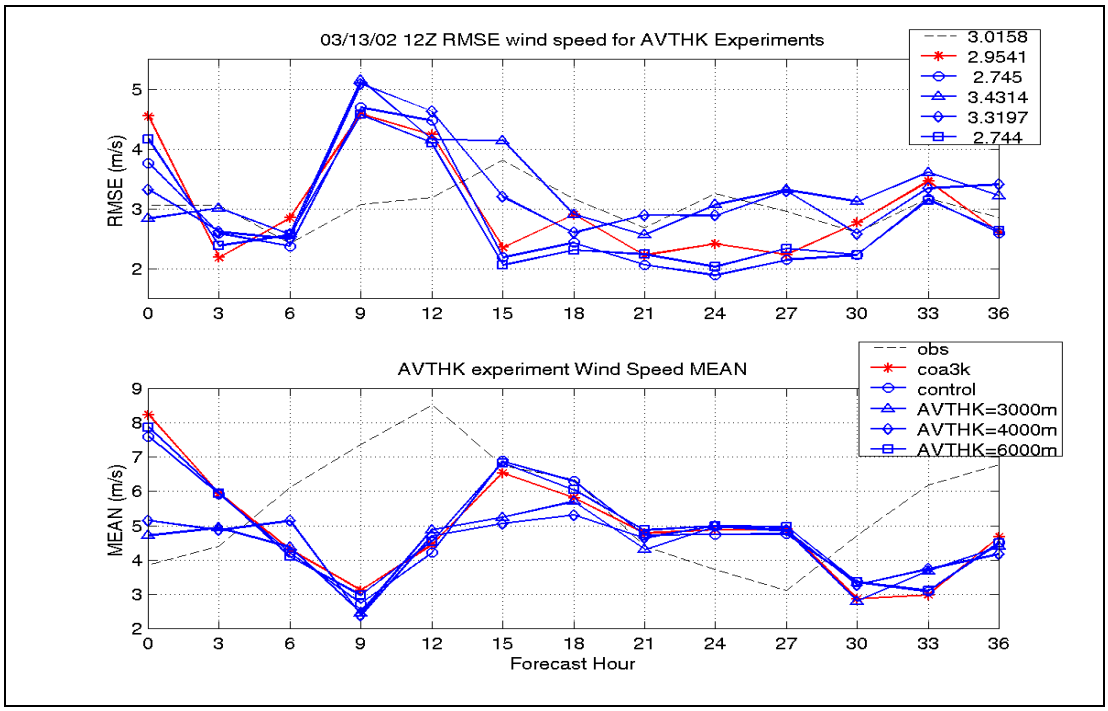

Figure 53. 13MAR02 12Z RMSE Wind Spd. AVTHK Experiments

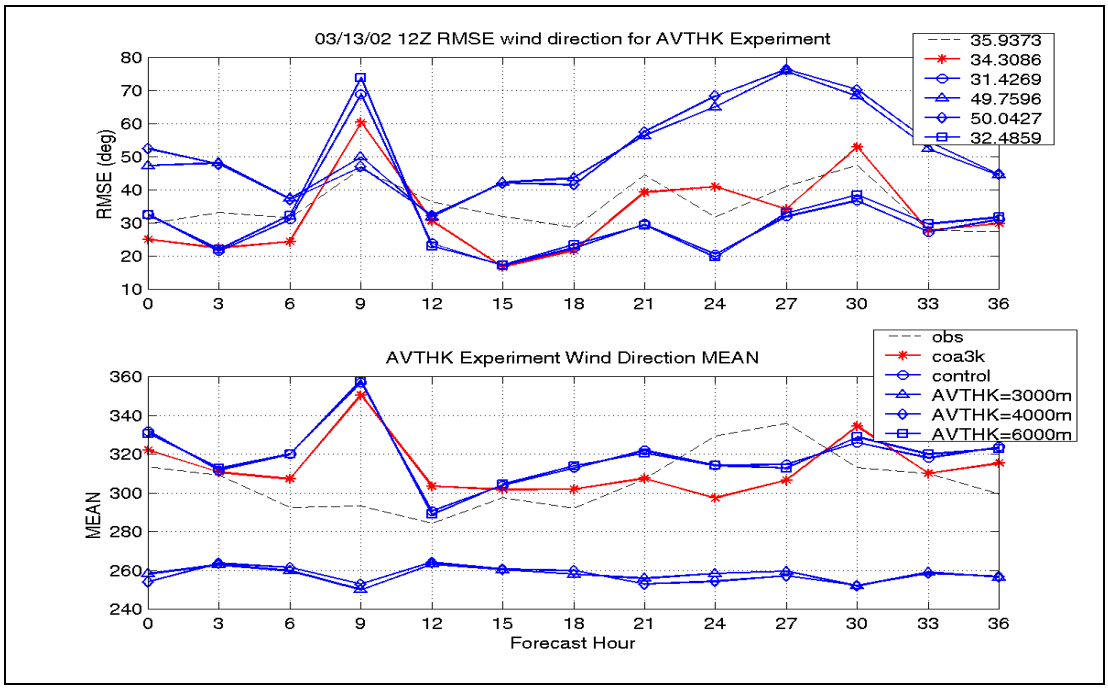

Figure 54. 13MAR02 12Z RMSE Wind Dir. AVTHK Experiments

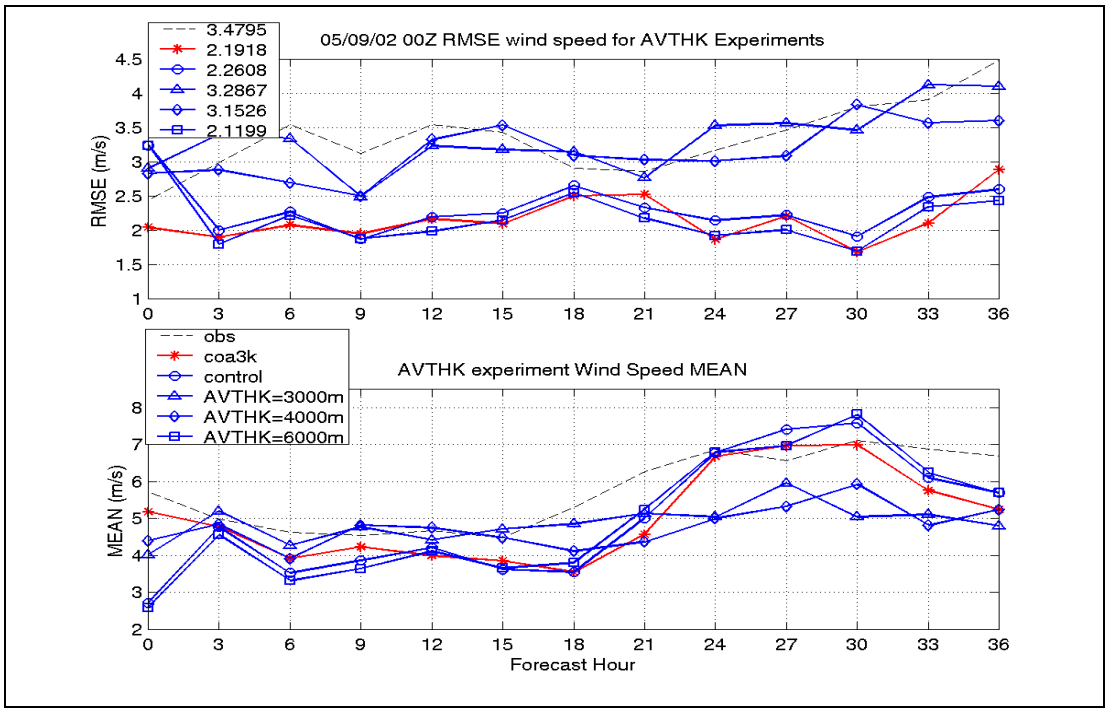

Figure 55. 09MAY02 00Z RMSE Wind Spd. AVTHK Experiments

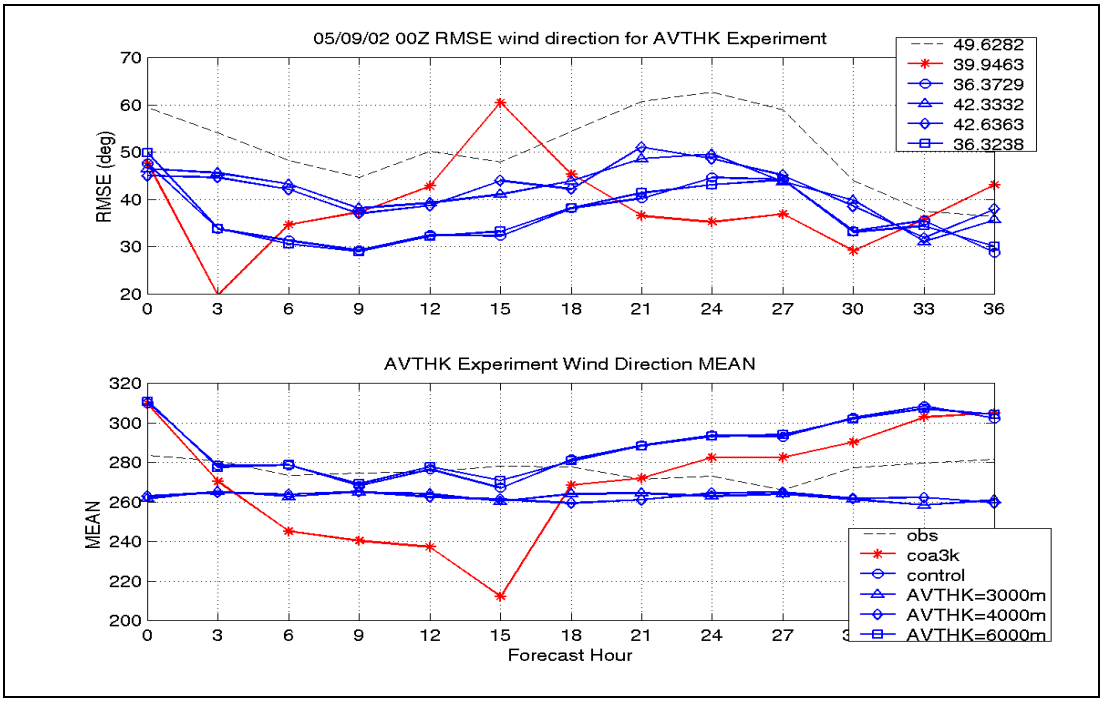

Figure 56. 09MAY02 00Z RMSE Wind Dir. AVTHK Experiments

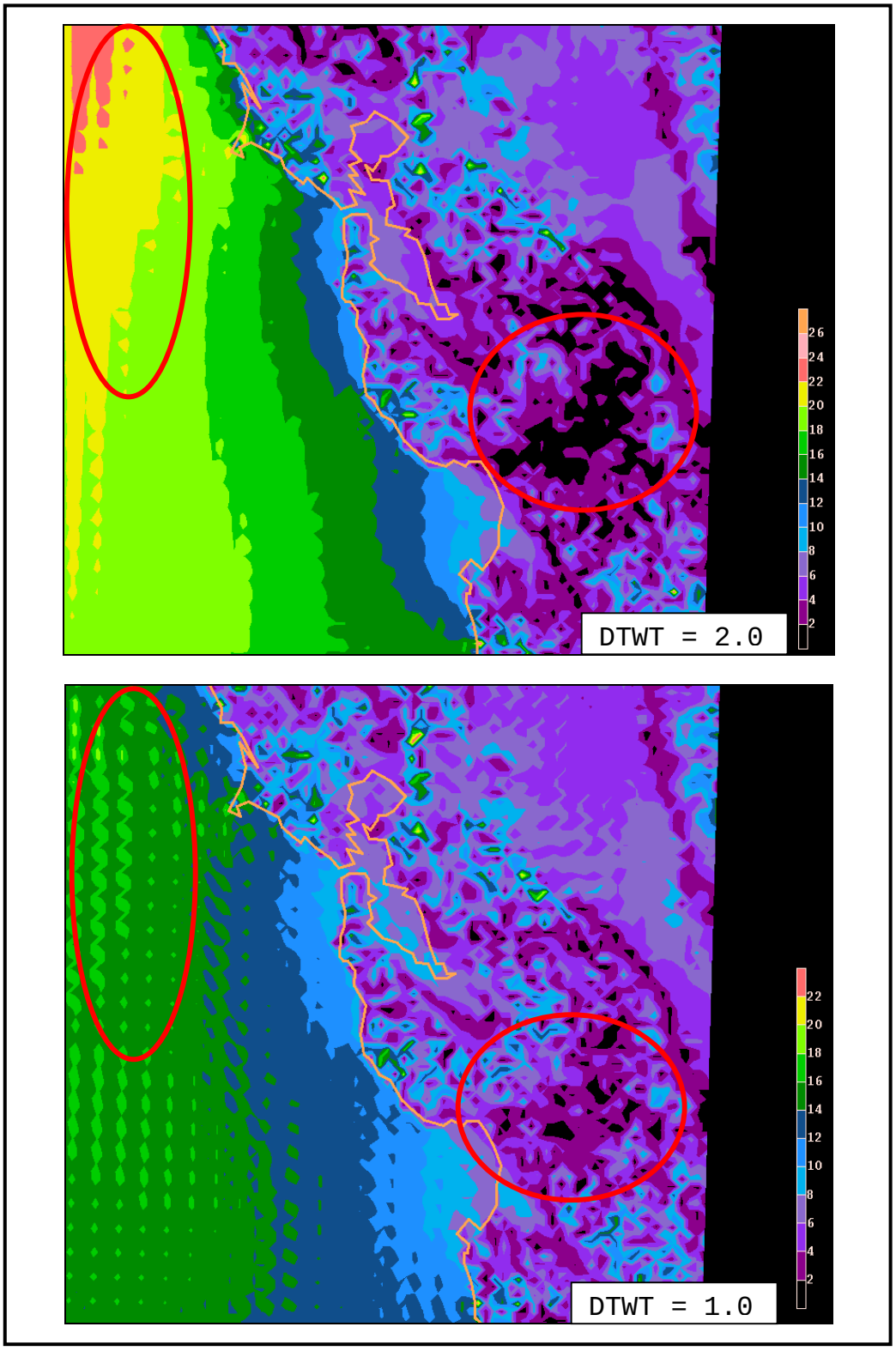

Figure 57. 09MAY02 06Z Isotachs 10 m DTWT Experiments

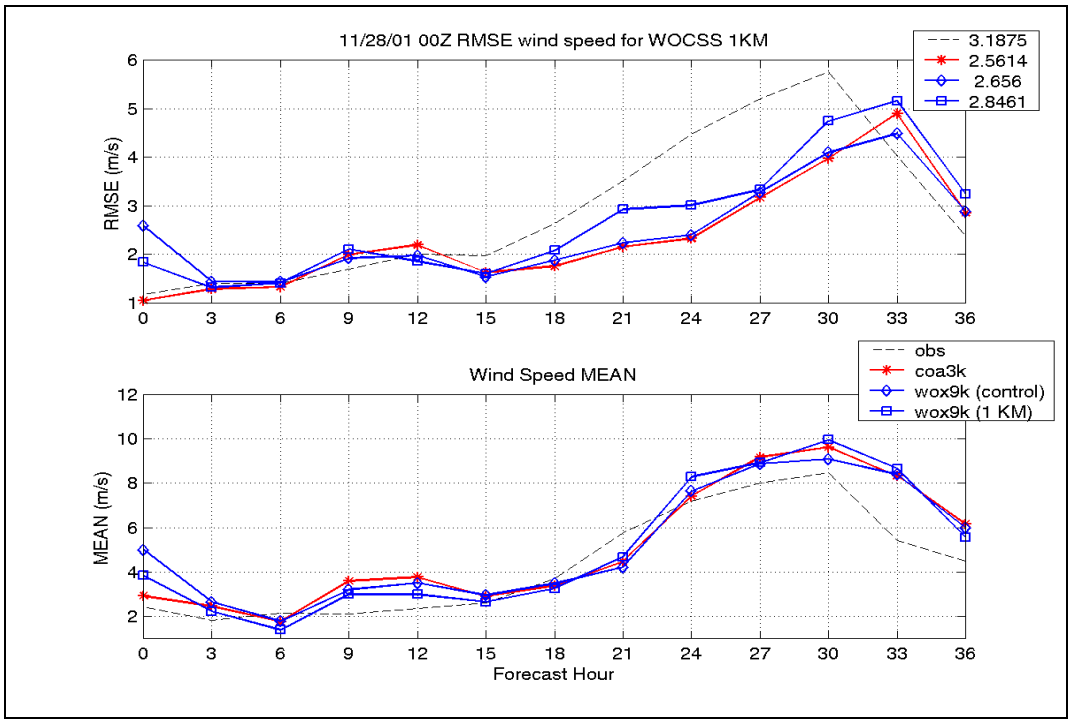

Figure 58. 28NOV01 WOCSS 1KM Experiment Wind Speed RMSE

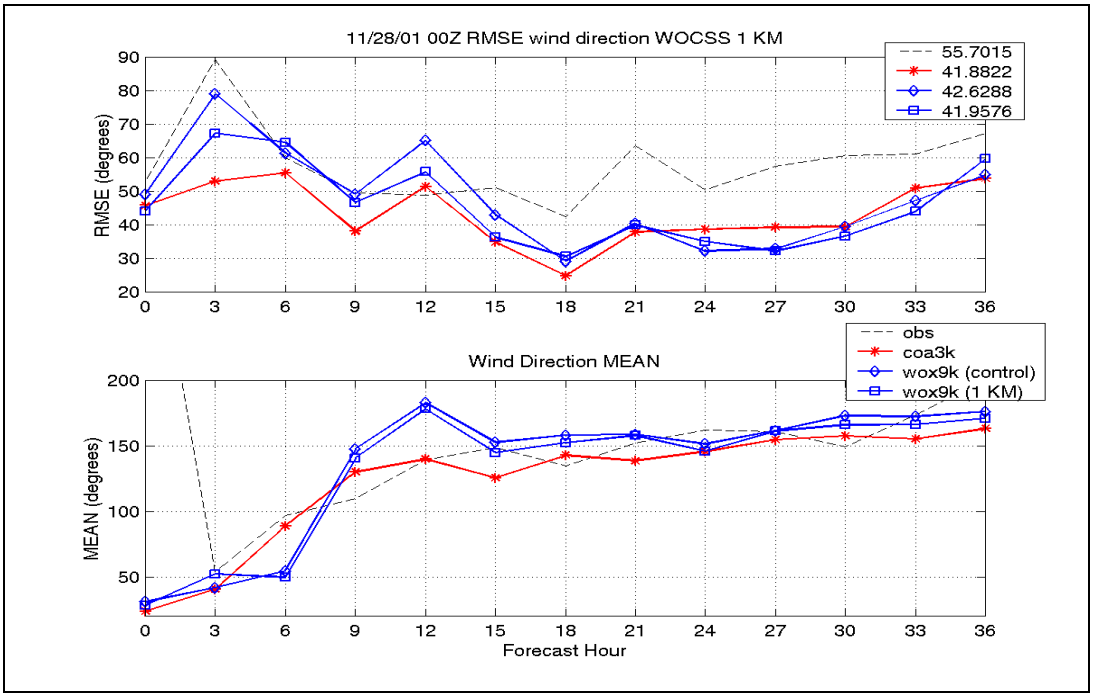

Figure 59. 28NOV01 WOCSS 1KM Wind Direction RMSE

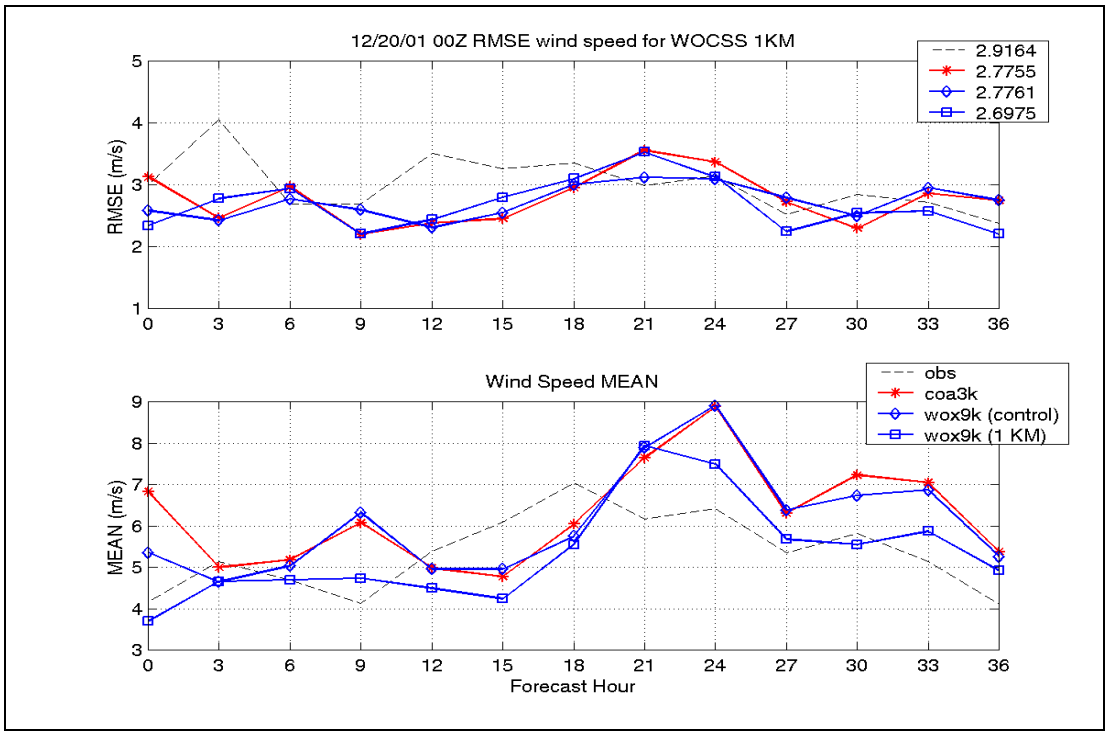

Figure 60. 20DEC01 WOCSS 1KM Experiment Wind Speed RMSE

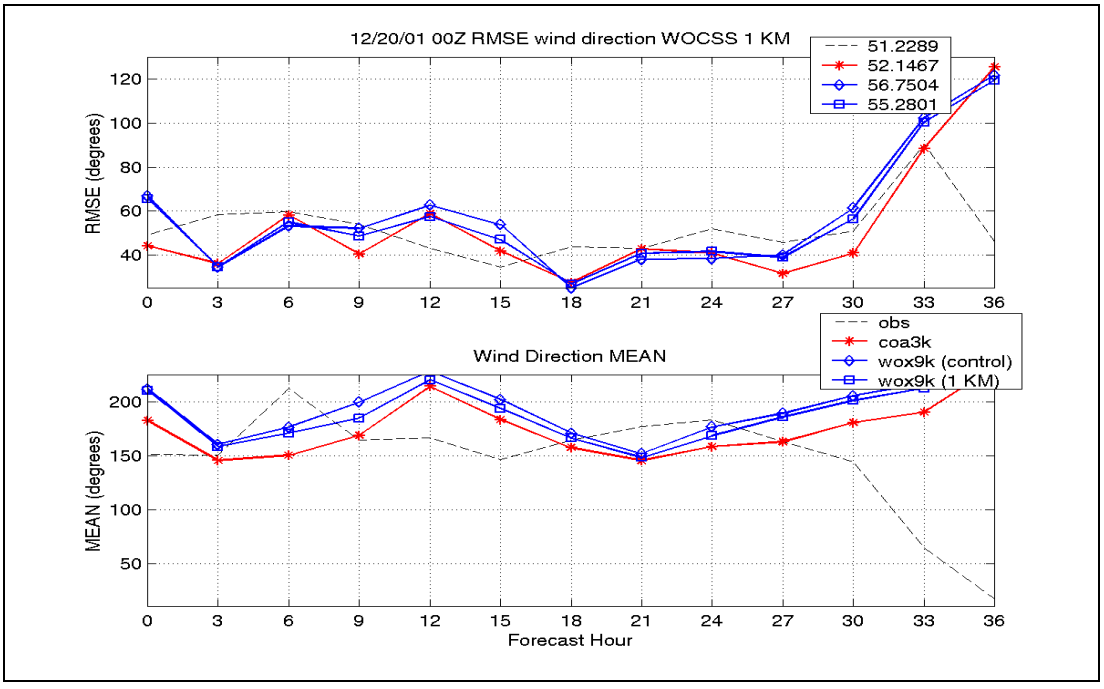

Figure 61. 20DEC01 WOCSS 1KM Wind Direction RMSE

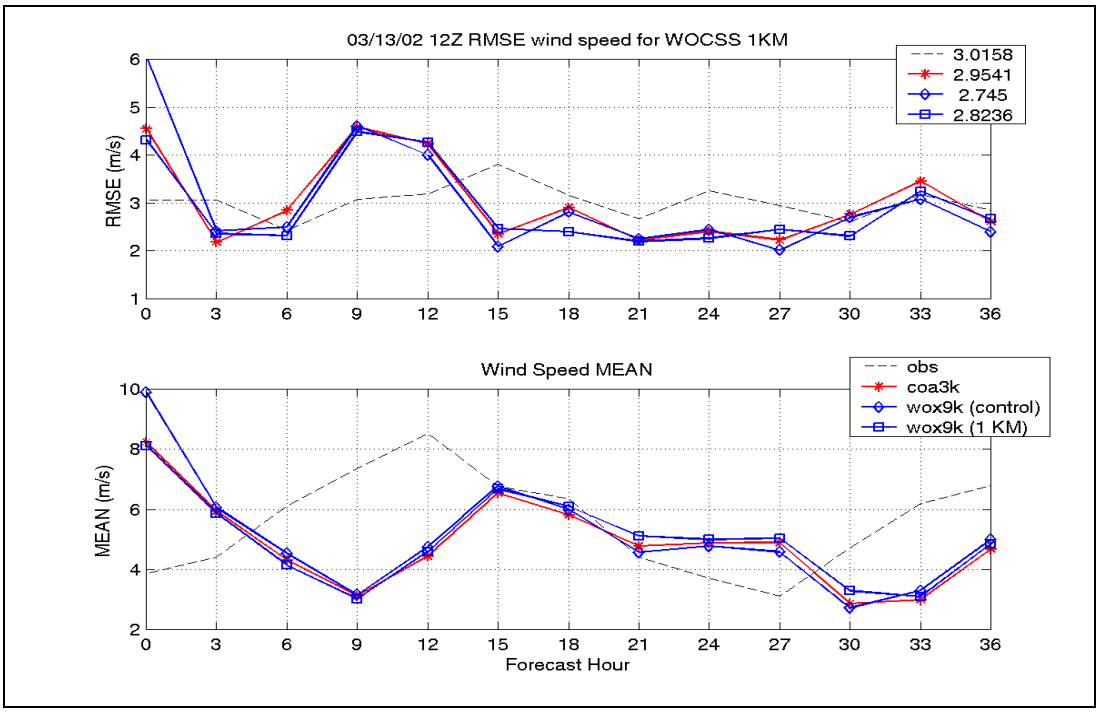

Figure 62. 13MAR02 WOCSS 1KM Wind Speed RMSE

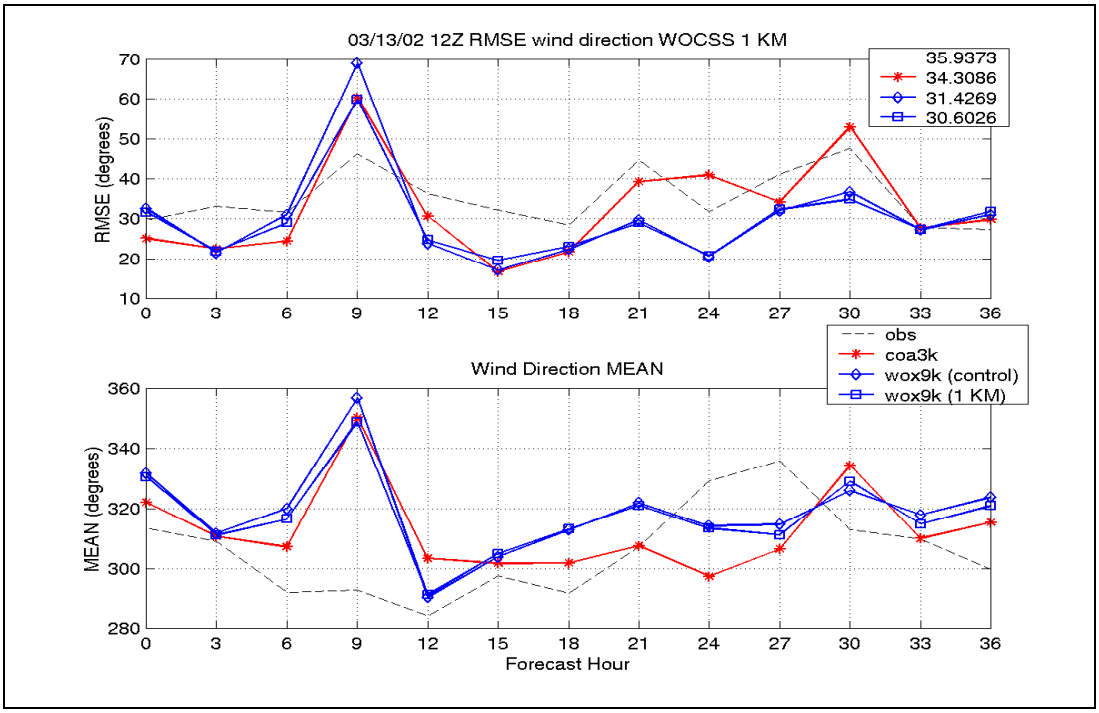

Figure 63. 13MAR02 WOCSS 1KM Wind Direction RMSE

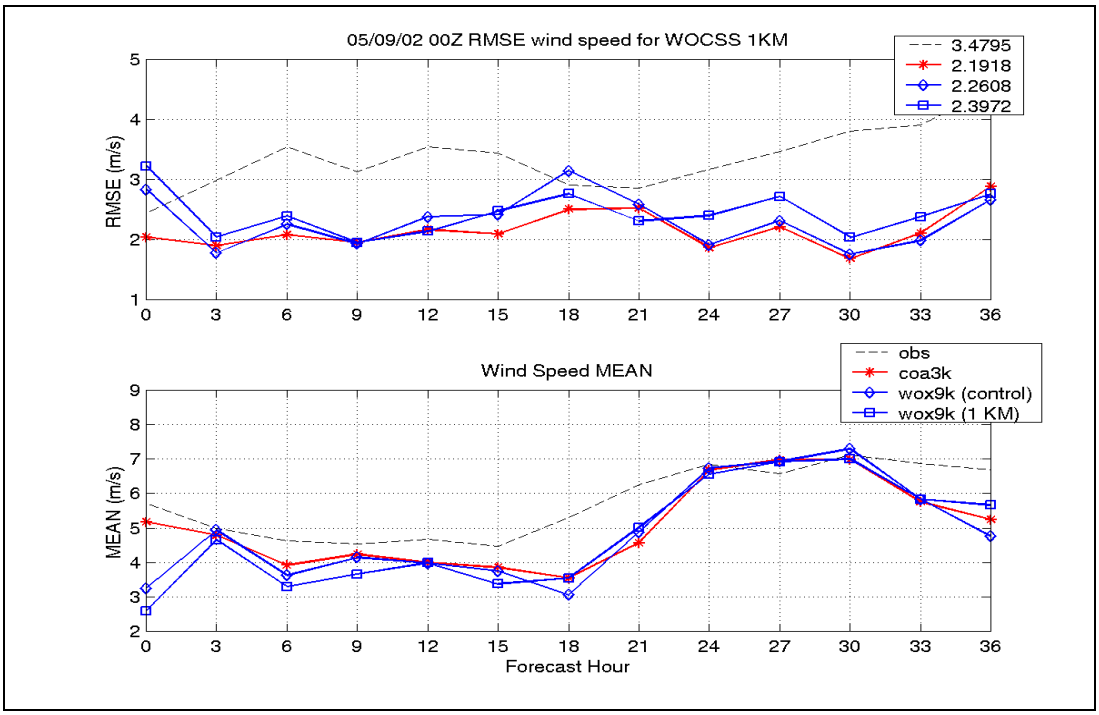

Figure 64. 09MAY02 WOCSS 1KM Wind Speed RMSE

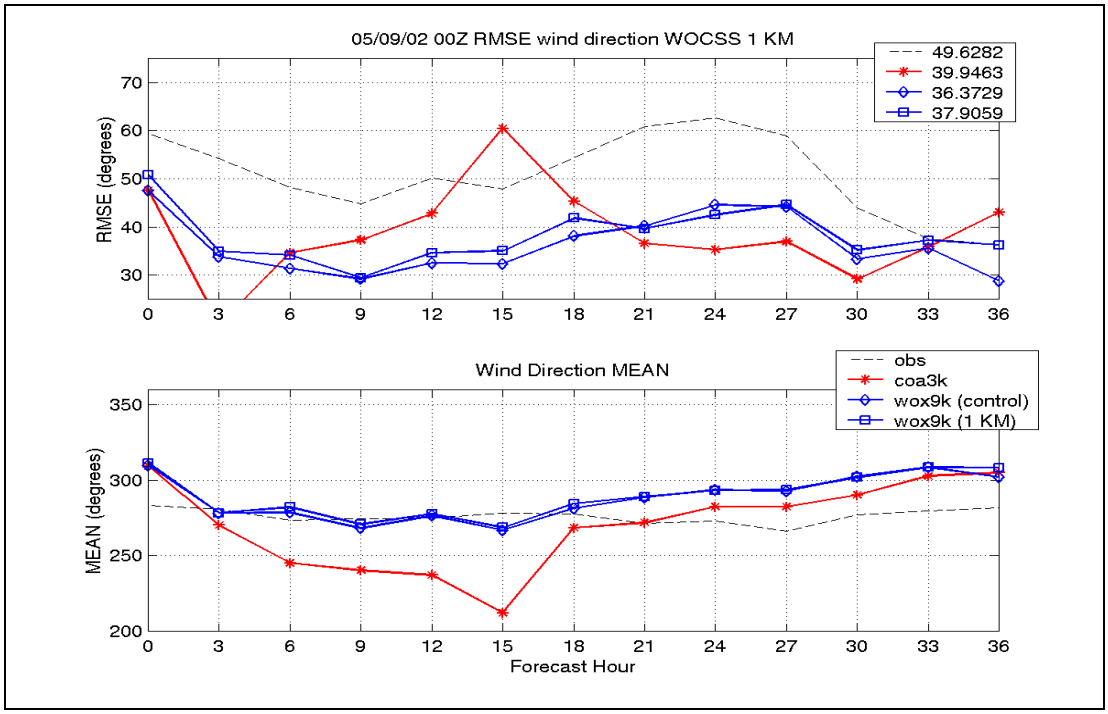

Figure 65. 09MAY02 WOCSS 1KM Wind Direction RMSE

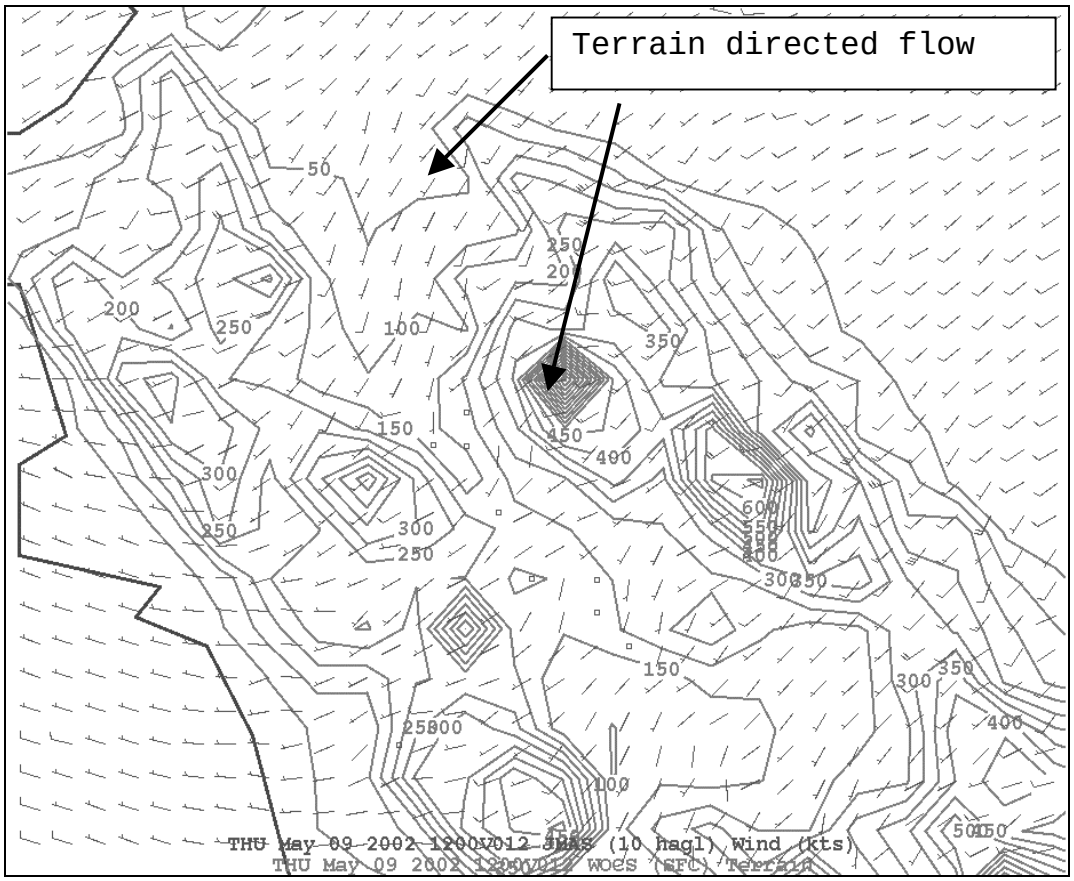

Figure 66. 09MAY02 12Z 1KM 10 m Winds (Diablo Range)

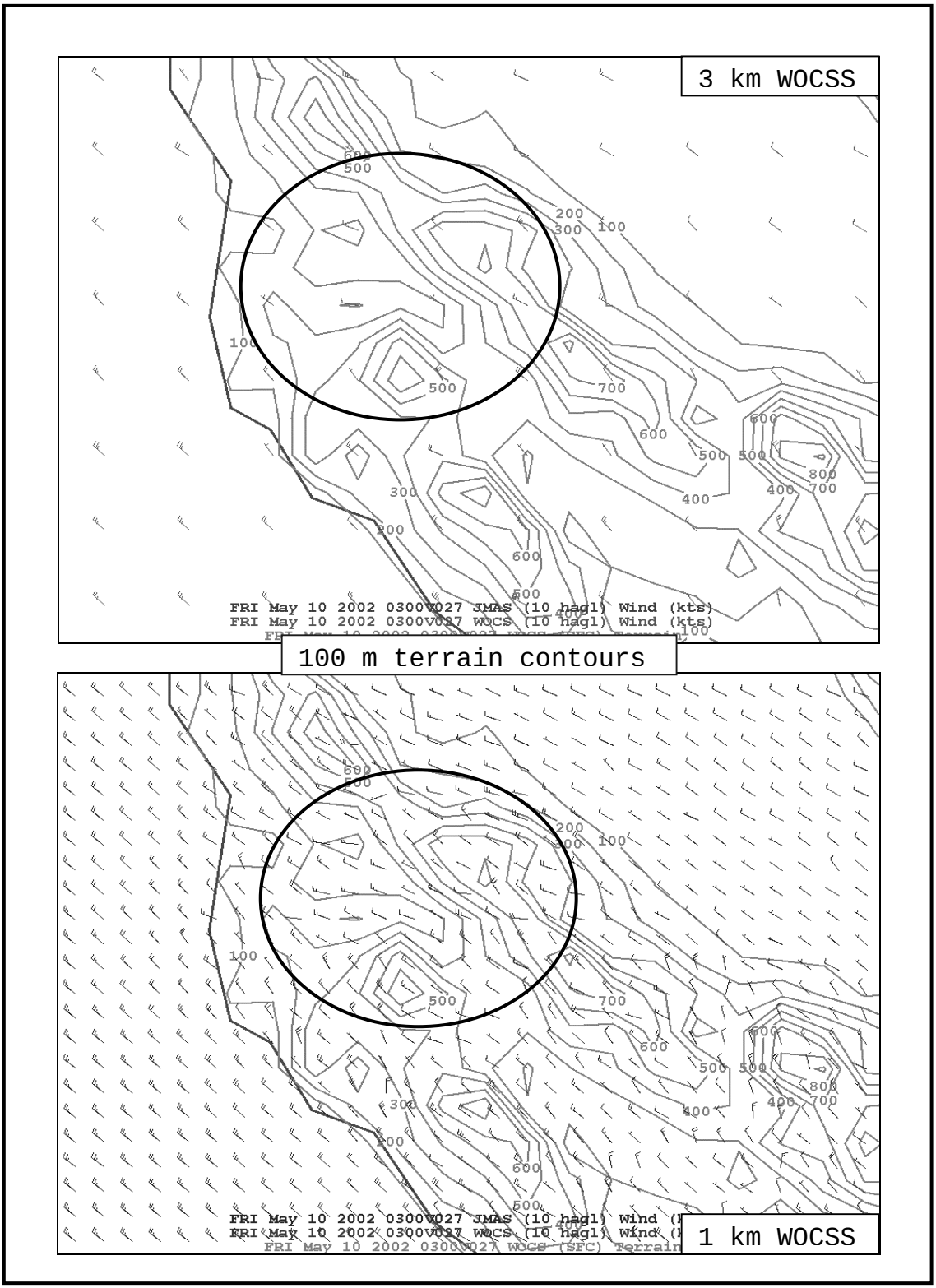

Figure 67. 09MAY02 12Z 3km(top)/1km(bottom) 10 m Winds

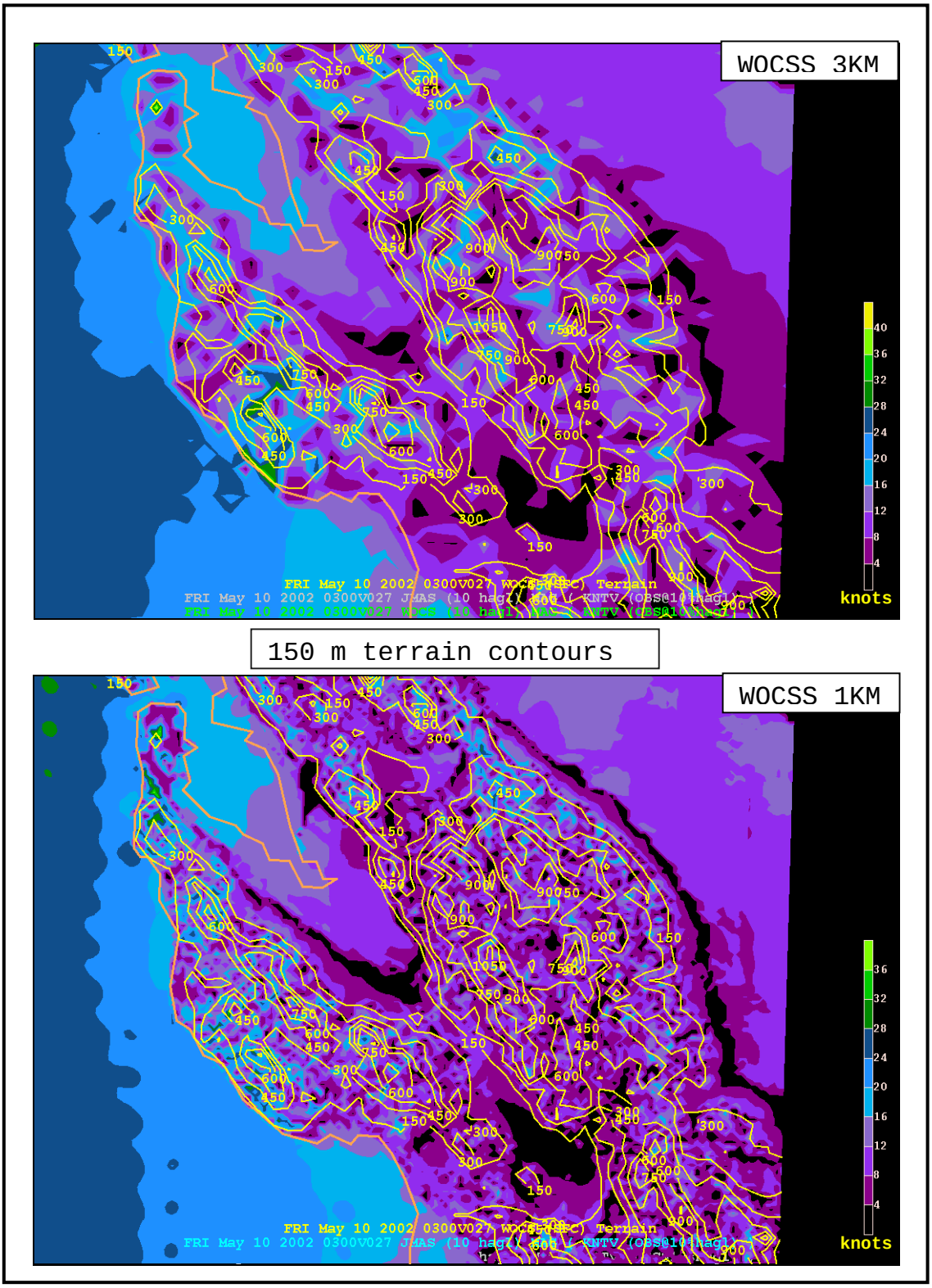

Figure 68. 10MAY02 03Z WOCSS 1KM/3KM 10 m Isotachs with 3 km terrain contoured

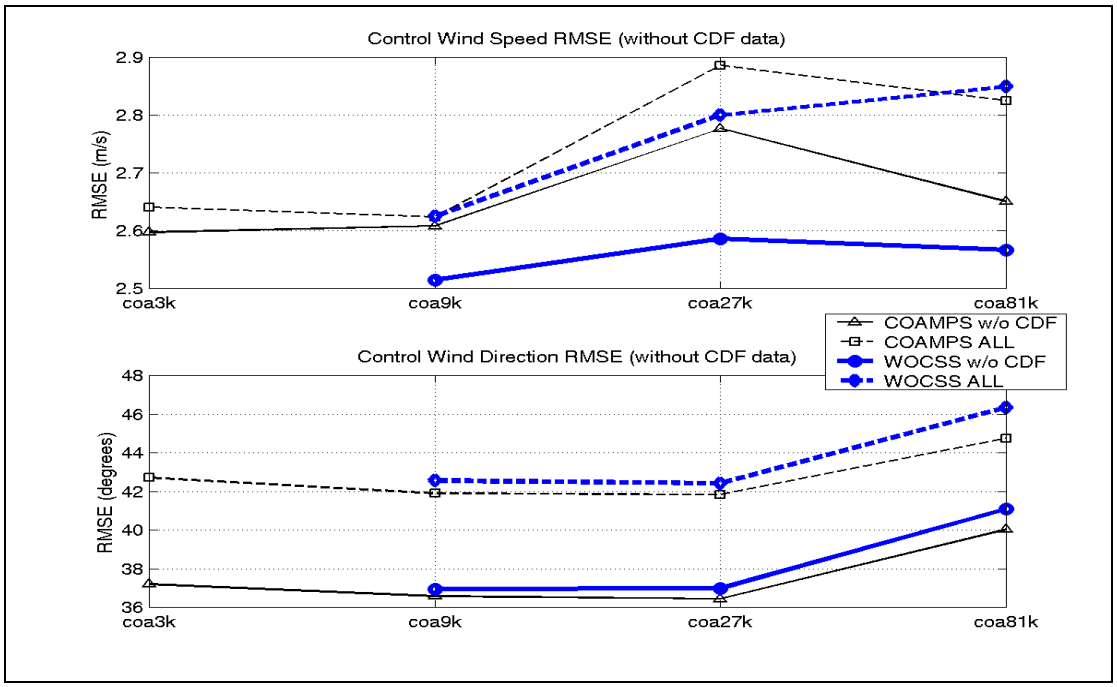

Figure 69. All Cases RMSE Without CDF Data

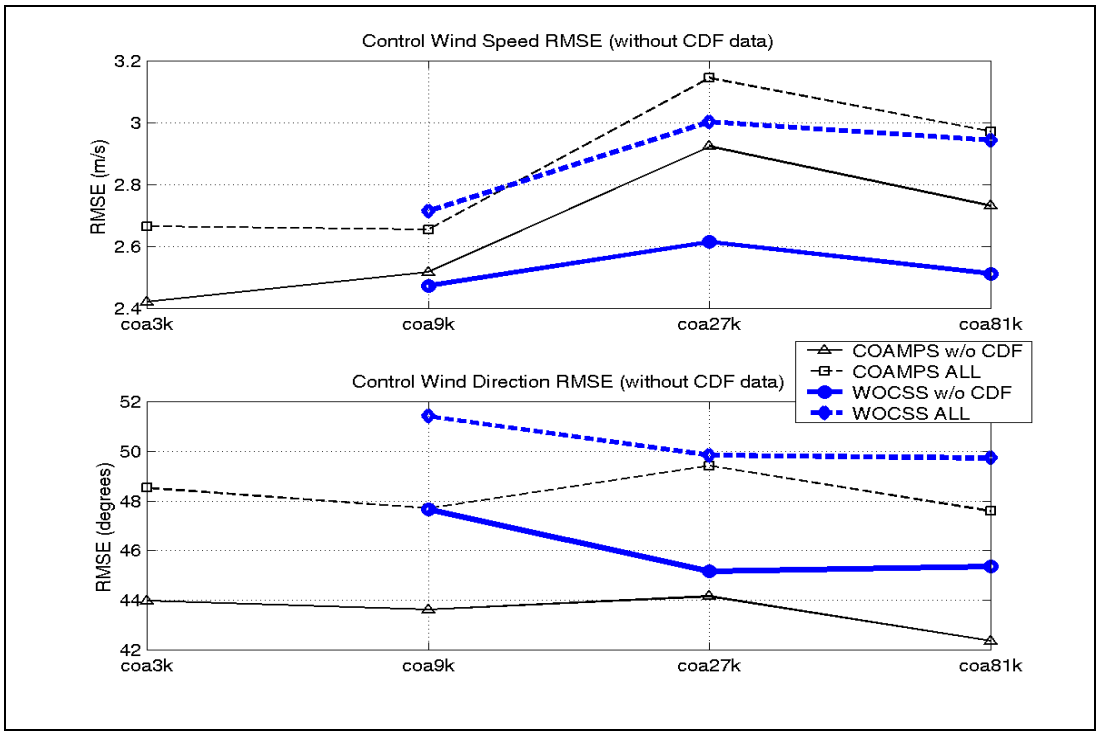

Figure 70. Frontal Cases RMSE Without CDF Data

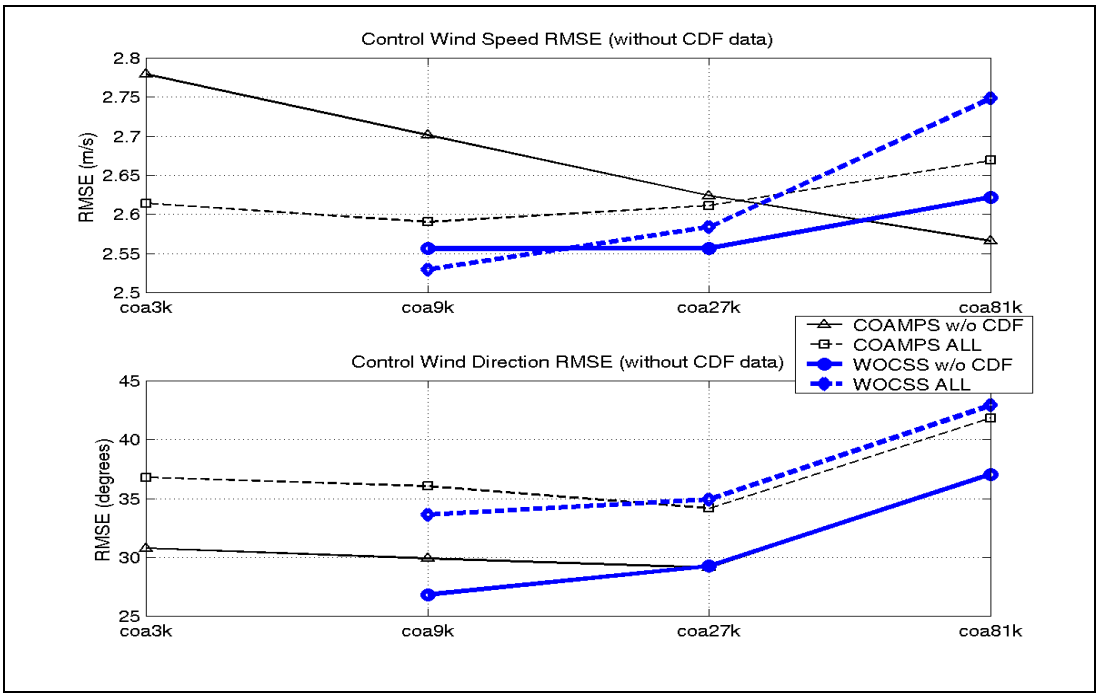

Figure 71. Non-Frontal Cases RMSE Without CDF Data

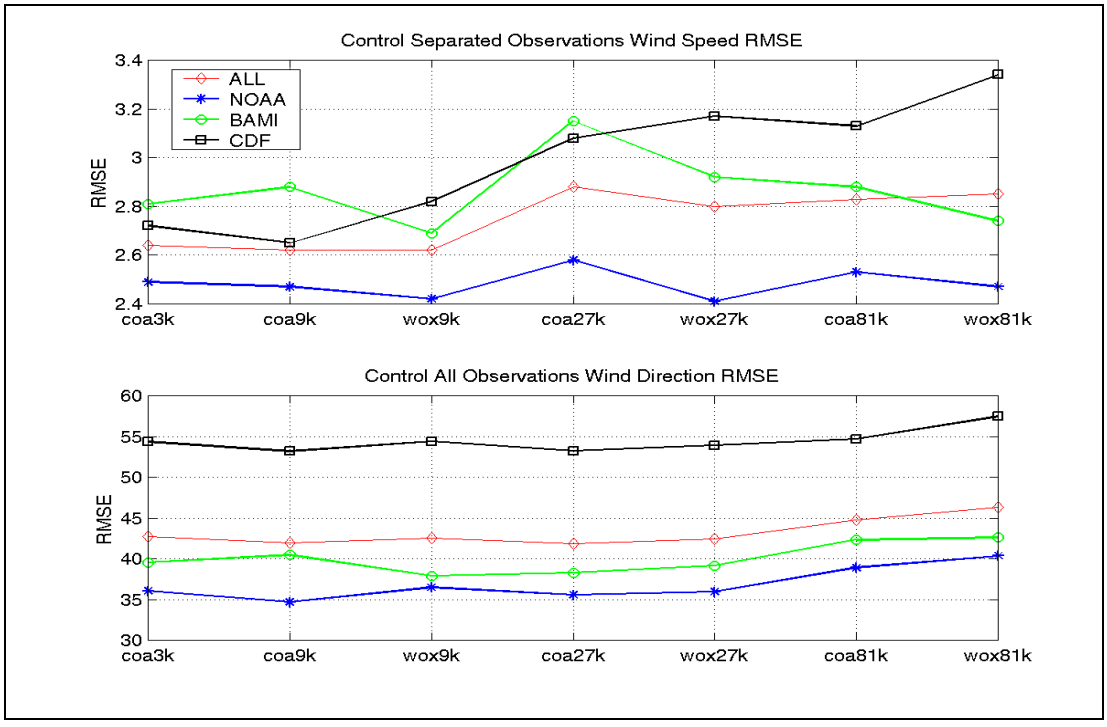

Figure 72. RMSE for Each Model Separated by Data Agency

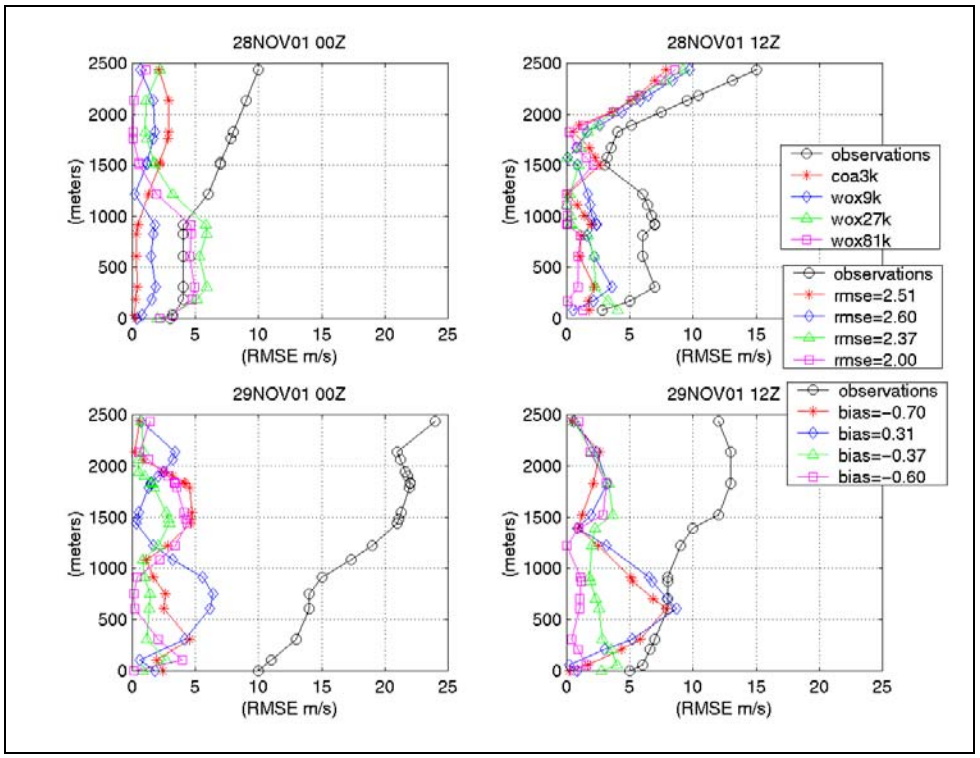

Figure 73. OAKU Sounding RMSE Wind Speed (28NOV01)

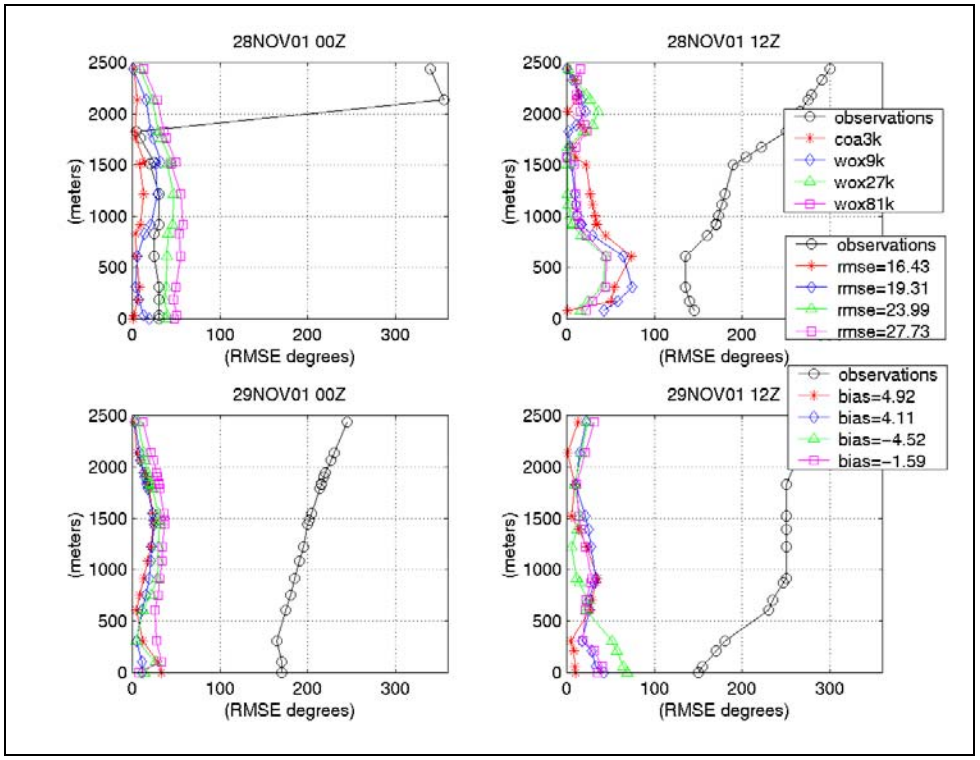

Figure 74. OAKU Sounding RMSE Wind Direction (28NOV01)

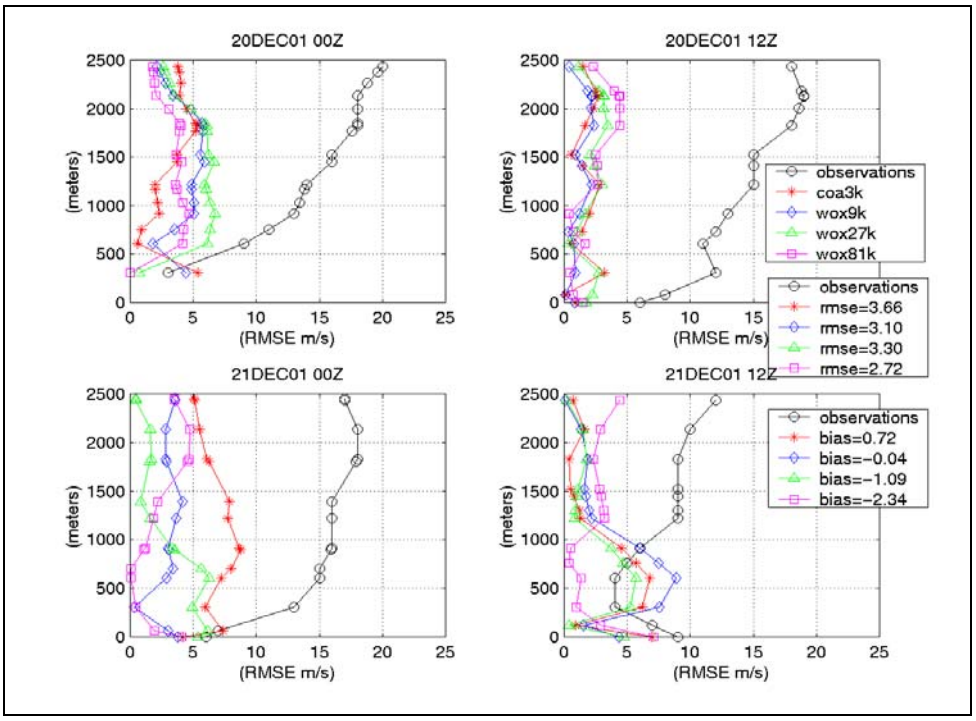

Figure 75. OAKU Sounding RMSE Wind Speed (20DEC01)

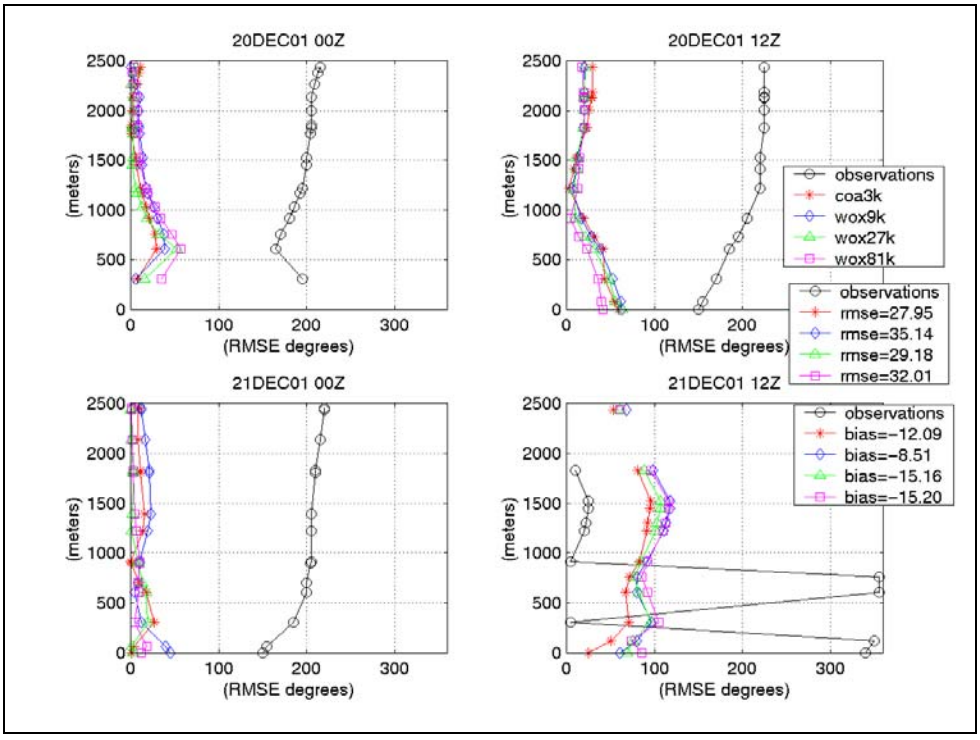

Figure 76. OAKU Sounding RMSE Wind Direction (20DEC01)

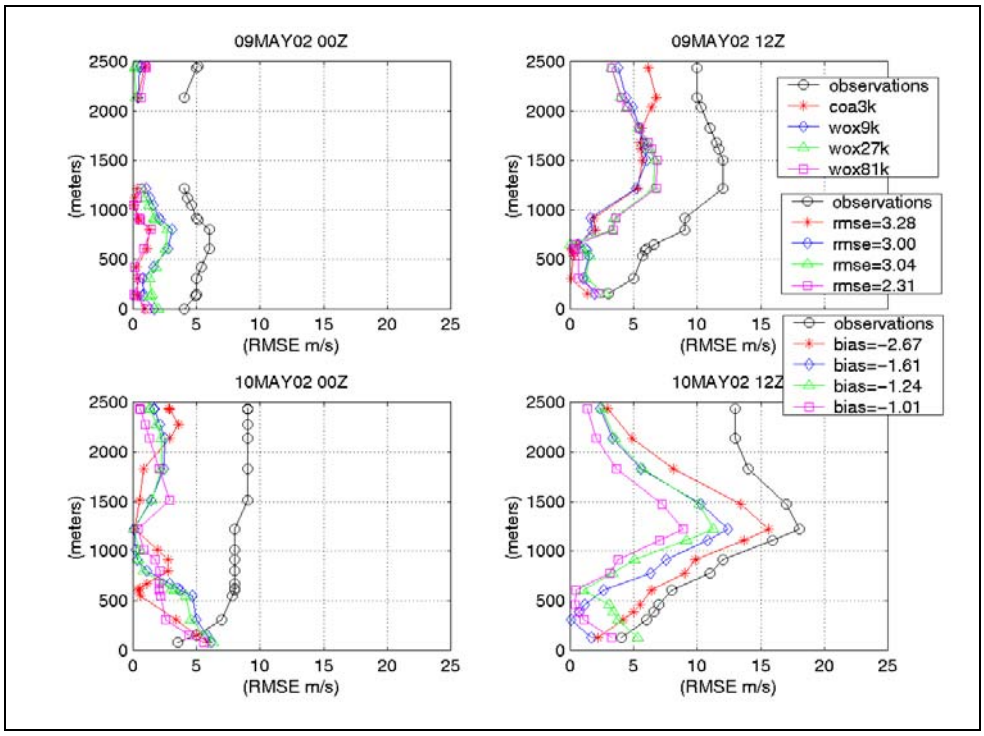

Figure 77. OAKU Sounding RMSE Wind Speed (09MAY02)

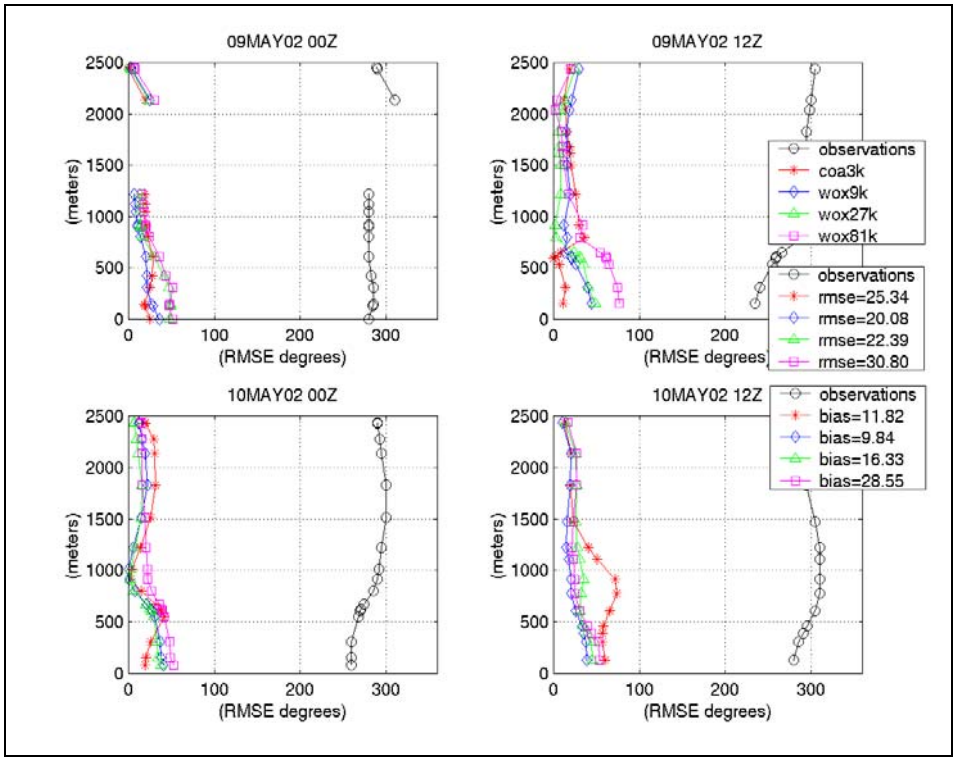

Figure 78. OAKU Sounding RMSE Wind Direction (09MAY02)

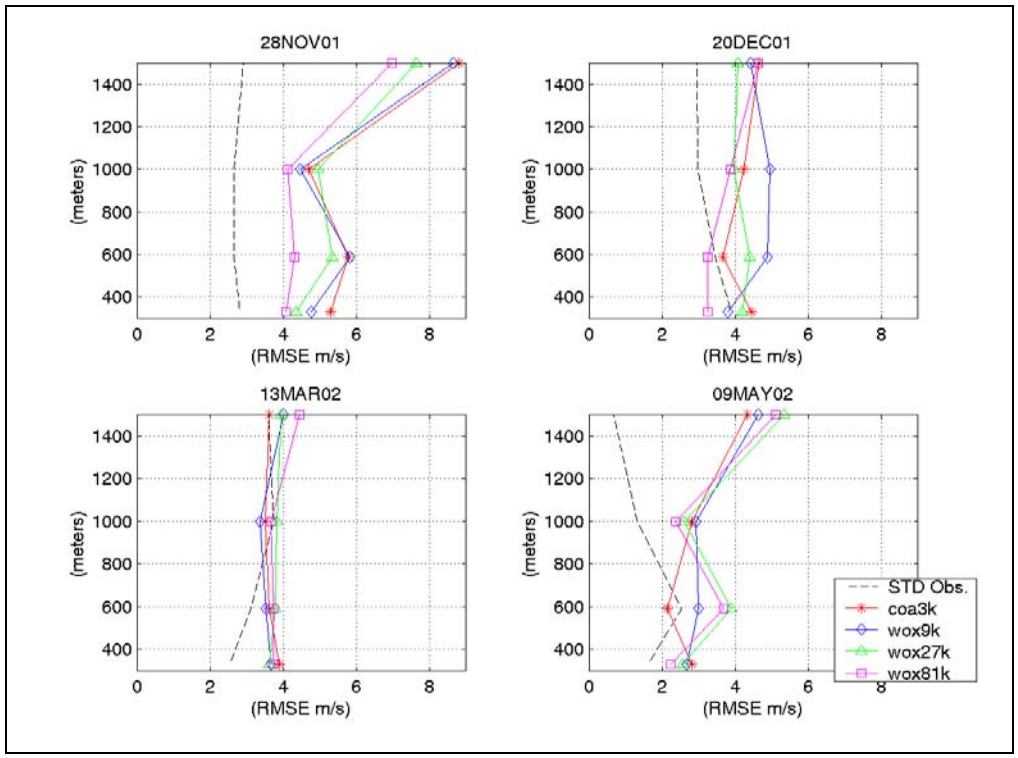

Figure 79. Vertical Profiler RMSE Wind Speed

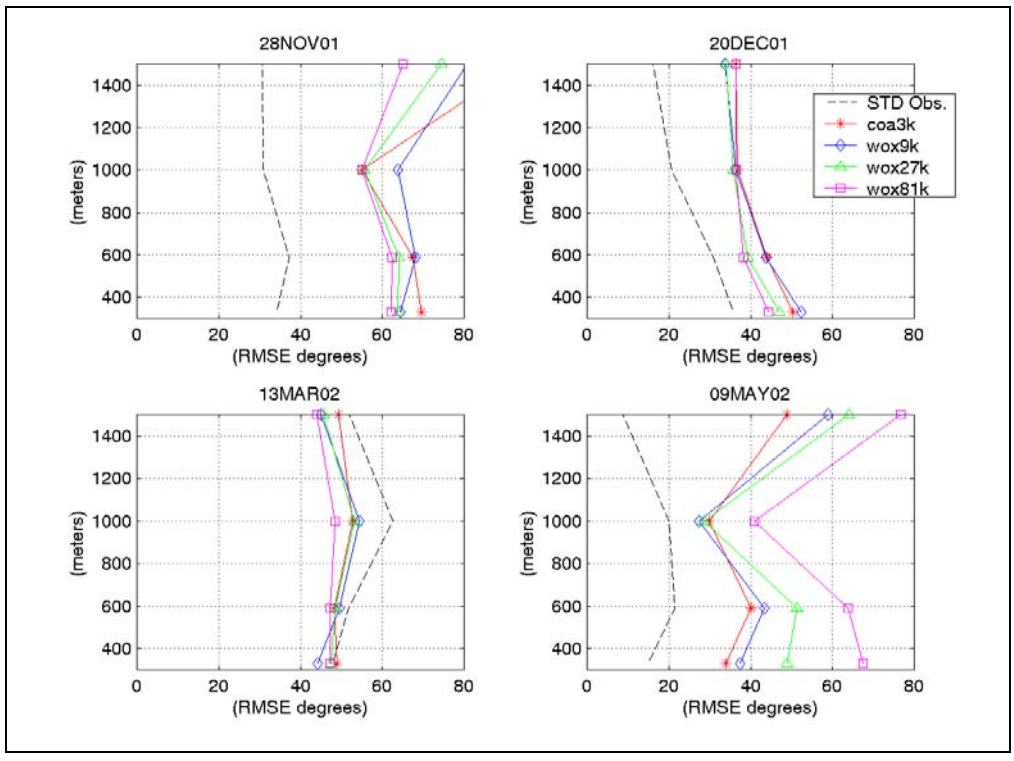

Figure 80. Vertical Profiler RMSE Wind Direction

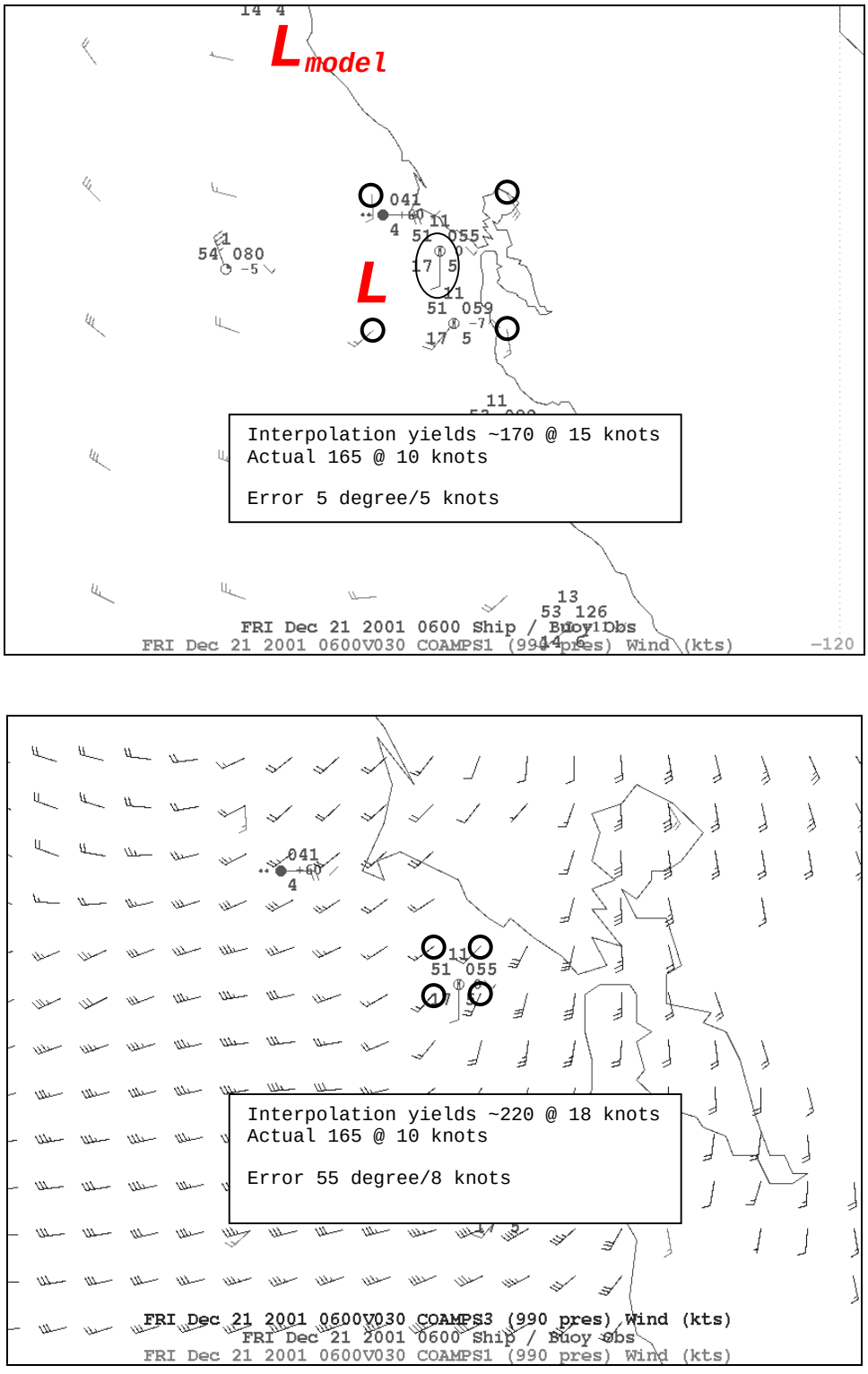

Figure 81. 21DEC02 06Z coa81k (Top) and coa9k (Bottom) 10 m Winds

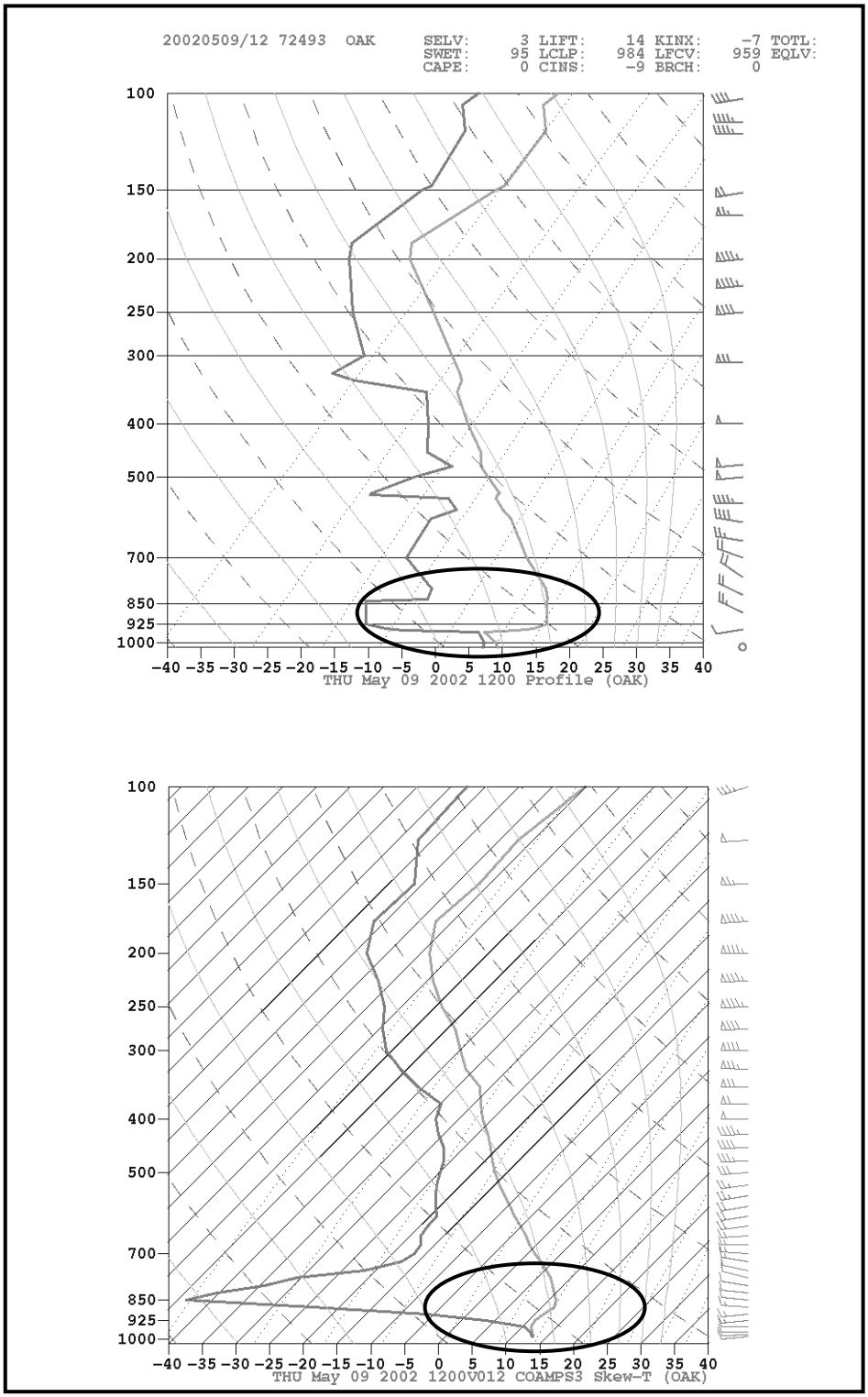

Figure 82 09MAY02 12Z Oakland Sounding Actual(Top) and coa9k Model(Bottom)

THIS PAGE INTENTIONALLY LEFT BLANK

Station Name	Station ID	Source	Lat	Long	Elev.(m)
NOAA Stations					
Napa	APC	NOAA	38.22	-122.28	10
Concord	CCR	NOAA	37.99	-122.05	11
Hayward	HWD	NOAA	37.66	-122.11	21
Livermore	LVK	NOAA	37.69	-121.81	117
Monterey	MRY	NOAA	36.59	-121.84	67
Moffett Field	NUQ	NOAA	37.40	-122.04	19
Oakland	OAK	NOAA	37.71	-122.23	26
Palo Alto	PAO	NOAA	37.46	-122.11	2
Reid/Hillview SJC	RHV	NOAA	37.33	-121.81	41
Stockton	SCK	NOAA	37.88	-121.22	10
San Francisco	SFO	NOAA	37.61	-122.36	26
San Jose	SJC	NOAA	37.35	-121.92	25
Salinas	SNS	NOAA	36.66	-121.61	25
San Carlos	SQL	NOAA	37.51	-122.25	1
Travis AFB	SUU	NOAA	38.26	-121.94	22
Watsonville	WVI	NOAA	36.93	-121.80	48
NOAA B #12	46012	NOAA	37.45	-122.70	0
NOAA B #26	46026	NOAA	37.75	-122.82	0
NOAA B #42	46042	NOAA	36.75	-122.42	0
NOAA B #13	46013	NOAA	38.23	-123.33	0
Tomasini Pt.	TMPC1	CNRFC	38.117	-122.85	12
Total Stations	21		Average Elevation		23.55

Table 1. NOAA Observation Sites

Station Name	Station ID	Source	Lat	Long	Elev.(m)
BAMI Stations					
Del Monte Beach	DMB	NPS	36.61	-121.87	8
Ft. ORD	ORD	NPS	36.69	-121.76	51
Pt. Sur N.S.	PTS	NPS	36.30	-121.89	12
Monterey Bay Aq.	MBA	NPS	36.62	-121.90	23
MBA B #1	M1B	MBARI	36.75	-122.01	0
MBA B #2	M2B	MBARI	36.69	-122.40	0
Bethel Island	BET	AQMD	38.01	-121.64	0
Ft. Funston	FUN	AQMD	37.71	-122.50	57
Kregor Peak	KRE	AQMD	37.94	-121.89	577
Livermore	LIV	AQMD	37.687	-121.783	137
Pt San Pablo	PAB	AQMD	37.96	-122.42	70
Richmond	RMD	AQMD	37.95	-122.40	111
San Martin	SMA	AQMD	37.08	-121.60	85
Sunol	SUN	AQMD	37.59	-121.88	140
Suisun	SUS	AQMD	38.22	-122.07	5
Vacaville	VCB	AQMD	38.38	-121.96	34
Hastings	CAHC1	CDF	36.551	-121.389	556
Ben Lomond	CKSC1	CDF	37.132	-122.17	802
Corralitos	CTOC1	CDF	36.991	-121.798	137
Diablo Grande	DBLC1	CDF	37.329	-121.294	564
Ft. ORD	FODC1	CDF	36.599	-121.753	234
Spring Valley	HSPC1	CDF	37.563	-122.436	328
La Honda	LAHC1	CDF	37.305	-122.254	130
Los Altos	LOAC1	CDF	37.358	-122.147	610
Los Gatos	LSGC1	CDF	37.203	-121.943	197
Las Trampas	LTRC1	CDF	37.834	-122.067	536
Mallory Ridge	LVMC1	CDF	37.817	-121.779	622
Mt. Diablo	MDAC1	CDF	37.867	-121.901	1173
OAK South	OKSC1	CDF	37.784	-122.160	305
OAK North	ONOC1	CDF	37.865	-122.221	396
Calaveras Road	PEAC1	CDF	37.553	-121.844	375
Black Diamond	PIBC1	CDF	37.95	-121.884	488
Briones	PLEC1	CDF	37.934	-122.118	442
Pulgas	PUGC1	CDF	37.475	-122.298	196
Rose Peak	RSPC1	CDF	37.502	-121.736	933
Ft. ORD #1	RTFC1	CDF	36.627	-121.798	140
Ft. ORD #2	RTGC1	CDF	36.627	-121.786	149
BAMI Stations	37		Average Elevation		279.92
CDF Stations	21		Average Elevation		433.47

Table 2. BAMI Observation Sites

Station Name	Station ID	Source	Lat	Long	Elev.(m)
Profiler Stations					
Livermore	LVR	AQMD	37.70	-121.90	65
Ft. ORD	NPS	NPS	36.69	-121.76	51
Richmond	RMD	NOAA	37.95	-122.40	111
Tracy	TCY	AQMD	37.69	-121.39	225
Vertical Sounding					
Oakland	OAKU	NOAA	37.733	-122.217	3

Table 3. Vertical Sounding Sites

Layer	Meters (AGL)
Layer 1 (~975mb)	304-359
Layer 2 (~950mb)	520-670
Layer 3 (~900mb)	938-1073
Layer 4 (~850mb)	1379-1623

Table 4. Profiler Observation Layers

Agency	Reported Precision		Reporting Average	Maintenance Schedule
NOAA/CNRFC	Wind Speed	0.1 m/s	2 minutes	6 month preventive
	Wind Direction	1.0°		Daily monitoring
	Temperature	0.1° C		yearly audit
NOAA/NBDC	Wind Speed	0.1 m/s	8 minutes	6 month preventive
	Wind Direction	1.0°		Daily monitoring
	Temperature	0.1° C		yearly audit
BAAQMD	Wind Speed	0.01 m/s	60 minutes	6 month preventive
	Wind Direction	1.0°		Daily monitoring
	Temperature	0.01° C		yearly audit
NPS	Wind Speed	0.01 m/s	1 minute prior to March, 2002 2 minutes after	Daily Monitoring
	Wind Direction	1.0°		Immediate Corrective
	Temperature	0.01° C		
MBARI	Wind Speed	0.1 m/s	1 minute	3-week check (variable)
	Wind Direction	1.0°		weekly monitoring
	Temperature	0.01° C		No auditing system
CDF	Wind Speed	0.25 mph	10 minutes	2-year preventive
	Wind Direction	2.0°		3-day monitoring
	Temperature	1.0° F		No auditing system

Table 5. Agency Maintenance and Precision Data (NOAA data-personal communications Carolina Horne NWS Monterey, BAAQMD data-personal communications Jeff Matsuoka BAAQMD San Francisco, NPS data-personal communications Dick Lind NPS Monterey, MBARI data-personal communications Mike Kelly MBARI Moss Landing, CDF data-personal communications Pete Gilbert CDF Sacramento)

Parameter	Code Variable	Value
Compression Factor	CMPRES	0.1
Ht. (m) highest sfc. over low pt.	AVTHK	5000
Iterations Limit (subroutine ba15)	NIT	20
Distance to weight power wt = 1/(Dist**DTWT)	DTWT	2
Max. adjustment near obs. 0 = no adj. & 1 = norm. adj.	ADJMAX	0.0
Roughness length in meters	ZZERO	0.05
Horizontal Resolution in km	N/A	3

Table 6. WOCSS Control Settings

Category	COAMPS Bias	WOCSS - COAMPS Difference	# Observations
Wind Speed	(m/s)	(m/s)	
Overall	0.24	-0.26	1983
Frontal	0.75	-0.52	1021
Non-Frontal	-0.31	-0.05	962
> 5 m/s	-1.65	-0.23	970
< 5 m/s	2.01	-0.28	1013
Frontal > 5 m/s	-1.34	-0.63	452
Frontal < 5 m/s	2.31	-0.39	569
Non-Frontal > 5 m/s	-1.89	0.11	517
Non-Frontal < 5 m/s	1.61	-0.14	445
28NOV01 Case	1.14	-0.22	528
20DEC01 Case	0.31	-0.83	493
13MAR02 Case	0.34	-0.25	532
09MAY02 Case	-0.65	0.09	430
Wind Direction	(degrees)	(degrees)	
Overall	13.97	6.46	1553
Frontal	6.33	5.01	780
Non-Frontal	21.67	8.23	773
> 5 m/s	14.25	4.41	790
< 5 m/s	10.96	6.86	763
Frontal > 5 m/s	4.99	4.88	433
Frontal < 5 m/s	10.92	5.98	347
Non-Frontal > 5 m/s	22.05	6.07	374
Non-Frontal < 5 m/s	21.02	9.12	399
28NOV01 Case	8.89	4.87	385
20DEC01 Case	9.23	5.45	395
13MAR02 Case	15.71	4.42	418
09MAY02 Case	28.17	11.87	355

Table 7. List of Biases/Differences by Category

Experiment	Model	Computation Time	# model obs
NIT = 10	wox9k	37-43 min.	736
	wox27k	7-9 min.	81
	wox81k	1.5 min.	9
NIT = 100	wox9k	45-51 min.	736
	wox27k	12-16 min.	81
	wox81k	3-5 min.	9
NIT = 1000	wox9k	69-79 min.	736
	wox27k	34-40 min.	81
	wox81k	20-24 min.	9
WOCSS 1KM	wox9k	6.5-8.5 hrs.	736
Control and All Other Experiments	wox9k	38-45 min.	736
	wox27k	8-10 min.	81
	wox81k	2 min.	9
Computing Platform: SGI Octane 300 MHz IP30 Processor, IRIX Operating System 6.5, CPU - MIPS R12000 Processor Chip, Memory - 640 MB			

Table 8. Computation Time for Experiments

WOCSS Levels	AVTHK = 3000m	AVTHK = 4000m	AVTHK = 5000m	AVTHK = 6000m	COAMPS
Sigma Levels	meters AGL	meters AGL	meters AGL	meters AGL	meters AGL
0	0	0	0	0	0
0.003	9	12	15	18	10
0.005	15	20	25	30	25
0.02	60	80	100	120	40
0.04	120	160	200	240	65
0.06	180	240	300	360	100
0.08	240	320	400	480	160
0.1	300	400	500	600	275
0.12	360	480	600	720	500
0.14	420	560	700	840	850
0.16	480	640	800	960	1275
0.18	540	720	900	1080	1750
0.2	600	800	1000	1200	2250
0.3	900	1200	1500	1800	2750
0.4	1200	1600	2000	2400	3250
0.6	1800	2400	3000	3600	3750

Table 9. WOCSS/COAMPS Vertical Levels

Model	**Layer 1**	**Layer 2**	**Layer 3**	**Layer 4**
RMSE	Speed/Direction	Speed/Direction	Speed/Direction	Speed/Direction
	(m/s)/(degrees)	(m/s)/(degrees)	(m/s)/(degrees)	(m/s)/(degrees)
coa3k	4.41/53.84	4.07/50.91	4.19/46.04	5.60/56.91
coa9k	4.25/51.94	4.37/50.51	4.21/48.51	5.40/51.80
wox9k	3.93/52.58	4.65/51.46	4.41/48.39	5.56/51.01
coa27k	4.16/48.83	4.51/47.59	4.09/43.74	5.00/51.75
wox27k	3.96/51.94	4.45/48.92	4.19/45.79	5.31/49.48
coa81k	3.48/49.82	3.66/48.97	3.62/46.02	4.94/53.90
wox81k	3.49/52.03	3.56/48.91	3.86/45.83	5.28/47.41
STD	3.09/36.12	3.08/36.61	3.01/34.12	3.08/30.27
Bias				
coa3k	0.02/7.54	-0.01/1.43	-0.16/0.43	-1.76/-11.60
coa9k	0.78/7.99	0.91/3.44	0.49/0.40	-1.40/-9.02
wox9k	0.82/10.57	1.20/7.49	0.72/5.19	-1.25/-9.32
coa27k	1.67/13.55	1.40/4.58	0.25/-0.42	-1.51/-14.32
wox27k	1.53/13.20	1.51/5.11	0.44/8.17	-1.65/-10.08
coa81k	1.04/11.91	0.74/5.49	-0.26/5.73	-1.86/-13.57
wox81k	1.13/22.32	0.90/8.43	-0.30/6.38	-2.18/-17.99
# Observations	101	103	100	78

Table 10. Profiler Statistics

THIS PAGE INTENTIONALLY LEFT BLANK

LIST OF REFERENCES

Arakawa, A., and J.M. Chen, 1987: Closure Assumptions in the Cumulus Parameterization Problem. *Short and Medium Range Numerical Weather Prediction.* T. Matsuno, Ed., Meteor. Soc. Japan, Universal Academy Press, 107-131.

Baker, N.L., 1992: Quality Control for the U.S. Navy Operational Database. *Wea. Forecasting*, 7, 250-261.

Baskett, R.L., R.L. Lee, W.A. Nuss, R. D. Bornstein, D.W. Reynolds, T. Umeda, and F.L. Ludwig, 1998: The Bay Area Mesonet Initiative (BAMI): A Cooperative Effort to Develop and Operate a Real-time Mesoscale Network in the Greater San Francisco and Monterey Bay Areas. Preprints, *Second Conf. on Coastal Atmospheric and Oceanic Prediction and Processes*, Phoenix, Arizona, Amer. Meteor. Soc., J30-J35.

Bhumralkar, C.M., R.L. Mancuso, F.L. Ludwig, and D.S. Renne, 1980: A Practical and Economic Method for Estimating Wind Characteristics at Potential Wind Energy Conversion Sites. *Sol. Energy*, 25, 55-65.

Cox, R.M., J. Sontowski, R.N. Fry, C.M. Dougherty, and T.J. Smith, 1998: Wind and Diffusion Modeling for Complex Terrain. *J. Appl. Meteor.*, 37, 996-1009.

Doyle, J.D, 1997: The Influence of Mesoscale Orography on a Coastal Jet and Rainband. *Mon. Wea. Rev*., 125, 1465-1488.

Endlich, R.M., 1967: An Iterative Method for Altering the Kinematic Properties of Wind Fields. *J. Appl. Meteor.*, 6, 837-844.

-----, F.L. Ludwig, C.M. Bhumralkar and M.A. Estoque, 1982: A Diagnostic Model for Estimating Wind at Potential Sites for Wind Turbines. *J. Appl. Meteor.*, 21, 1441-1454.

-----, 1984: Wind Energy Estimates by Use of a Diagnostic Model. *Bound.-Layer Meteor*., 30, 375-386.

Fast, J.D., B.L. O'Steen, and R.P. Addis, 1995: Advanced Atmospheric Modeling for Emergency Response. *J. Appl. Meteor.*, 34, 626-649.

Hodur, R.M., 1997: The Naval Research Laboratory's Coupled Ocean/Atmosphere Mesoscale Prediction System (COAMPS). *Mon. Wea. Rev*., 125, 1414-1430.

Horel, J., and Coauthors, 2002: MesoWest: Cooperative Mesonets in the Western United States. *Bull. Amer. Meteor. Soc.*, 83, 211-225.

Hunt, J.C., and W.H. Snyder, 1980: Experiments on Stably and Neutrally Stratified Flow Over a Three-dimensional hill. *J. Fluid Mech*., 96, 671-704.

Kuypers, M.A., 2000: *Understanding Mesoscale Error Growth And Predictability*, Master's Thesis, Naval Postgraduate School, Monterey, California, September 2000.

Lange, R., 1978: A Three-dimensional Particle-in-cell Model for the Dispersal of Atmospheric Pollutants and Its Comparison to Regional Tracer Studies. *J. Climate Appl. Meteor.*, 28, 665-679.

Lorenc, A.C., 1986: Analysis Methods for Numerical Weather Prediction. *Quart. J. Roy. Meteor. Soc.*, 112, 1177-1194.

Lorenz, E.N., 1982: Atmospheric Predictability Experiments With a Large Numerical Model. *Tellus*, 36A, 505-513.

Ludwig, F.L., J.M. Livingston, and R.M. Endlich, 1991: Use of Mass Conservation and Critical Dividing Streamline Concepts for Efficient Objective Analysis of Winds in Complex Terrain. *J. Appl. Meteor*., 30, 1490-1499.

-----, and D. Sinton, 2000: Evaluating an Objective Wind Analysis Technique with a Long Record of Routinely Collected Data. *J. Appl. Meteor*., 39, 335-348.

Mass, C.F., D. Owens, K. Westrick, and B.A. Colle, 2002: Does Increasing Horizontal Resolution Produce More Skillful Forecasts? *Bull. Amer. Meteor. Soc.*, 83, 407-430.

McNider, R.T., K.E. Johnson and R.W. Arritt, 1984: Transferability of Critical Dividing Streamline Models to Larger Scale Terrain. *Conference Volume-Fourth Joint Conf. on Applications of Air Pollution Meteorology*, Boston, Amer. Meteor. Soc., J25-J27.

Miller, Miguel, 1996: *Climate of San Jose*. NOAA Technical Memorandum NWS WR-259

Mohammed, R.M., 2000: *Forecasting Mesoscale Winds on Complex Terrain using a Simple Diagnostic Model*, Master's Thesis, Naval Postgraduate School, Monterey, California, September 2000.

Molinari, J. and M. Dudek, 1992: Parameterization of Convective Precipitation in Mesoscale Numerical Models: A Critical Review. *Mon. Wea. Rev.*, 120, 326-342.

Monterrosa, O.E., 1999: *Comparison of TAMS/RT Surface Wind, Temperature, and Pressure Fields with Surface Observations and Model Analyses in the SOCAL Area*, Master's Thesis, Naval Postgraduate School, Monterey, California, December 1999.

Null, Jan, 1995: *Climate of San Francisco.* NOAA Technical Memorandum NWS WR-126.

Nuss, W.A., and D.W. Titley, 1994: Use of Multiquadric Interpolation for Meteorological Objective Analysis. *Mon. Wea. Rev.*, 122, 1611-1631.

Perkey, D.J., 1986: Formulation of Mesoscale Numerical Models. In: Mesoscale Meteorology and Forecasting, P.S. Ray, Ed., *Am Meteor. Soc.*, 573-596.

Poulos, G.S., and J.E. Bossert, 1995: An Observational and Prognostic Numerical Investigation of Complex Terrain Dispersion. *J. Appl. Meteor.*, 34, 650-669.

Sheppard, P.A., 1956: Air Flow Over Mountains. *Quart. J. Roy. Meteor. Soc*., 82, 528-529.

Sherman, C.A., 1978: A Mass-consistent Model for Wind Fields Over Complex Terrain. *J. Appl. Meteor*., 17, 312-319.

Thompson, W.T., T. Haack, J.D. Doyle, and S.D. Burk, 1997: A Nonhydrostatic Mesoscale Simulation of the 10-11 June 1994 Coastally Trapped Wind Reversal. *Mon. Wea. Rev.*, 125, 3211-3230.

Thykier-Nielsen, S.,T. Mikkelsen, R. Kamada, and S.A. Drake, 1990: Wind Flow Model Study for Complex Terrain. Preprints, *Ninth Symp. On Turbulence and Diffusion*, Copenhagen, Denmark, Amer. Meteor. Soc., 421-424.

Troen, I., and A.F. de Bass, 1986: A Spectral Diagnostic Model for Wind Flow Simulations in Complex Terrain. *Proc. EWEC '86 European Wind Energy Association Conf. and Exhibit*, Rome, 243-250.

WebMET.com: The Meteorological Resource Center, *Radar Wind Profiler*, [http://www.webmet.com/metmonitoring/ 914.html]. 02 August 2002.

Williams, M., and T. Yamada, 1990: A Microcomputer-based Forecasting Model: Potential Applications for Emergency Response Plans and Air Quality Studies. *J. Air Waste Manage. Assoc.*, 40, 1266-1274.

INITIAL DISTRIBUTION LIST

1. Defense Technical Information Center
   Ft. Belvoir, VA

2. Dudley Knox Library
   Naval Postgraduate School
   Monterey, CA

3. Chairman, Code MR/Wx
   Department of Meteorology
   Naval Postgraduate School
   Monterey, CA

4. Chairman, Code OC/Ga
   Department of Oceanography
   Naval Postgraduate School
   Monterey, CA

5. Professor Douglas K. Miller
   Department of Meteorology
   Naval Postgraduate School
   Monterey, CA

6. Professor Wendell A. Nuss
   Department of Meteorology
   Naval Postgraduate School
   Monterey, CA

7. Commander
   Naval Meteorology and Oceanography Command
   Stennis Space Center, MS

8. Dr. Francis L. Ludwig
   Dept. of Civil Env. Engineering
   Stanford University
   Stanford, CA

9. Dr. Francis M. Fujioka
   PSW Forest Fire Laboratory
   Riverside, CA

10. Dr. Duane E. Stevens
    University of Hawaii at Manoa
    Honolulu, HI

11. Lieutenant Shawn G. Gallaher
    Monterey, CA

12. Dr. David Bright
    National Weather Service
    Tucson, AZ

13. Brad Colman
    NOAA/National Weather Service
    Seattle, WA

14. Dr. James D. Doyle
    Naval Research Laboratory
    Monterey, CA

15. Pete Gilbert
    California Department of Forestry
    Sacramento, CA